Momentum-space atom correlations in strongly interacting Bose gases

David Clément

UNIVERSITÉ PARIS-SACLAY

École doctorale de Ondes et Matières (ED 572)

Laboratoire Charles Fabry (UMR 8501 CNRS)

Mémoire présenté pour l'obtention du

Diplôme d'habilitation à diriger les recherches

Discipline : Physique

par

David CLEMENT

Momentum-space atom correlations in strongly interacting Bose gases

Rapporteurs :

JEAN DALIBARD
THIERRY GIAMARCHI
DAVID GUERY-ODELIN

Date de soutenance : 14 Octobre 2019

Composition du jury :

ALAIN ASPECT	(Invité)
IMMANUEL BLOCH	(Examinateur)
JEAN DALIBARD	(Rapporteur)
DANIELLE DOWEK	(Examinatrice)
THIERRY GIAMARCHI	(Rapporteur)
DAVID GUERY-ODELIN	(Rapporteur)
CHRISTOPH WESTBROOK	(Invité)

Contents

Chapter 1

Introduction

This manuscript for the Habilitation à diriger des Recherches presents my research activity as a post-doctoral fellow at the LENS laboratory (Florence, Italy) and as a Maitre de conférence (associate professor) at the laboratory Charles Fabry (Palaiseau, France), covering a period of time ranging from 2008 to 2019. Over these years, I have participated to investigating various scientific questions in quantum physics, with two main features shared by these works. On the one hand, a central motivation has been to unveil the role of (quantum) correlations between the individual particles in interacting quantum systems. As it shall be explained below, one intriguing aspect of quantum physics lies in the possibility for the particles to be correlated (for instance when entangled) in a way for which there exist no classical counterpart. Understanding how new ground-states and dynamics emerge as a result of these correlations is a fascinating objective for a physicist. On the other hand, identifying the role of correlations in interacting quantum systems in an experiment requires a high degree of control – ideally at the single particle level – and adequate probes to reveal the correlation signals. One type of experimental platforms that was shown to be suited for these tasks are quantum gas experiments. All the works presented in this manuscript have been performed with quantum gas apparatus, with either an atomic species of Rubidium or of Helium.

My scientific curiosity for correlated quantum matter was initially triggered by the literature associated with the topic of my PhD thesis, the localization of matter-wave in disorder. Although a large part of my PhD work has been devoted to looking for localization phenomena of non-interacting matter-waves, the scientific context of this research was very much inspired by solid-state physics and the prediction of P. W. Anderson to describe electronic insulators [5]. As I was lucky to participate to the early days of the quest for localization phenomena with quantum gases, I went through a literature which was that of condensed-matter physicists and got acquainted with some concepts associated with interacting quantum systems, especially in an attempt to draw for myself a physical picture of the interplay between disorder and interaction in solids. In addition, the period of my PhD thesis also coincided with the flourishing of two experimental techniques that brought weakly-interacting quantum gases in the regime of strong interactions: the use of optical lattices and of Feshbach resonances. Optical lattices can be used to simulate cristalline structures for the atoms, and Feshbach resonances allow for tuning the strength of the inter-particle interactions. Several landmarks experiments were reported at that time and by the end of my PhD I was very much impressed and interested to learn more about these experimental tools. My decision to proceed with a post-doctoral stay in the group of M.

Inguscio derives from this motivation: the group at LENS had obtained important results both with loading atoms in optical lattices and from varying the interaction strength thanks to Feshbach resonances. I spent three years in Florence studying one-dimensional (1D) Bose gases thanks to the use of optical lattices.

My post-doctoral experience then played a central role in the building of the research project I presented for the position of Maître de Conférence at the Institut d'Optique. It was indeed during my stay in Italy that I realised that global probes are not the most suited techniques to study correlations in quantum systems, contrary to local – ideally single-particle-resolved – probes. The difference between a local and a global probe I am referring to is simply that the later averages the signal measured by the local probe. When the averaging effect is too large, the signals of interest are affected and may even vanish. These ideas were spreading among the quantum gas community at the time of my post-doctoral stay and the first experimental probes sensitive to individual atoms were being demonstrated [160]. These results as well as discussions with colleagues certainly had an influence on me. My personal experience in the lab also had a strong impact. While we have obtained some interesting results on 1D Bose gases during my stay in Florence, our work was limited in some aspect by our way of probing the system. As it will be detailed in the first chapter, we used a light scattering technique – referred to as Bragg spectroscopy – to study the response of the 1D gases when a momentum and an energy is deposited. The probe was global in two aspects: on the one hand the light was shown over the entire gas, irrespective of the local atomic density which happens yet to be a crucial parameter in the response of a 1D gas to such an excitation; on the other hand the response was characterised in the experiment by estimating the total energy deposited in the 1D gases, without distinguishing excitations of different momenta for instance. In an attempt to overcome the limitations associated with global probes, a central technical aspect of my project to investigate interacting quantum matter consists in using the single-atom-resolved method of detection that was pioneered by my (future) colleagues at the Institut d'Optique. This technique relies on the properties of metastable Helium atoms and it had been used for analogs of quantum optics experiments. My plan was to extend its scope to probe interacting quantum systems.

The following paragraphs puts my research activity in the international context and briefly summarise the main scientific results.

1.1 Scientific context: probing many-body physics through atom correlations

The laws and models drawn by physicists attempt at describing the world that surrounds us. A better understanding of this environment has always derived from new experimental observations. It happened that theoretical predictions have led experimentalists to developed innovative tools of observation, or that the advent of novel techniques have yielded new pieces of information by itself, without a previous support from theory. In both the situations the role played by the techniques of observation is central as it provides access to information with which our knowledge is confronted. In this respect, I believe that a central aspect of the role of an experimentalist is to establish new observation tools that yield original pieces of information about physical systems that we do not fully understand. A broad area of modern physics where a full description, and understanding, is still lacking in situations of interest is quantum many-body physics. A quantum many-body system

consists of an ensemble of interacting quantum particles where the interplay between interaction[1] and quantum fluctuations plays a central role. More precisely, many-body physics refers to situations where the physics can not be described at the mean-field level, *i.e.* that the description of strongly interacting (many-body) systems requires keeping track of some correlations present between the individual constituents. As we shall explain below, this requirement is at the origin of our difficulties to capture the physics of strongly correlated quantum systems both in theory and experiments. Overcoming these difficulties is important as quantum many-body systems cover a large variety of situations that would benefit from a deeper understanding, from solid-state superconductors and topological matter to neutron stars. In addition, the results of quantum simulation could potentially lead to novel technologies based on engineered quantum matter with strong correlations, as underlined by the launch of the European flagship on quantum technologies.

Quantum simulation with AMO platforms. Quantum theory provides a framework where many-body problems can be exposed because all the information – and correlations – is encoded in the complete wave-function characterising the system under study. But obtaining this information often turns out impossible when the number of particles exceeds a few dozens. In some special cases, it is possible to capture the correlations of interest by using perturbative approaches on top of a well-known solution. In many cases, many-body perturbative theories are yet not sufficient and the description of many-body systems requires the knowledge of multi-particle correlations. This implies an exponential growth of the Hilbert space with the number of particles, a scaling that poses the limit of a few dozens of particles mentioned previously for the most advanced numerical approaches (developed on classical computers). In addition, today's understanding of many-particle entanglement is somehow limited and dealing with many-particle entanglement remains an extremely difficult task – the very definition of multi-partite entanglement is not obvious [102]. This poses difficulties to theoretical approaches for many-body physics because many-particle entanglement is often at the heart of strongly correlated systems [159, 47].

In a celebrated contribution from 1982 [76], R. Feynman introduced an idea, which we now refer to as "quantum simulation", to overcome the limits posed by numerical calculations to solve many-body problems. Discussing the impressive development of (classical) computers at that time, R. Feynman noted that classical computers would probably not be able to deal with the simulation of a large number of quantum particles, for the reasons discussed above. As an alternative, he proposed to "*Let the computer itself be built of quantum mechanical elements which obey quantum mechanical laws*". This apparently simple suggestion has deeply impacted our view to address many-body problems and led scientists to look for building a novel type of experimental apparatus. To follow the direction indicated by R. Feynman, the machine should not only be made of elements behaving quantum mechanically but it also requires an unprecedented level of control for what was possible at the time: the parameters for the quantum simulation should be under an excellent control as that encountered when performing a numerical simulation on a classical computer.

Over the past decades, physicists have worked to master various experimental platforms in the direction indicated by Feynman's suggestion, among which are quantum gas experiments. Nowadays, the exquisite control on the microscopic parameters provided by working with quantum gases has permitted to implement a large series of Hamiltonians [20], varying in a controlled manner central parameters of many-body problems: the

[1]Here, interactions is intended in a broad meaning which includes the way particles interact with each other but which also covers decoherence processes, viewed as an interaction with the environment.

statistics (boson, fermion), the dimension (from 1D to 3D), the interactions (its strength through Feshbach resonances but also its type, from short-range to long-range) and the environment (from lattice geometries of almost any kind to disordered potentials). It resulted in many fascinating experiments along the line of the quantum simulation: the investigation of the BEC-BCS crossover with fermions [177, 239, 49, 27, 121], of the Fermi Hubbard Hamiltonian in the presence of doping [146], of the many-body localization phenomena in disorder [196, 51, 139] and many others. Today's enthusiasm for the use of AOM platforms to investigate many-body physics – quantum gases, ions, superconducting qbits, etc – is (partially) rooted in Feynman's early proposal. But it should be stressed that it also derives from the capabilities provided by these platforms to probe many-body phenomena at the level of individual particles. As mentioned previously, single-particle-resolved methods of detection are the most appealing kind of local probes, from which particle correlations are directly extracted. From measuring the full particle distribution in a given degree of freedom (*e.g.* the position, the momentum, the spin, ...), correlations at any order can indeed be obtained in principle. Of course, experiments are often limited to low orders of correlation, due to the presence of technical noise and the necessity to accumulate a lot of statistics to reach a correct signal-to-noise ratio on the correlation functions, but these single-atom-resolved measures of correlations go beyond what is commonly measured in solid-state systems, as we shall explain below.

Probing many-body physics at the single particle level. Probing the correlations between some degree of freedom of individual particles in experiments is a difficult task. In condensed matter physics, imaging the position – and correlations – of individual electrons is hardly possible and this led physicists to obtain information about many-body systems from measuring their response to a perturbation. By perturbation we intend a mean to deposit some energy and/or momentum into the system. Experimental probes then consist in quantifying how much energy and/or momentum is transferred to the system under investigation. These methods includes the measurements of transport properties [224, 227] as well as momentum-resolved scattering techniques like Angle-Resolved Photo-Emission Spectroscopy (ARPES) [63] and neutron scattering [221]. With the definition given previously, these approaches are global probes of many-body systems. While emblematic signatures of many-body physics were obtained in condenser matter through these global probes, some correlations are difficult to reveal without being in the position to observe single quantum particles. For instance, to my knowledge, there exists no direct observation of the momentum correlations associated to Cooper pairs. In conventional superconductors, the celebrated theory proposed by Bardeen, Cooper and Schrieffer to support the existence of superconductivity relies on a mechanism of pairing between two electrons which is mediated by the phonons. This so-called Cooper pairing mechanism has been identified in conventional superconductors through various properties, for instance those of the superconducting gap probed through the specific heat [216]. Nevertheless, a Cooper pair is assumed to be made of two electrons with opposite momenta, a correlation for which a direct observation is missing. An experiment with single-electron-resolved detection in the momentum-space could provide the mean for such an observation.

In contrast to solids, probing the individual particles of a many-body state is amenable in dilute systems made of a few quantum particles, "few" meaning much less than the Avogadro number $\sim 10^{23}$, a typical situation in AMO physics. This possibility is illustrated by the 2012 Nobel prize that rewarded a tremendous progress in the development of experimental tools to manipulate and observe single quantum objects like ions [229] and photons

[95]. In most of the experiments performed along the line of research highlighted by the 2012 Nobel prize, the physics that was investigated is that of one or a few (typically less than a dozen) of quantum particles with no or weak interactions. But the techniques associated to these works have doubtlessly played a central role in the flourishing of AMO platforms probing many-body physics at the single particle level. This includes trapped ions [29], quantum gases [20] and arrays of Rydberg atoms [15] (one should also include platforms for quantum simulation based with solid-state devices like superconducting q-bits [14]).

In the quantum gas community, optical techniques – fluorescence, absorption and phase contrast imaging – have been the central method used to probe atoms [119]. Optical probes remains central nowadays as well but, on the one hand fluorescence techniques sensitive to individual atoms have been implemented and, on the other hand alternative methods to image single particles have been developed (see [160] for a review). Fluorescence imaging of individual atoms was obtained in dipole traps [193, 2] and then extended to optical lattices – thanks to quantum gas microscopes [11, 199] and in arrays of Rydberg atoms [155] – and to image atoms after an expansion [31]. The non-optical methods yielding single-atom sensitivity range from using cavities [161], micro-channel plates [192] or electron guns [85]. While most of these approaches permit to measure position-space and/or spin resolved correlations between individual particles, recent experiments have been capable of probing momentum-space correlations as well [73, 98, 42, 17]. Investigating the momentum degree of freedom lies at the center of the project I developed at the Institut d'Optique.

Momentum-resolved measurements of correlations. Two celebrated momentum-resolved probes of solid-state systems were mentioned above, the ARPES and neutron scattering. These techniques had an important impact in condensed matter but they also had a strong influence on the quantum gas community. Some words about these two aspects need to be exposed here. On the one hand, ARPES and neutron scattering have shown to yield important information of many-body systems: their low-energy excitations, their quantum coherence or the presence of pairing mechanisms. In this context, the description of many-body physics often relies on the low-energy excitation spectrum. The reason is somehow two-fold. Firstly, the low-energy excitation spectrum captures physical features of the ground-state and it allows one to describe the response of the system to small perturbations. Secondly, a direct comparison of the outcomes from experiments with theory is possible because there exist both the above-mentioned experimental techniques and theoretical approaches allowing one to calculate the low-energy properties. On the other hand, the success associated to these momentum-resolved probes have been a strong motivation behind many works with quantum gases over the past two decades. This includes the activity I participated to during my post-doctoral stay in Italy. Landmark experiments have been reported with analogs of both the techniques for cold atoms, from the Bragg spectroscopy to measure the Bogoliubov spectrum of weakly-interacting bosons [162], to the photoemission spectroscopy to investigate strongly interacting fermions [207].

As stated above, what is more with AOM platforms is the possibility to measure the momentum and correlations between individual quantum particles, *i.e.* to go beyond probing the global response of the system. This implies that a more precise characterisation of many-body phenomena is at hand. For instance, one could in principle directly observe the pairing of two atoms in the momentum-space from measuring the two-body correlation functions at opposite momenta. This could reveal the Cooper pairing of fermions as well as the pairing mechanism associated to quantum depleted bosons. It could also allow

one to probe many-particle entanglement through the measure of many-body correlation functions. These promising perspectives have motivated the activity developed with metastable Helium gases at the Institut d'Optique. And this manuscript describes the probe I have implemented at Institut d'Optique, which can provide access to the momentum-space correlations between individual atoms, *i.e.* an innovative tool of observation with which I hope we will be able to obtain original information about the many-body physics we aim at understanding.

1.2 Brief summary of the post-doctoral activity

During my post-doctoral stay in the group of C. Fort and M. Inguscio at LENS, I devoted the larger part of my work to the investigation of one-dimensional Bose gases. In one dimension, the particles are confined to move along one direction only and the number of degrees of freedom is therefore reduced with respect to higher-dimensional systems. As a consequence, the interplay between quantum fluctuations and interaction is enhanced [86, 43]. In the context of quantum simulation, one-dimensional systems are of special interest as there exist exact theoretical approaches that allow one to use these systems as testbeds of many-body theories. All thermodynamics quantities can be calculated numerically for instance [86, 43]. In addition, the physics in one dimension can be very surprising and thus fascinating. An emblematic example of the "weirdness" of 1D physics is provided by how the strength of the interaction changes with the particle density: the lower the density, the more correlated the system is! Our intuition that the importance of interaction (and the associated correlations) decreases with the particle density is drawn from higher dimensions. While the kinetic energy varies similarly in any dimensions, the linear scaling of the interaction energy in 1D with the inverse particle distance yields the fascinating assertion that the strongly interacting regime is approached by reducing the particle density.

Following the seminal works of the Weiss and Bloch groups [122, 164] we have realized an array of 1D Bose gases of Rubidium-87 atoms by loading a 3D Bose-Einstein condensate into a 2D optical lattice. This approach has one practical and important benefit with respect to the the realization of a single 1D gases: it allows to reach the regime of strong correlations and low temperatures [21]. This stems from the large transverse trapping frequencies and the fact that evaporation to BEC is not performed in 1D. On the other hand, we have to deal with an array of 1D systems. Since the atom number in the various 1D tubes varies from one tube to another, the measured quantities are mostly averaged over 1D gases with different properties and this complicates the comparison with theoretical predictions with respect to investigating a single 1D system.

Light scattering techniques were used to probe the properties of 1D interacting bosons. It relies on a two-photon transition which allows one to deposit a finite energy and a finite momentum into the gas [52]. When the two-photon transition leaves the excited atoms into a state identical to that before the excitation, this technique is very similar to that of neutron scattering (see Chap. 2). During the initial stage of my PhD thesis, I had used the Bragg spectroscopy to investigate phase fluctuations in elongated BECs and upon arriving in Florence I built a similar setup. With this experimental tool, we have investigated the dynamical structure factor of 1D Bose gases across the superfluid-to-Mott transition [54] and the low-energy spectrum of 1D Bose gases, finding an experimental signature of the presence of the two Lieb modes (*i.e.* beyond Luttinger liquid theory) [70, 71].

In addition, we have demonstrated that, when the 1D gases are loaded into a periodic potential, one can probe the one-particle spectral function, similarly to the quantity which is obtained from Angle-Resolved Photo-Emission Spectroscopy in solids [63]. The idea here is to use the lattice structure to perform the two-photon transition from the lowest-energy band of the lattice towards an excited band, thus effectively removing one particle from the many-body ground-state lying in the lowest-energy band. We have performed experiments of this kind in the Mott phase, in an attempt to measure the coherence of the quasi-particles of the Mott state [53, 72].

1.3 Brief summary of the research activity at Laboratoire Charles Fabry

I joined the laboratoire Charles Fabry (LCF) at the Institut d'Optique in late 2010 as Maitre de Conférence. In agreement with my colleagues from the Quantum gases group at LCF, I started a new experimental activity aiming at using metastable Helium gases to probe many-body phenomena via the measure of momentum-space correlations. The year 2011 was mainly devoted to designing and raising funding for the building of a novel apparatus. We started mounting the first parts of the apparatus in late 2011 with the newly arrived PhD student L. Hoendervanger. It took us three years to complete the building and obtain our first Bose-Einstein condensate (BEC) of metastable Helium-4 on February 17th, 2015. The journey to BEC was the success of a team work that included three PhD students (L. Hoendervanger, Y. Fang, Q. Bouton), one post-doc fellow (R. Chang) and one engineer (F. Nogrette), along with several graduate students. During this period, we have benefited from the advices of all the experienced colleagues of the Quantum Gas group at LCF and in particular from the expert of metastable Helium, A. Aspect, D. Boiron and C. Westbrook.

The experimental sequence we have implemented to reach Bose-Einstein condensation was original for metastable Helium gases. At the time I designed our apparatus, all the (few) metastable Helium experiments (Boiron/Westbrook (France); Vassen (Netherlands); Truscott (Australia); Zeilinger (Switzerland)) were starting with a magneto-optical trap and red molasses to load a Ioffe-type magnetic trap where radio-frequency towards quantum degeneracy was performed [225]. Two limitations were associated to this type of experimental sequences: the typical duration for BEC was rather long ($\sim 25 - 30$ s) as compared to other atomic species and the final magnetic trap did not allow to look for magnetic Feshbach resonances. I decided to attempt a technique initially developed with Rubidium atoms [133]: using a magnetic quadrupole trap to efficiently load an optical dipole trap. In the case of metastable Helium though, the presence of Penning collisions in laser-cooled spin mixtures prevents from working with high atomic densities [225]. An efficient evaporation in the magnetic quadrupole trap requires a sufficiently high atomic density for the elastic collision rate to be high enough. The density in the quadrupole trap depends on both the density and the temperature of the gas before the loading. This implies that we need to compensate the low densities associated with metastable Helium molasses with reaching the lowest possible temperatures. We have thus investigated in details the equilibrium temperature of the red-molasses phase which led us to the first observation of 3D laser-cooled molasses at the Doppler limit ($T \sim 40\mu$K) [45]. The Doppler limit could not have been previously observed in 3D optical molasses with alkali atoms because sub-Doppler mechanisms play a central role and set the equilibrium temperatures []. To further lower the temperature, we have implemented the first gray molasses for metastable

Helium-4 (inspired by the early works on Velocity Selective Coherent Population Transfer [8]) and obtained temperatures below the Doppler limit ($T \sim 15\mu$K) [28]. These unprecedented results put us in the position of loading a quadrupole trap with adequate collisional rates (for radio-frequency evaporation) and in turn to obtain a large number of atoms in a crossed optical dipole trap from which BECs are produced. To avoid the presence of Penning collisions in the optical trap, a magnetic bias is used and we produce spin-polarized BECs in the spin state $m_J = +1$. The approach we have developed yields the production of pure BECs every 6 seconds in an optical trap, thus leaving the possibility to play with magnetic bias fields to investigate Feshbach resonances in future.

During the building of the apparatus, we dedicated a substantial part of lab work to the He* detector [99, 154]. The He* detector which consists in a stack of micro-channel plates mounted on top of a delay-line anode allows one to reveal the three-dimensional positions (and correlations) of individual atoms after a time-of-flight, as pioneered by my colleagues at LCF [192]. A brief description of the He* detector is provided in Chap. 3. Building upon the knowledge acquired by D. Boiron and C. Westbrook on the He* detector, we collaborated to upgrade the detector that the two metastable Helium apparatus at LCF would use. On the one hand, we have performed a series of experiments to testing various configurations of the detector, which actually did not result in any convincing improvement of the detection efficiency and of the resolution [99]. On the other hand, we have collaborated with D. Heurteau and R. Sellem from the LUMAT fédération to develop a novel time-to-digital converter based on a FPGA architecture. This work successfully ended in an improved detection rate of the particles and a better spatial resolution [154]. During the past years, we have also tested new types of micro-channel plates and fast electronics, reaching even better spatial resolutions.

With the experiment built and the detector installed, the first set of experiments we performed was triggered by the observation of algebraically decaying tails in the time-of-flight distributions of harmonically-trapped BECs. Several features suggested to relate the presence of these tails to the quantum depletion of the trapped BEC [44]. This conclusion raised many discussions with colleagues, several of them putting forward the fact that the presence of interaction during the initial expansion should wash out the signature of the in-trap quantum depletion in the measured distributions [175]. We have recently revisited this experiment and we found that the tails are associated with the presence of spin impurities. In the transfer from the magnetic quadrupole, a small fraction (less than 1% of the total atom number) of the atoms is transferred in the optical trap in the spin state $m_J = 0$. We have identified that the interplay of the impurities with the spin-polarized BEC (in $m_J = +1$) is at the origin of the observed momentum tails, and that the later are not a signature of the quantum depletion. An understanding of the above mentioned interplay is the object of current investigation. The attention received by this work has triggered two collaborations: an experimental collaboration with the group of Z. Hadzibabic (Cambridge, UK) where studies were performed to identify the quantum depletion in BECs of Potassium with variable interaction strength [135]; a theoretical work with L. Sanchez-Palencia (Palaiseau), A. Minguzzi (Grenoble) and P. Vignolo (Nice) to investigate the contact in interacting 1D Bose gases [232].

More recently, the second phase of my research project was initiated with the investigation of strongly interacting lattice bosons. This scientific direction was implemented on the apparatus by a fully renewed set of young researchers that includes three PhD students (H. Cayla, C. Carcy, A. Tenart) and one post-doc fellow (M. Mancini). From the comparison of the measured distributions with ab-initio Quantum Monte-Carlo (QMC)

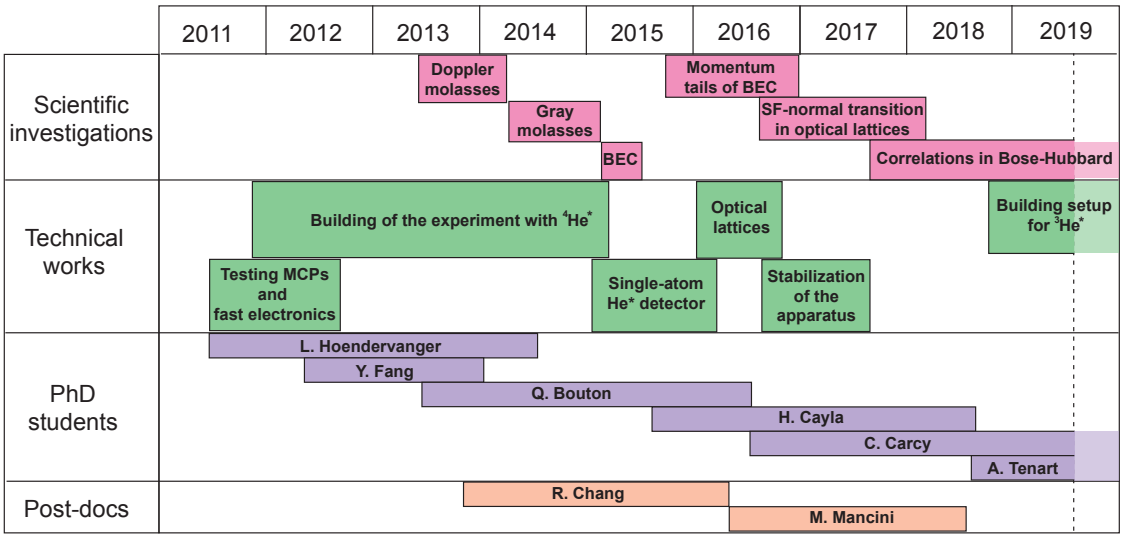

Figure 1.1: Overview of the research activity at Laboratoire Charles Fabry.

calculations performed by G. Carleo, we have validated our method to access the three-dimensional atom distribution in momentum-space [42]. We have also investigated the superfluid-to-normal transition and shown our capability to calibrate the temperature of the lattice gas with a good approximation. More recently, we have performed further studies of the superfluid-to-Mott transition with metastable Helium atoms [36]. Deep in the Mott regime we have observed perfectly contrasted many-body correlations associated to the bosonic statistics. On approaching the Mott transition, we have measured the modification of the spectral weight of the quasi-particles. QMC calculations realized by T. Roscilde has allowed us to quantify the temperature of the gas across the superfluid-to-Mott transition, pinpointing the position of the experiment in the finite-temperature phase diagram of the Bose-Hubbard Hamiltonian. On-going investigations now concentrate on the critical regime of the Mott transition, with the aim of identifying the role of thermal fluctuations on the measured quantities and of finding signatures of the quantum nature of the transition in the n-body momentum-space correlations.

Future research directions. In the years to come, the scientific directions will be driven by the aim of identifying, and possibly of quantifying, the presence of many-body correlations deriving from the interplay of quantum fluctuations and interaction. An alternative wording of this central objective is the investigation of multi-particle entanglement in many-body quantum systems. On the one hand, this encompasses the detection of pairing mechanisms in the momentum space that are expected to be found in many-body ground-states. Pairing of two atoms – *e.g.* a Bogoliubov pair for bosons and a BCS pair for fermions – can be viewed as first-order corrections to mean-field theories, *i.e.* the most simple type of beyond mean-field correlations. In these pairing mechanisms, the momentum conservation associated with the elastic two-body interaction process implies that the atoms forming the pair have opposite momenta. The presence of such pairing could thus be directly revealed by measuring 2-body correlations at opposite momenta, as provided by the He* detector.

On the other hand, quantum fluctuations and interaction are expected to yield many-body correlations in the critical regime of quantum phase transitions – beyond the mere example of 2-body correlations associated to pairing mechanisms. The current investigation of the critical regime of the 3D Bose-Hubbard hamiltonian goes along this line with

the aim of unveiling the presence of many-body correlations in the crossover towards the Mott state. In the future, similar investigations could also be extended to other interesting phase diagrams, including the Bose-Hubbard hamiltonian in reduced dimensions, the Hubbard hamiltonian with polarized fermions, and dissipative (Bose or Fermi) Hubbard systems. In this context, our project would strongly benefit from close collaborations with theory colleagues.

Performing these experiments necessitates to upgrade the existing apparatus. Firstly, the investigations of the BCS-type pairing and of lattice fermions require to add the fermionic species ^{3}Helium* on the apparatus. Note that the outstanding capacities of the He* detector illustrated in this manuscript with bosons are also valid for the detection of individual fermions ^{3}Helium*. Secondly, understanding how to use on-site Penning losses to induce a controlled dissipation in Hubbard ground-states is another prerequisite for the above-mentioned scientific objectives. It will thus be the object of experimental studies in the years to come.

Chapter 2

Light scattering study of interacting one-dimensional Bose gases

In this section, I present some pieces of work I participated to during my post-doctoral stay (2007-2010) in the group of M. Inguscio and C. Fort in Florence (Italy). This activity was centered on the use of inelastic scattering of light to measure spectral functions in one-dimensional (1D) Bose gases. I first briefly discuss the probe we have implemented and the physical quantities it provides access to (2.1). Then I describe some of the results we obtain when probing strongly correlated 1D bosons of Rubidium 87 atoms, in the absence (2.2) and in the presence of a periodic potential (2.3). My post-doctoral stay has coincided with the PhD of N. Fabbri and all the works presented here have been obtained by the amazing "BEC1" team formed by Nicole (Fabbri), Leo (Fallani), Chiara (Fort), Massimo (Inguscio) and myself.

2.1 Bragg spectroscopy: measuring spectral functions

The theoretical description of the dynamics of strongly correlated systems in terms of low-energy excitations (*e.g.* using Green functions) is widespread in condensed matter physics [140]. As explained in the introduction, the knowledge of these low-excitations modes provide information on the many-ground state and on its response to excitations (in the linear regime of response). Measuring these excitations in the experiment is thus central. From a practical point of view, two measurable quantities related to the low-energy spectrum are often put forward: the one-particle spectral function $\mathcal{A}(\mathbf{k},\omega)$ and the dynamical structure factor $\mathcal{S}(\mathbf{k},\omega)$, where $\mathbf{k}$ and $\hbar\omega$ correspond to the momentum and the energy transferred to the system. The one-particle spectral function $\mathcal{A}(\mathbf{k},\omega)$ quantifies the overlap between the many-body wave-function with one added particle (or hole) and the true excited one-particle (or one-hole) state. It can be obtained from techniques like the Angle-Resolved Photo-Emission Spectroscopy (ARPES). The dynamical structure factor $\mathcal{S}(\mathbf{k},\omega)$ describes the spectral weight of an excitation in the many-body wave-function whose momentum is $\mathbf{k}$ and energy $\hbar\omega$. It can be measured through inelastic neutron scattering for instance. We shall briefly define and describe those two quantities, before explaining how we have implemented a method to obtain them both in our cold-atom experiment.

The one-particle spectral function $\mathcal{A}(\mathbf{k},\omega)$. Consider a many-body quantum system of bosons that can be described by a set of many-body wave-functions $|\varphi_j\rangle$. The one-particule spectral function is defined as $\mathcal{A}(\mathbf{k},\omega) = \mathcal{A}^+(\mathbf{k},\omega) + \mathcal{A}^-(\mathbf{k},\omega)$ with

$$\mathcal{A}^+(\mathbf{k},\omega) = \frac{1}{\mathcal{Z}} \sum_{j,j'} (\mathrm{e}^{-\beta E_{j'}} - \mathrm{e}^{-\beta E_j}) |\langle \varphi_{j'} | a(\mathbf{k})^\dagger | \varphi_j \rangle|^2 \, \delta(E_{j'} - E_j - \hbar\omega) \tag{2.1}$$

and

$$\mathcal{A}^-(\mathbf{k},\omega) = \frac{1}{\mathcal{Z}} \sum_{j,j'} (\mathrm{e}^{-\beta E_{j'}} - \mathrm{e}^{-\beta E_j}) |\langle \varphi_{j'} | a(\mathbf{k}) | \varphi_j \rangle|^2 \, \delta(E_{j'} - E_j - \hbar\omega), \tag{2.2}$$

where $a(\mathbf{k}$ is the annihilation operator for a particle with momentum $\mathbf{k}$, $\beta = 1/k_B T$ is the inverse temperature and E_j is the energy of the wave-function $|\varphi_j\rangle$. The functions $\mathcal{A}^+(\mathbf{k},\omega)$ and $\mathcal{A}^-(\mathbf{k},\omega)$ describe respectively the one-particle addition and the one-particle removal spectra of the many-body wave-function. Note that the one-particle spectral function is directly related to the retarded Green function $G(\mathbf{k},\omega)$ by $\mathcal{A}(\mathbf{k},\omega) = -1/\pi \, \mathrm{Im}[G(\mathbf{k},\omega)]$.

As mentioned previously, ARPES is a mean to measure $\mathcal{A}(\mathbf{k},\omega)$ in solid-state materials [63]. An incident photon is shone onto the material and excites one electron in the bulk. The excited electron is then detected after it has escaped the solid piece, with an angular resolution that gives rise to the name of the technique. In the most simple picture, the excited electron is considered to propagate freely outside the bulk. Actual ARPES experiments are analysed with less stringent but more complicated approximations.

The dynamical structure factor $\mathcal{S}(\mathbf{k},\omega)$. The dynamical structure factor is defined as

$$\mathcal{S}(\mathbf{k},\omega) = \frac{1}{\mathcal{Z}} \sum_{j,j'} (\mathrm{e}^{-\beta E_{j'}} - \mathrm{e}^{-\beta E_j}) |\langle \varphi_{j'} | a(\mathbf{k}-\mathbf{q})^\dagger a(\mathbf{q}) | \varphi_j \rangle|^2 \, \delta(E_{j'} - E_j - \hbar\omega), \tag{2.3}$$

with similar notations as before. $\mathcal{S}(\mathbf{k},\omega)$ corresponds to creating an excitation of momentum $\mathbf{k}$ and energy $\hbar\omega$ in the many-body system, in contrast to $\mathcal{A}(\mathbf{k},\omega)$ which is associated with extracting one particle from the many-body state. The dynamical structure factor can also be written in terms of density-density correlations as pointed out by Van Hove. It is proportional to terms of the type $\langle \rho(\mathbf{k},0)^\dagger \rho(\mathbf{q}-\mathbf{k},\omega) \rangle$ as it is the space and time Fourier transform of the position-space density correlation $\langle \rho^\dagger(\mathbf{x},t)\rho(\mathbf{x}',0) \rangle$. In condensed-matter physics, the dynamical structure factor $\mathcal{S}(\mathbf{k},\omega)$ can be extracted from inelastic neutron scattering experiments. The solid-state sample is shone with neutrons that scatter off by depositing energy and momentum into the system.

Two-photon Bragg spectroscopy. In the cold atom community, Bragg spectroscopy refers to a coherent two-photon transition induced by two laser beams (see Fig. 2.2) and which leaves the internal state of the atom unchanged while transferring a momentum $\hbar\mathbf{k}$ and an energy $\hbar\omega$ to the atom [206, 162]. The absorption-stimulated emission process can also be viewed as the diffraction of the atom onto a grating of light formed by the interference of the two laser beams and moving at velocity $\hbar\mathbf{k}/m$. This second picture shares an analogy with the Bragg diffraction of a coherent beam of light or electrons on a cristalline structure. It is at the origin of the name for the technique.

Upon my arrival in Florence, we started the project of implementing and using Bragg spectroscopy as a probe of many-body lattice gases. We were not the first ones aiming at

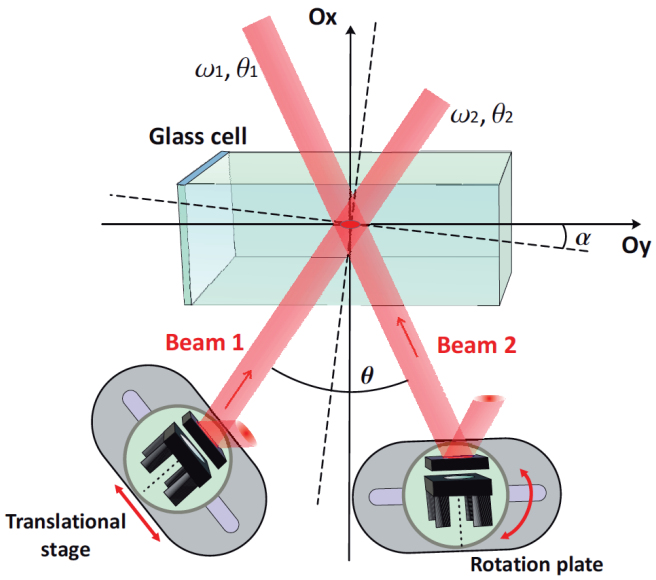

Figure 2.1: Experimental implementation of the Bragg spectroscopy. *[Adapted from the PhD thesis of N. Fabbri]* Two laser beams - referred to as Bragg beams - are shone onto the atoms through the glass cell. Mechanical mounts (translation and rotation stages) allow us to modify the angle between the two beams and thus to change the momentum $\hbar\mathbf{k}$ transferred to the atoms. In addition (not shown here) the two beams are derived from the same laser source to ensure phase coherence but detuned from one another with acousto-optic modulators. This permits to tune to the energy $\hbar\omega$ transferred to the atoms.

measuring the low-energy excitation spectra in lattice systems since it had been probed with amplitude modulation of the lattice in the group of T. Esslinger a few years earlier [209]. But our motivation to realize the spectroscopy with two laser beams as indicated in Fig. 2.1 was two fold. On the one hand, there were some doubts that the experiments with amplitude modulation were conducted in the linear response regime. On the other hand, it was clear that some interesting features of the spectrum could be revealed only with a net momentum transfer $\mathbf{k} \neq 0$ to the atoms, while no momentum is transferred to the atoms through the method of amplitude modulation. Several theory works were indeed indicating the scientific interest in implementing a spectroscopy at non-zero momentum transfer [158, 179, 174, 105].

In the presence of a lattice, an additional degree of freedom for the experimental probing of low-energy excitations is provided by the band structure. I would like to briefly illustrate it here, a more detailed discussion being given in [52]. When the lattice amplitude is high enough, the lowest energy bands are well separated in energy and the wave-functions of individual atoms in different bands have a very small overlap. Under this hypothesis, one can neglect inter-band interactions. Here, we will restrict ourselves to the three lowest energy bands and use the notation $|n_0,n_1,n_2\rangle$ to describe the many-body state with n_i atoms in the ith band. In the absence of inter-band interactions, $|n_0,n_1,n_2\rangle \simeq |n_0\rangle \otimes |n_1\rangle \otimes |n_2\rangle$ where $|n_0\rangle = |\varphi_i\rangle$ is the many-body wave-function we are interested in and containing initially all the N atoms. Let us write the creation (annihilation) operators of a particle with momentum $\hbar\mathbf{k}$ in the band i as $c^\dagger_{i,\mathbf{k}}$ ($c_{i,\mathbf{k}}$).

We first consider a two-photon Bragg transition within the lowest energy band (left-column of Fig. 2.2). The amplitude of the scattering induced by the Bragg beams contains

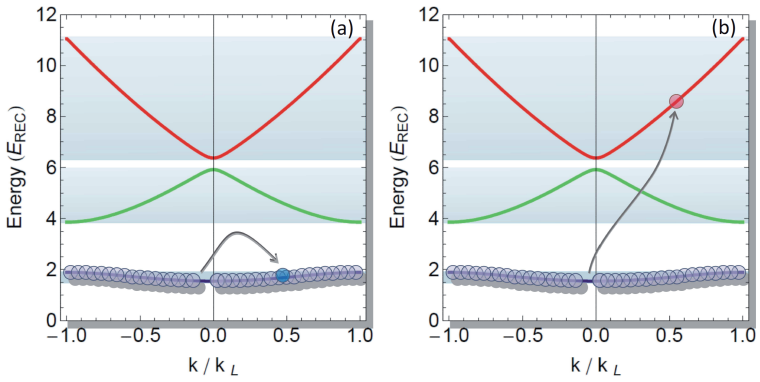

Figure 2.2: Bragg excitations in the presence of lattice band structure. *[Adapted from the PhD thesis of N. Fabbri]* When the Bragg spectroscopy is performed within the lowest energy band (left) one measures the dynamical structure factor $\mathcal{S}(\mathbf{k},\omega)$. When the Bragg spectroscopy is performed from the lowest energy band towards a highly excited band (right) one measures a quantity related to the one-particle spectral function $\mathcal{A}(\mathbf{k},\omega)$.

terms like

$$\begin{aligned} |\langle n_0',n_1',n_2'|c^\dagger_{0,\mathbf{k}-\mathbf{q}}c_{0,\mathbf{q}}|N,0,0\rangle|^2 &\simeq \\ |\langle N,0,0|c^\dagger_{0,\mathbf{k}-\mathbf{q}}c_{0,\mathbf{q}}|N,0,0\rangle|^2 &\simeq \\ |\langle\varphi_f|c^\dagger_{0,\mathbf{k}-\mathbf{q}}c_{0,\mathbf{q}}|\varphi_i\rangle|^2 &= |\langle\varphi_f|a^\dagger(\mathbf{k}-\mathbf{q})a(\mathbf{q})|\varphi_i\rangle|^2 \end{aligned} \tag{2.4}$$

from which one can identify the type of term that enters the definition of the dynamical structure factor $\mathcal{S}(\mathbf{k},\omega)$. When doing appropriate summing, one finds the dynamical structure factor. This is in line with the interpretation of $\mathcal{S}(\mathbf{k},\omega)$ since the Bragg spectroscopy is performed within the lowest energy band and it deposits energy and momentum in the many-body ground-state.

We now consider a two-photon Bragg transition towards the second-excited energy band (right-column of Fig. 2.2). The amplitude of the scattering contains terms like

$$\begin{aligned} |\langle n_0',n_1',n_2'|c^\dagger_{2,\mathbf{k}-\mathbf{q}}c_{0,\mathbf{q}}|N,0,0\rangle|^2 &\simeq \\ |\langle N-1,0,1|c^\dagger_{2,\mathbf{k}-\mathbf{q}}c_{0,\mathbf{q}}|N,0,0\rangle|^2 &\simeq \\ |\langle\varphi_f|c_{0,\mathbf{k}}|\varphi_i\rangle|^2 &= |\langle\varphi_f|a(\mathbf{k})|\varphi_i\rangle|^2 \end{aligned} \tag{2.5}$$

that can be identified with the terms appearing in the definition of the one-particle spectral function $\mathcal{A}(\mathbf{k},\omega)$. A central feature here is to use the band structure of the lattice to remove one atom from the ground-state wave-function and excite it well above the later. As mentioned previously, an atom promoted into a high-energy band hardly interacts with the atoms belonging to the lowest energy band when the lattice potential is deep. To a good approximation the excited atom can thus be considered as a free atom. The two-photon Bragg transitions we used to remove one atom from the Mott insulator is illustrated in Fig. 2.8. The band structure makes it possible to probe both $\mathcal{S}(\mathbf{k}_0,\omega)$ and $\mathcal{A}(\mathbf{k}_0,\omega)$ with the two-beam Bragg setup by adequately playing with the intra- and inter-band transitions.

Before probing strongly-interacting systems, the first experiment we conducted aimed at demonstrating that we could use two-photon Bragg spectroscopy to probe the spectrum

of a lattice Bose gas, in particular to address the different bands. The most simple lattice gas is a 3D Bose-Einstein Condensate loaded into a one-dimensional optical lattice. The band structure can be exactly calculated and the resonances of the dynamical structure factor $\mathcal{S}(\mathbf{k}_0,\omega)$ when the gas is probed at a fixed $\mathbf{k}_0$ are known. Some of our measurements are shone in Fig. 2.3. They are in good agreement with the calculated Bogoliubov spectrum in the lattice and they demonstrated that we could indeed address the different bands of the lattice by tuning the energy transferred to the atoms.

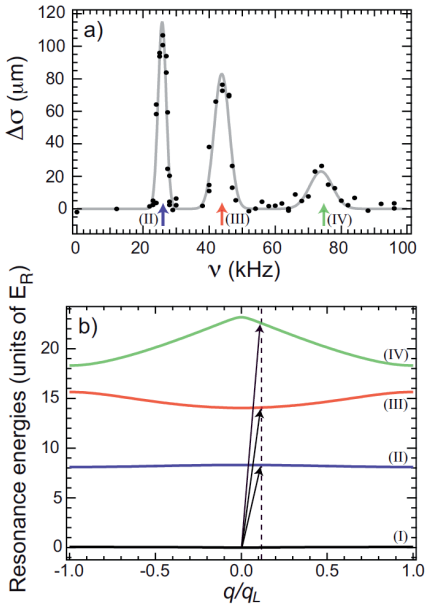

Figure 2.3: Bragg spectrum of a 3D BEC loaded into a 1D lattice. **(a)** Spectrum of excitations of a 3D BEC loaded into a 1D optical lattice as measured in the experiment. The different resonances can be unambiguously associated with the different bands of the 1D lattice. The Bragg transitions associated to each lattice band are depicted in **(b)**.

2.2 Signatures of beyond Luttinger liquid theory in 1D Bose gases

In order to simulate a one-dimensional system in an experiment, one must confined the particles such that all degrees of freedom associated with the directions transverse to the 1D axis are frozen. Take a harmonically trapped gas with frequencies $\omega_x/2\pi$ and $\omega_\perp/2\pi$ respectively along the 1D and the transverse axis. The energy gap $\hbar\omega_\perp$ between the transverse ground-state and the first transverse excited state defines the energy scale associated with 1D physics along the 1D axis: if all the energies of the system (in particular the thermal energy k_BT and the chemical potential μ) are much smaller than $\hbar\omega_\perp$, the particles are in the transverse ground-state within a good approximation.

We have realized one-dimensional Bose gases by loading a 3D ^{87}Rb Bose-Einstein condensate into two orthogonal optical lattices. To ensure the gas to be in the 1D regime we use a 2D lattice of amplitude $V_\perp = s_\perp E_R$ with $s_\perp = 35$ and $E_R = h^2/2m\lambda_L^2$ (λ_L is the lattice wavelength). For such an amplitude of the transverse lattice, we have shown that

$k_B T \ll \hbar\omega_\perp$ and $\mu \ll \hbar\omega_\perp$. Considering contact interactions and a homogeneous trap, the gas is described by the Lieb-Liniger Hamiltonian [132, 156]:

$$H = \frac{\hbar^2}{2m}\int dx\, \frac{d\psi^\dagger}{dx}\frac{d\psi}{dx} + \frac{g_{1D}}{2}\int dx\, \psi^\dagger\psi^\dagger\psi\psi, \tag{2.6}$$

where the 1D interaction strength is $g_{1D} = 2\hbar\omega_\perp a_s$, with a_s the 3D scattering length [156].

Regimes of 1D Bose gases. The regime of an homogeneous 1D gas with density ρ is characterized by two dimensionless parameters, γ and τ [120]. Firstly, γ is the ratio of the mean-field interaction to the kinetic energy to bring two particles at distance ρ^{-1},

$$\gamma = \frac{m g_{1D}}{\hbar^2 \rho}. \tag{2.7}$$

The ratio γ takes two asymptotic values, $\gamma \to 0$ and $\gamma \to +\infty$, which correspond to radically different ground-states at low temperature. For $\gamma \ll 1$, the interaction energy is much smaller than that to position particles at distance ρ^{-1}: the particles are delocalized and weakly interact via a mean-field potential. The corresponding ground-state is a weakly-interacting Bose-Einstein condensate. For $\gamma \gg 1$, the low energy cost associated to the kinetic energy implies that particles are typically separated by a distance ρ^{-1} and hardly overlap with each other. The corresponding ground-state is the Tonks-Girardeau (TG) gas where bosons are "fermionized", *i.e.* that the impenetrability of adjacent bosons due to the strong correlations mimics an effective Pauli principle. It is interesting to note that for a fixed interaction strength g_{1D} the gas would go from a weakly-interacting BEC to a strongly-correlated TG gas upon *decreasing* the density ρ. This dependency of the regime of correlations with the density is counter-intuitive as in a 3D gas it goes the opposite way. It illustrates the fascinating properties that a 1D system can have!

Secondly, τ is the ratio of the temperature to the temperature of quantum degeneracy ($T_d = (\hbar\rho)^2/2m$),

$$\tau = \frac{2mk_B T}{(\hbar\rho)^2}, \tag{2.8}$$

or, better, the ratio t referred to as the reduced temperature and which is density-independent,

$$t = \frac{2\hbar^2 k_B T}{m g_{1D}^2}. \tag{2.9}$$

The Lieb-Liniger model. The celebrated Lieb-Liniger Hamiltonian describes 1D bosons with contact interaction[131, 156]. While it is easy to write, it turns out difficult to calculate its physical properties [43]. The Lieb-Liniger Hamiltonian supports two modes of particle-hole excitation, the Lieb-I and Lieb-II modes. These modes emerge naturally when describing a 1D uniform system as a Fermi sea: while in 2D and 3D it is possible to excite arbitrary low-energy excitations for a continuum of momentum k (see Fig. 2.4a), in 1D the surface of the Fermi sea is reduced to two points where excitations can be created (see Fig. 2.4b). It yields one excitation with vanishing k (local in the Fermi surface) called the mode Lieb-I, and one excitation with momentum $k \simeq 2k_F$ with $k_F = \pi\rho$ (connecting the two points of the Fermi surface) called the mode Lieb-II. The Lieb-I mode corresponds to a quasi-particle excitation that connects to the Bogoliubov excitation present at small γ while the Lieb-II mode is of quasi-hole nature and disappears when $\gamma \ll 1$ (see Fig. 2.5).

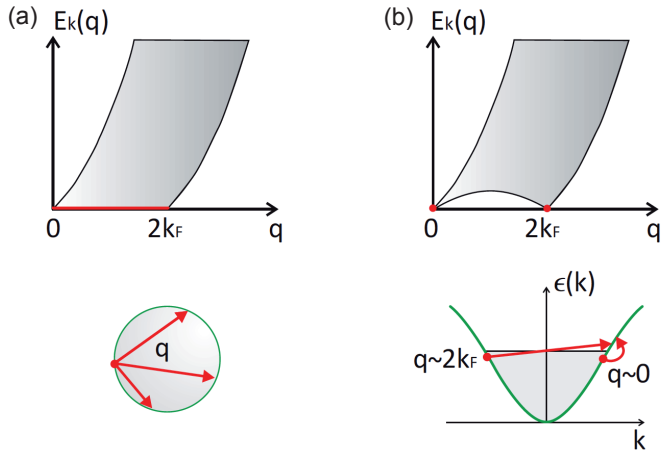

Figure 2.4: Cartoon on low-energy excitations in a fermionic gas. **(a)** 2D and 3D case **(b)** 1D case. k_F is the Fermi wave-vector.

The Luttinger liquid theory. The Luttinger liquid theory has served as a useful paradigm for the description of one-dimensional quantum fluids in the limit of low energies [86]. This theory is based on a linearization of the dispersion relation of the particles in the fluid, with the low-energy excitations being collective ones. The scientific interest shown in the Luttinger description of 1D quantum fluids stems from the simplification of the theoretical treatment but it has also demonstrated accurate in describing numerous experiments, from electronic 1D chains and 1D carbon nanotubes to 1D Bose and Fermi quantum gases [43]. Experimental realizations where signatures of beyond Luttinger liquid physics have been reported are indeed scarse and we are aware of a single work with 1D electrons [12]. On the opposite, theoretical works describing the physics beyond the Luttinger liquid paradigm are numerous (see [43, 107] for a review).

An emblematic example of the breakdown of the Luttinger liquid approach is the modification of the one-particle spectral function $\mathcal{A}(\mathbf{k},\omega)$ [40] and of the dynamical structure factor $\mathcal{S}(\mathbf{k},\omega)$ [39, 163] of 1D bosons as interactions (γ) are increased. In mean-field regime of interaction ($\gamma \ll 1$) the spectral weight is well described by the Luttinger liquid theory while at large interactions ($\gamma \gg 1$) the presence of the Lieb-II mode can not be neglected and the spectral weight spreads between the two Lieb modes (see Fig. 2.5). Observing the contribution of the Lieb-II mode in the spectral functions of 1D bosons is a strong motivation to measure the dynamical structure factor.

Bragg spectroscopy of 1D Bose gases. In the experiment we have probed the dynamical structure factor $\mathcal{S}(\mathbf{k},\omega)$ of an ensemble of 1D Bose gases at various momentum transfers k [70]. When the gases made from the 2D lattice are independent from each other (*i.e.* at sufficiently high amplitude of the 2D lattice), we have observed a Lorentzian lineshape for $\mathcal{S}(k,\omega)$ as a function of ω. In 2011 we have interpreted these data along the lines of previous works probing phase fluctuations in elongated 3D BEC using similar Bragg spectroscopy [180]. In the weakly-interacting regime, described by the Bogoliubov spectrum (see Fig. 2.5a), the effect of finite temperature is to populate low-excitation modes that are phonons. The typical correlation length of the in-trap phase is given by the phonon mode whose energy equals the temperature. In addition, when the Bragg beams transfer a large momentum (with respect to the momentum associated to the energy scale given by the chemical potential), the Bragg spectrum can be mapped onto the in-trap momentum

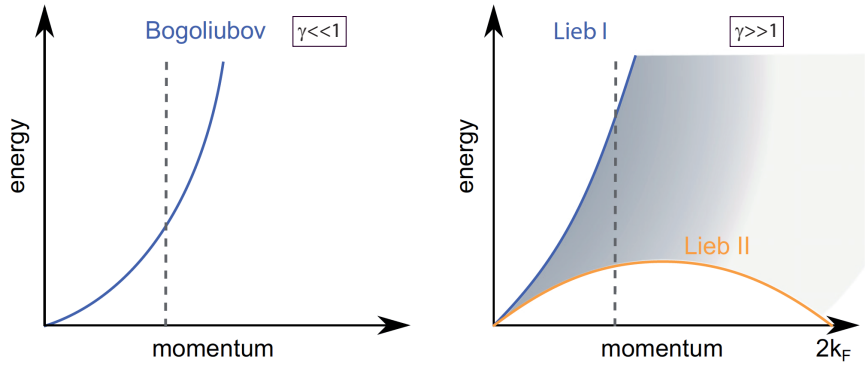

Figure 2.5: Low-energy spectrum of 1D Bose gases. **(a)** Bogoliubov spectrum of a weakly-interacting Bose gas. All the spectral weight is centered on the relation dispersion of the Luttinger model. The notion of quasi-particle is valid in this regime. **(b)** Spectrum of a strongly-interacting 1D Bose gas with a non-zero spectral weight covering a large area limited in between the two Lieb modes. Excitations are only collective ones in this regime.

distribution [180, 162, 70]. We first interpreted our experimental data as a measurement of the momentum distribution, the width of which reflects the correlation length of the phase[1]. It turned out that we were wrong and that our observation had to be linked to the presence of the Lieb-II mode, as introduced above, a much more appealing conclusion for our work!

In contrast to the 3D elongated BEC described by the Bogoliubov spectrum [180], the presence of strong correlations in 1D prevents the use of the Bogoliubov approximation in the regime of our experiment. More precisely, the contribution of the Lieb-II mode to the dynamical structure factor can not be neglected when $\gamma \simeq 1$, as in the experiment. The correct analysis of the data came a few years later with the development of theoretical and numerical techniques allowing one to fully include both finite interaction and temperature effects in the calculation of $\mathcal{S}$ [163]. Our theory colleagues M. Panfil and J.-S. Caux, who have been developing this numerical approach, have thus given us the key to a correct understanding of our measurements. In particular, the statement that the contribution of the Lieb-II mode has to be taken into account stems from the comparison of these most advanced numerics with the experimental data [71]. Thus, the interpretation of the measured $\mathcal{S}(\mathbf{k},\omega)$ became radically different: in the strongly interacting picture the spectral broadening derives from zero-temperature correlations induced by interactions (the finite temperature effect was shown to be small [71]). This observation related to the continuous spectrum of excitations spread between the two Lieb modes is a direct signature of beyond Luttinger liquid physics.

In Fig. 2.6 some examples of measured Bragg spectra of 1D Bose gases are compared with the finite-temperature theory of [163] and taking into account the presence of an array of 1D quantum fluids [71]. Since the temperature can not be simply extracted from a measurement of the time-of-flight distribution in the regime of correlated 1D bosons, τ is an adjustable parameter in the comparison with the theory. On the one hand, the agreement between theory and experiment is excellent for small values of τ (typically $0.5 < \tau < 1$). This indicates that the 1D gases are strongly degenerated, a regime which is hardly accessible

[1]The momentum distribution is the Fourrier transform of the first-order correlation function in position, $g_1(x,x')$.

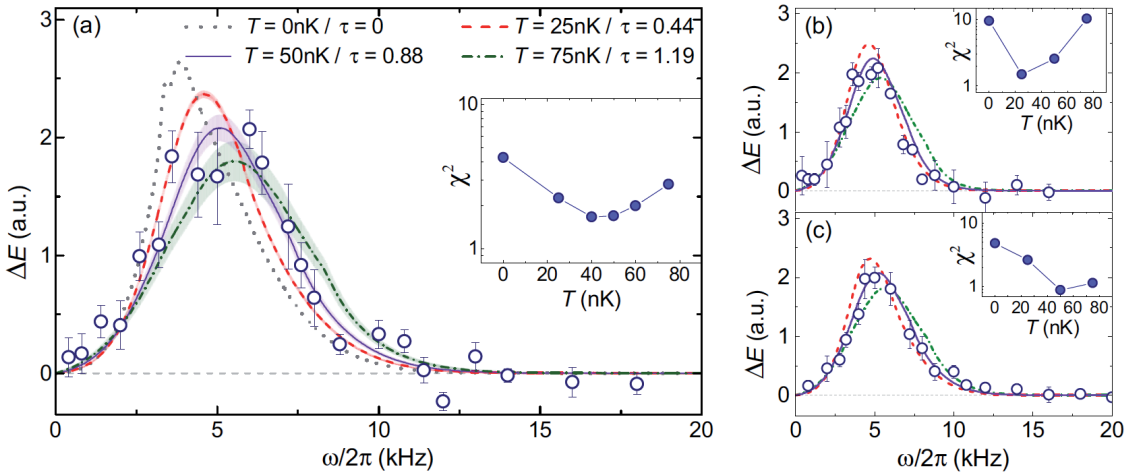

Figure 2.6: Experimental Bragg spectrum of 1D Bose gases. **(a)-(c)** Bragg spectra measured in the experiment (dots) for different transverse trapping frequencies in the 1D Bose gases. The lines are ab-initio calculated spectra with the appraoch of [163]. The reduced temperature fitting best the experimental data is small, $\tau < 1$. Consequently the width of the spectra is dominated by the zero-temperature contributions coming from the extended region of non-vanishing spectral weight (see Fig. 2.5).

with one-dimensional realization on atom chip [178]. On the other hand, the contribution of the finite temperature to the spectrum can be identified but it is clear that the spectral weight derives mainly from the zero-temperature contribution of the Lieb-Liniger model.

Our work has inspired colleagues from the Nagerl group (Innsbruck) who have proceeded similarly to us but probing 1D Bose gases with Bragg spectroscopy at larger parameters γ. This was possible by tuning the interaction strength with a Feshbach resonance [147]. The spectra they measured are qualitatively similar to the one we have found, thus indicating that the regime $\gamma \sim 1$ is indeed a regime of strong interaction, clearly beyond that of weakly-interacting systems.

2.3 Spectroscopy of lattice 1D bosons across the Mott transition

Phases of the Bose-Hubbard hamiltonian. An emblematic example of a strongly-correlated Hamiltonian inspired by solid-state physics is the Hubbard hamiltonian. It is an approximate model that describes an ensemble of interacting quantum particles in the lowest energy band of a lattice potential. It contains two terms, an on-site interaction U and a tunnelling energy J, but it is sufficient to describe a conductor-insulator phase transition, the celebrated transition towards a Mott insulator. In the 2000's, this quantum phase transition has been observed with ultra-cold gases loaded into optical lattice, both with bosons [90, 209, 205] and with fermions [112, 195]. These experiments were performed in a trap thus implementing a trapped version of the homogeneous Hubbard hamiltonian where an additional energy scale, the site-to-site potential energy shift $m\omega_T^2 a^2/2$ (where $\omega_T/2\pi$ is the trapping frequency and $a = \lambda/2$ is the lattice spacing), appearing on top of U and J. A major consequence of realizing the Hubbard hamiltonian in a trap is the possible co-

existence of different phase of matter, such as the simultaneous presence of Mott insulator and superfluid regions in the case of bosonic particles [21].

In the following we will concentrate on the bosonic Hamiltonian, the so-called Bose-Hubbard Hamiltonian, that we have implemented in the experiment and probed via Bragg spectroscopy. The hamiltonian writes

$$H = -J\sum_{j,l}(b_j^\dagger b_l + \text{h.c.}) + \sum_j \frac{U}{2} n_j(n_j - 1) + \sum_j \frac{m\omega_T^2 a^2 j^2}{2} n_j \tag{2.10}$$

where U and J are respectively the on-site interaction and tunnelling energy parameters, $\omega_T/2\pi$ the trap frequency, m the atomic mass, a the lattice spacing and $n_j = b_j^\dagger b_j$ the atom number on a site labelled j. The zero-temperature ground-state of this hamiltonian undergoes a quantum phase transition from a superfluid state (at low ratio U/J) to a Mott insulating state (at large U/J). The critical ratio U/J where the transition occurs depends on the dimensionality and the filling of the lattice system. The university class of the phase transition in homogeneous one-dimensional system also strongly changes with the filling factor: it is a BKT-type transition at unit filling while it is belongs to the mean-field university class when crossed by changing the chemical potential [43]. In addition, as mentioned earlier, the presence of a trap complicates this picture as superfluid and Mott phases can co-exist in separate regions of the trap. These different aspects make the observation of the criticality associated to the Mott phase transition extremely difficult with trapped ultracold atoms. Nonetheless an interesting question that can be addressed using quantum gases is the characterization of the quantum phases on both sides of the phase transition. One approach to this aim, as introduced previously, consists in measuring the low-energy spectrum. Contrary to solid-state experiments, one should stress that the high degree of control on ultracold gases allows one to study perfectly periodic lattices, without disorder nor phonons, and thus to investigate the properties of the "clean" Bose-Hubbard Hamiltonian.

Probing $\mathcal{S}(k,\omega)$ in 1D Bose gases across the Mott transition. In the experiment, we realized one-dimensional Bose gases by loading a 3D Bose-Einstein condensate into two orthogonal optical lattices whose amplitude is $V_\perp = s_\perp E_R = 35E_R$. Adding a third optical lattice of varying amplitude $V_y = s_y E_R$ along the direction of the 1D gases permits to explore the different many-body phases across the Mott transition. The experimental procedure, which includes a thermalization time at low lattice amplitude after the Bragg excitation (see Fig. 2.7(a)), aims at measuring the energy deposited by the Bragg beams in the gas. In Fig. 2.7(c)-(h) we plot the measured Bragg spectra as a function of s_y [54]. Note that in this paragraph we concentrate on a Bragg excitations whose energy $\hbar\omega$ belongs to the lowest-energy band of the optical lattice.

The modification of the nature of the ground-state from a superfluid to a Mott insulator appears in a striking manner on the recorded low-energy spectra: at small s_y the response exhibits a single broad peak while, at large s_y the spectrum shows a complex structure with multiple resonances. In addition, the amplitude of the response drastically drops as the atomic system enters the insulating regime. We have shown that the width of the Bragg spectra is an adequate indicator to pinpoint the phase transition as it yields a value of the ratio U/J compatible with Monte-Carlo calculations [181].

A more detailed analysis of the spectra reveals several interesting features associated to the many-body quantum states. On the superfluid side of the transition we observed

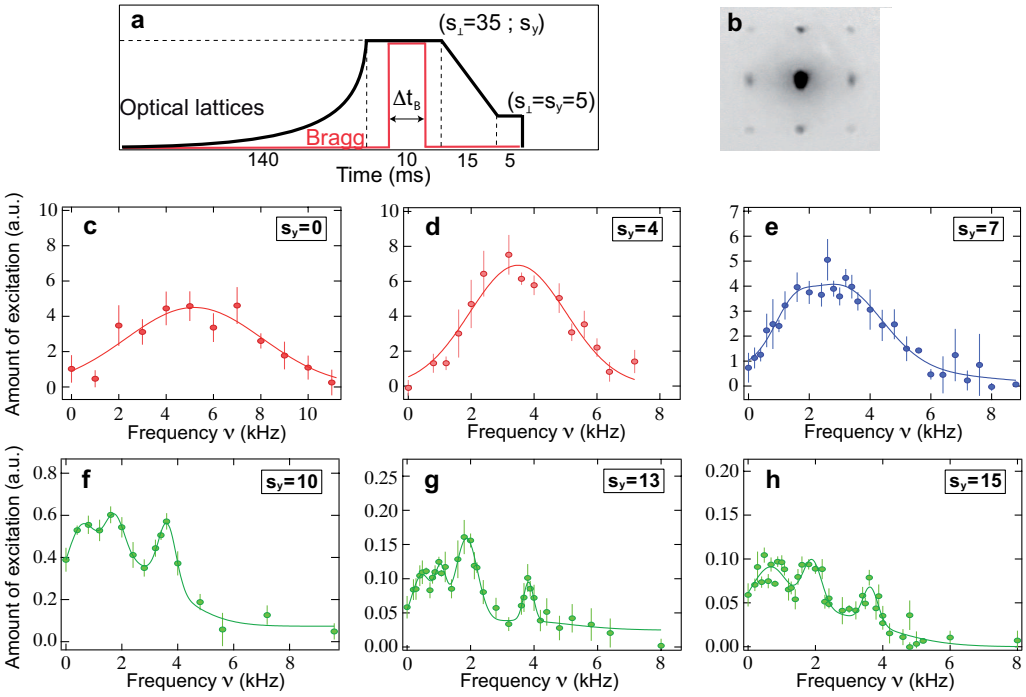

Figure 2.7: Dynamical structure factor $\mathcal{S}(k_0,\omega)$ of 1D Bose gases across the Superfluid-to-Mott transition. **(a)** Experimental sequence: after loading the 3D BEC in 3D optical lattice ($s_\perp = 35$, sy) with an exponential ramp, the 1D gases are excited with the Bragg beams. The optical lattice is then linearly ramped down to $s_\perp = sy = 5$ in 15 ms. After a waiting time of 5 ms, both the optical lattices are abruptly switched off and an absorption image is taken after a time-of-flight of 20 ms. **(b)** Typical absorption image in the absence of the Bragg excitation. **(c)–(h)** Spectra in the lowest energy band measured across the Superfluid-to-Mott Insulator transition. Lines are guides to the eye. Note the drop in the amplitude of the response (vertical scale).

anisotropic line-shapes that could be associated to the presence of a gapped mode. Indeed, it is theoretically predicted that strongly-interacting 1D lattice bosons exhibit two types of excitations [198, 105, 148]: the Goldstone mode which relates to the Bogoliubov excitation present in the weakly-interacting regime and a gapped mode, the Higgs mode, with non-vanishing spectral weight close to the edge of the Brillouin zone. The momentum transferred by the Bragg excitation used in our experiment $k = 0.96k_a$ (with $k_a = 2\pi/a$) was indeed particularly suited to probe this gapped mode. A more recent experiment in the Bloch group using a modulation of the lattice amplitude in two-dimension lattice superfluids (thus effectively probing the gas at the edge of the Brillouin zone as well) has unambiguously revealed the presence of the Higgs mode [68].

In the Mott region, the Bragg spectra are rich of several resonances. We associated two of these peaks to elementary excitations of the Mott state, *i.e.* to particle-hole excitations [54]. A particle-hole excitation above the Mott state is gapped with an energy close to U when probed at $k \simeq k_a$ and large U/J ratio. Similar observations were previously reported with amplitude modulation spectroscopy [209]. On the other hand, resonances observed in the Bragg spectrum at energies lower than the Mott gap were not present in lattice modulation experiments. By transferring a net momentum k, the Bragg beams are in principle capable of exciting atoms belonging to the normal or superfluid phase that co-exist with

the Mott state. They could as well as excite particle-hole states that are activated at finite temperature [179]. While we attributed the observed novel spectral features to these excitations, we were not in the position of extracting physical quantities of interest (like the temperature) due to a lack of theoretical modelling and to a poor signal-to-noise in the experiment. Along these lines, a different spectroscopy method based on the laser excitation of single site in Ytterbium lattice gases has recently demonstrated the possibility to quantify the presence of normal and superfluids [116] while the quantum gas microscopes have shown the capability to measure the entropy (and the temperature) in the Mott state from the on-site fluctuations of atoms (see for instance [199]).

Towards measuring $\mathcal{A}(k,\omega)$ in the Mott insulator state. As discussed at the beginning of this chapter, performing Bragg spectroscopy in the presence of an optical lattice permits in principle to remove a particle from the lowest energy band, and thus from the many-body ground-state, and measure of the one-particle spectral function $\mathcal{A}(k,\omega)$. This assumes that the particle promoted to the excited band does not interact with the atoms in the ground-state, *i.e.* belonging to the lowest energy band. As we shall recall later, we ensured theoretically that this condition is met when exciting atoms to the third band of the lattice from a Mott insulator state. A sketch of the experiment is given in Fig. 2.8(a) where the Bragg excitation towards the third band of the lattice is illustrated. As compared to the previous experiments where the energy range of the Bragg excitation was $\hbar\omega \in [0,3]E_R$, here we transfer a similar momentum k with the Bragg beams but we investigate an energy range spanning $\hbar\omega \in [7,12]E_R$.

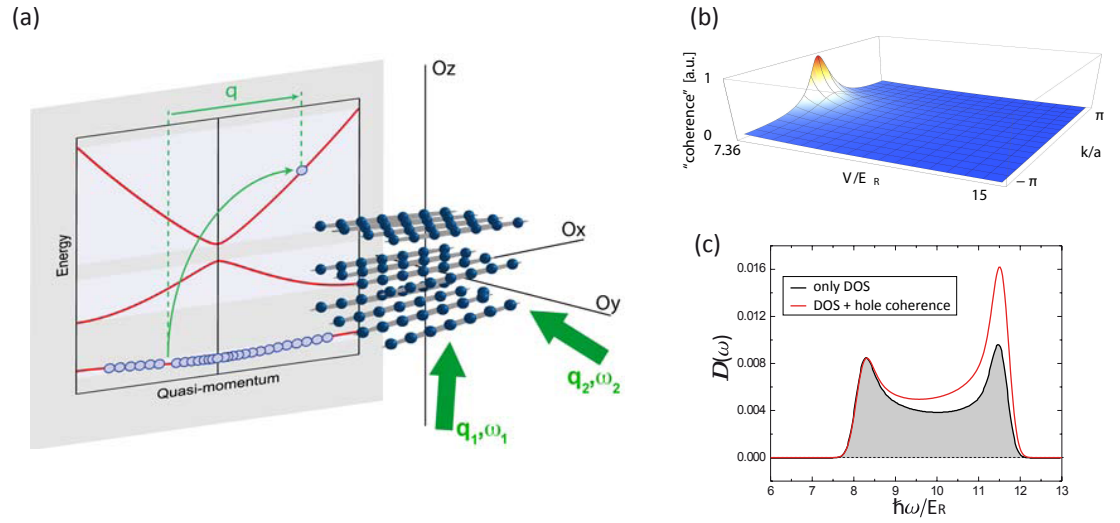

Figure 2.8: One-particle spectral function in a Mott insulator. **(a)** Schematics of the experiment. An array of 1D Bose gases in the Mott state is excited by two Bragg beams which energy difference $\hbar(\omega_1 - \omega_2)$ is set to promote atoms into the third band of the lattice. The small overlap of the atom wavefunction in the third band with the Mott state permits the measurement of the one-particle spectral function $\mathcal{A}(k,\omega)$. **(b)** One-particle spectral function (referred to as "coherence") of a hole in the Mott state. **(c)** The Bragg spectrum results from the combination of the density of state (DOS) in the third band with the spectral function of a hole in the Mott state. The spectral weight $\mathcal{A}(k,\omega)$ of the hole manifests as an asymetry in the amplitude of the Van Hove singularities of the DOS.

In experiments like ARPES, the particle (*i.e.* the electron) which is extracted from the many-body state couples to the continuum of free particles and the probability of excitation depends only on the one-particle spectral function of the initial many-body state. Our scheme differs from the ARPES picture because the density-of-state (DOS) of the final state must be taken into account. Indeed the atom which is extracted from the Mott state is promoted to the excited band whose DOS is not flat. As a consequence, the probability for an excitation above the Mott state depends on $\mathcal{A}(k,\omega)$ of the initial Mott state but also on the DOS of the final state (third excited band). Note that the excited particle in the third excited band is free (to a good approximation) and the DOS is this easy to calculate. The DOS in the excited band of an optical lattice exhibits a peculiar shape taking high values at the edge of the Brillouin which are associated to Van Hove singularities [104]. An example for our experimental parameters is provided in Fig. 2.8(c) (black curve).

The one-particle spectral function $\mathcal{A}(k,\omega)$ is related to the imaginary part of the Green function G in a simple manner, $\mathcal{A}(k,\omega) = -\pi^{-1}\mathrm{Im}[G(k,\omega + i0^{+})]$. In order to calculate $\mathcal{A}_h(k,\omega)$ associated to creating a hole in the Mott state we described the propagation of a hole in a generalized Bogoliubov approach [105]. It yields the Green function G_h associated to a hole in the form of

$$G_h(k,\omega) = \frac{f(k)}{-i\omega - \omega_h(k)} \tag{2.11}$$

where $\omega_h(k)$ denotes the dispersion relation of a hole in the lowest energy band and $f(k)$ is the momentum distribution of the quasi-particle excitation above the Mott state. The function $f(k)$ reflects the coherence of the quasi-particles and it is the quantity that we aimed at measuring and it is plotted in 2.8(b). As intuitively expected, $f(k)$ is peaked around $k = 0$ and its amplitude decreases when U/J increases since the hole can hardly move around the lattice when the tunnelling is reduced.

When performing the full calculation for the energy transfer induced by the Bragg excitation in the Mott state, we obtain the red curve in 2.8(c) which is clearly distinct from the mere DOS of the final energy band. We have shown that the contribution of finite interaction between the excited hole and the Mott can be safely neglected and we have measured the skewness of the energy spectra to characterize the asymmetric shape induced by the hole coherence [72]. In Fig. 2.9 we plot spectra at different lattice amplitude along the 1D tubes to illustrate the presence of the asymmetry in the experiment as well as the reduction of the weight W associated to $\mathcal{A}_h(k,\omega)$ when U/J increases.

It is important to note that the measured energy spectra correspond to a rather complicated weighted sum over the hole spectral function $\mathcal{A}_h(k,\omega)$ and is not proportional to the spectral function itself. For this reason, input from a theoretical model of the Green's function in the Mott insulator was needed to extract a measure of the hole coherence. For this we used a Bogoliubov-like theory that takes into account zero-point fluctuations around the mean-field Mott wave-function. The non-trivial hole coherence stems from these zero-point fluctuations. In this respect, it is clear that it is the fruitful collaboration with the theory colleagues S. Huber and E. Altman that made the interpretation of the measurements possible.

It would be interesting to directly measure the single hole spectral function and, thereby, obtain quasiparticle energies, coherence factors, and decay times in a model independent way. In principle, this can be done using a band-mapping technique to count how many particles are excited to a particular k state in the upper band [53]. A more direct approach

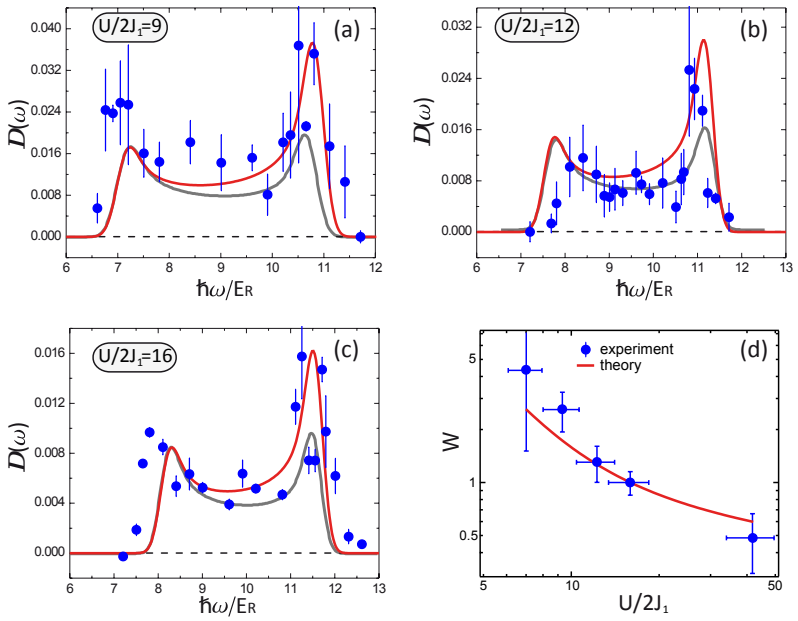

Figure 2.9: Measured Bragg spectra from a Mott insulator with an excitation towards the third band of the lattice. **(a)**-**(c)** The experimental data (blue dots) are shown along with the DOS of the third band (grey line) and expected weight that takes into account the coherence of the hole (red line). **(d)** Total spectral weight as a function of the ratio $U/2J$ of the lattice along the 1D gases.

to the measurement of $\mathcal{A}(\mathbf{k},\omega)$ exists. It consists in using a single radio-frequency photon to change the internal state of one atom, possibility towards a final state that does not interact with the initial internal one. This technique is called photoemission spectroscopy and it has been widely used, for instance to probe the one-particle energy spectrum of fermions [207].

2.4 Associated peer-reviewed publications

[1] *"Exploring correlated 1D Bose gases across from the superfluid to the Mott insulator state by inelastic light scattering"*
D. Clément, N. Fabbri, L. Fallani, C. Fort and M. Inguscio
Phys. Rev. Lett. 102 155301 (2009)

[2] *"Excitations of a Bose-Einstein condensate in a one-dimensional periodic potential"*
N. Fabbri, D. Clément, L. Fallani, C. Fort, M. Modugno, K. M. R. van der Stam and M. Inguscio
Phys. Rev. A 79 043623 (2009)

[3] *"Multi-band spectroscopy of inhomogeneous Mott insulator states of ultracold bosons"*
D. Clément, N. Fabbri, L. Fallani, C. Fort and M. Inguscio
New J. Phys. 11 103030 (2009)

[4] *"Bragg spectroscopy of strongly correlated bosons in optical lattices"*
D. Clément, N. Fabbri, L. Fallani, C. Fort and M. Inguscio
J. Low Temp. Phys. 158 5-15 (2010)

[5] *"Momentum-resolved study of an array of 1D strongly phase-fluctuating Bose gases"*
N. Fabbri, D. Clément, L. Fallani, C. Fort and M. Inguscio
Phys. Rev. A 83 031604(R) (2011)

[6] *"Quasiparticle dynamics in a Bose insulator by inter-band Bragg spectroscopy"*
N. Fabbri, S. D. Huber, D. Clément, L. Fallani, C. Fort, M. Inguscio, E. Altman
Phys. Rev. Lett. 109 055301 (2012)

[7] *"Dynamical structure factor of one-dimensional Bose gases: experimental signatures of beyond-Luttinger liquid physics"*
N. Fabbri, M. Panfil, D. Clément, L. Fallani, M. Inguscio, C. Fort and J.-S. Caux
Phys. Rev. A 91 043617 (2015)

Chapter 3

3D single-atom-resolved detection of quantum gases in the momentum space

In this chapter I describe the experimental apparatus that we built at Laboratoire Charles Fabry between 2012 and 2015. I describe the production of Bose-Eintein condensates of metastable ^{4}He*, highlighting the solutions we have chosen and implemented to reach a fast production of stable BECs. In a second part, I present the He* detector, a single-atom detector in three dimensions, that is central to the overall research project.

3.1 A novel approach to the production of ^{4}He* condensates

Since the advent of Bose-Einstein condensation [4] the techniques to cool degenerate quantum gases have made enormous progress. Among these improvements, trapping in far-off resonance optical dipole trap (ODT) have been central, allowing to dramatically improve the stability and cycle duration for many atomic species, either using all-optical cooling [16, 54] or magnetic-optical hybrid traps [133]. Another strong motivation for using ODT to produce quantum gases in the magnetic-free environment of an ODT that leaves the possibility to tune the atomic scattering length with a magnetic bias [58, 108]. Lastly, the use of optical traps has also led to building dedicated science chambers with a large numerical access, in contrast to apparatus that were built in the late 90's with magnetic traps (*e.g.* clover-leaf traps) requiring a large number of coils closely located to the gas. Reaching BEC in optical traps thus appear as the right choice to make.

Moreover, in the study of many-body phenomena one often seeks to make highly accurate measurements or search for rare events. In these situations convincing evidence can only be obtained by acquiring a large amount of data to increase the statistical significance of the results. Multi-particle correlations are a good example of such measurements and are often used in both particle physics [56] and quantum optics [143, 93]. Efforts to increase data acquisition rates constitute a major preoccupation for experimentalists. In this context, the fast and robust production of degenerate quantum gases becomes a prerequisite for experimental investigations.

These considerations motivated us to produce Bose-Einstein condensates of metastable Helium atoms He* in an optical trap. At the beginning of the project, reaching BEC in

ODT had yet to be realized with He^*, and the unusual characteristics of this atom – a light mass and a large internal energy – poses significant challenges. In non-polarized He^*, the atomic density is indeed severely limited by the presence of Penning collisions [13, 145, 125] preventing the use of all-optical cooling techniques without spin polarization. On the other hand, hybrid traps use magnetic quadrupoles in which one must minimize losses due to Majorana spin flips. Since the Majorana loss rate, at a given temperature, varies inversely with the particle mass [141], He^* is particularly unfavorable for this approach as well. Nevertheless the potential gain offered by these novel approaches was sufficiently great that it was worth some effort to try to circumvent these difficulties and to produce $^4He^*$ BECs in an optical trap. We observe our first BEC on the evening of February 17th, 2015.

3.1.1 The experimental apparatus

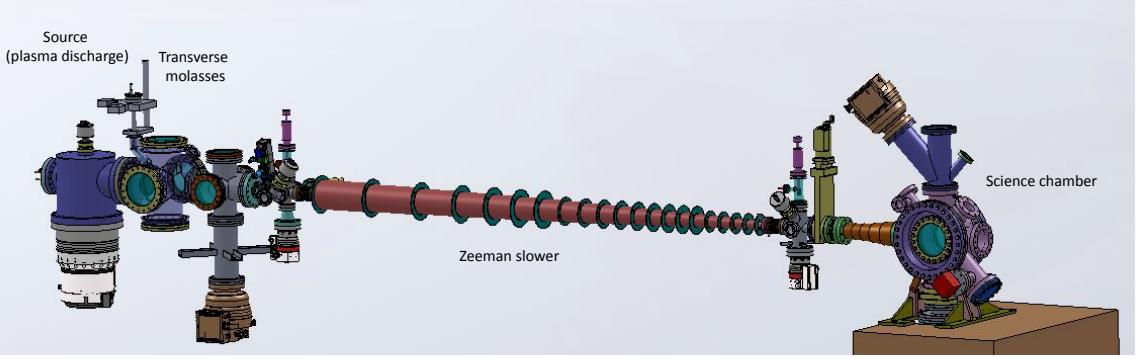

Figure 3.1: Experimental apparatus built at Institut d'Optique. From left to right: in the first chamber, Helium atoms are excited into the metastable state with a dc-discharge under vacuum ; in the second chamber, viewports allow to shine the atoms with the transverse molasses beams ; a 2.5 meters-long Zeeman slower brings atoms from ~ 1200 m/s to ~ 50 m/s ; the chamber to the right-end is the science chamber where Bose-Einstein condensates are produced.

The experimental apparatus. The machine we built ressembles many "old style" apparatus and can be divided in three sections (see figure 3.1): (1) the source; (2) the Zeeman slower; (3) the science chamber. The source of metastable is based on a dc-discharge between a needle and a skimmer, similar to other Helium experiments [13, 183, 211]. The need of a plasma to excite Helium atoms into the metastable state implies that the longitudinal atom velocity is quite large (~ 1200 m/s) and that a Zeeman slower is required. Cooling the source with liquid nitrogen allows one to keep a Zeeman slower of decent, but relatively large, length (about 2.5 meters long). The science chamber has a large numerical aperture and many viewports to shine the atoms with many optical beams.

A discharge plasma cell. Laser manipulation and laser cooling is at the basis of any cold atom experiments. The linewidth of an atomic transition being small compared to the transition wavelength, one uses the atoms themselves to set adequately the laser wavelength. This is often done by saturated absorption spectroscopy through a glass cell containing the

atomic species. In the case of metastable atoms, the situation is a bit more tricky as the transition to probe does not involve the ground-state. As a consequence, one needs to excite the gas to the metastable state in the glass cell where the spectroscopy is performed. In practice, ignition of a plasma in the cell provides enough excited atoms to the metastable state.

When we started building the new apparatus, we were given glass cells filled with Helium atoms by our colleagues D. Boiron and C. Westbrook. We decided to excite a radio-frequency plasma discharge in these cells. In contrast to dc-discharge cells [137] [129], rf discharges [46, 210, 103] are appealing because they lend themselves to the use of sealed glass cells with no internal metal parts. On the other hand, they have the drawback of radiating rf power into a laboratory in which many other sensitive electrical measurements are being performed. In addition, when rf power is generated by an external oscillator and amplifier, impedance matching to the discharge coil is important and mismatch can result in substantial losses. With the help of F. Moron (an electrician at Laboratoire Charles Fabry) we have developed an efficient, low cost apparatus [150] which provides good spectroscopic signals in a rf-discharge cell of helium. To avoid impedance matching problems, we use a Colpitts oscillator design in which the discharge coil is included as part of the oscillator circuit [55]. This rf-discharge cell has been working properly over the years.

A magneto-optical trap. The first stage of the experimental cycle consists in trapping atoms into a Magneto-Optical Trap (MOT). The MOT is made of $\sim 2.5 \times 10^9$ atoms in the 2^3S_1 state at a temperature of ~1 mK. Using a Compressed MOT stage (decreasing both the detuning and the laser intensity in 10 ms), we then load the atoms in an optical molasses red-detuned from the $2^3S_1 \rightarrow 2^3P_2$ transition. The red molasses have $\sim 2.5 \times 10^9$ atoms at a temperature of $\sim 100\mu$K. In the following we discuss the laser cooling of ^{4}He* in optical molasses and we describe the measurements we perform on Doppler laser cooling.

It is important to note here that the atomic densities in the MOT and the molasses are rather low ($\sim 10^{10}$ cm^{-3}) as compared to other atomic species like alkalii atoms ($\sim 5 \times 10^{11}$ cm^{-3}). This is due to the presence of two-body inelastic losses in a gas of metastable atoms like ^{4}He* [225]. The major inelastic losses present in metastable gases are so-called Penning collisions that result in the loss of two metastable atoms (see section 3.1.5). Since these collisions are assisted by near-resonant light [13, 125, 218, 30, 190], the MOT is loaded with a large detuning of the laser beams (typically $\delta \simeq 35\Gamma$) resulting in a spatially-extended MOT and a low atomic density. During the building of the apparatus, we have investigated the light-induced Penning collisions as reported in the PhD thesis of L. Hoendervanger [100].

3.1.2 Doppler and sub-Doppler laser cooling

Doppler laser cooling. The 2^3S_1 state of Helium-4 is degenerate and sub-Doppler laser cooling processes could in principle occur. As our first measurements on the molasses temperature were not indicating the presence of sub-Doppler mechanisms, we have investigating the properties of red-detuned molasses. We have shown that sub-Doppler laser cooling is not present in ^{4}He* molasses because of its low capture velocity: Doppler laser-cooled atoms are too fast to allow for efficient sub-Doppler cooling to play a role [45]. We have measured the celebrated "check mark" dependency of the temperature with the detuning for Doppler molasses in three dimensions (see Fig. 3.2a):

$$k_B T_{\mathrm{D}} = \frac{\hbar\Gamma}{2}\frac{1 + I_{\mathrm{tot}}/I_{\mathrm{sat}} + (2\delta/\Gamma)^2}{4|\delta|/\Gamma}, \tag{3.1}$$

where I_{tot} is the total intensity of all six laser beams, I_{sat} and Γ are respectively the saturation intensity and the line-width of the atomic transition. In the model of a two-level atom, T_D has a minimum value at a detuning $\delta = \Gamma/2k_B$ equal to $\hbar\Gamma/2$ for vanishing intensities. Recently, Doppler laser cooling was investigated in 3D red-detuned molasses of Lithium atoms [233].

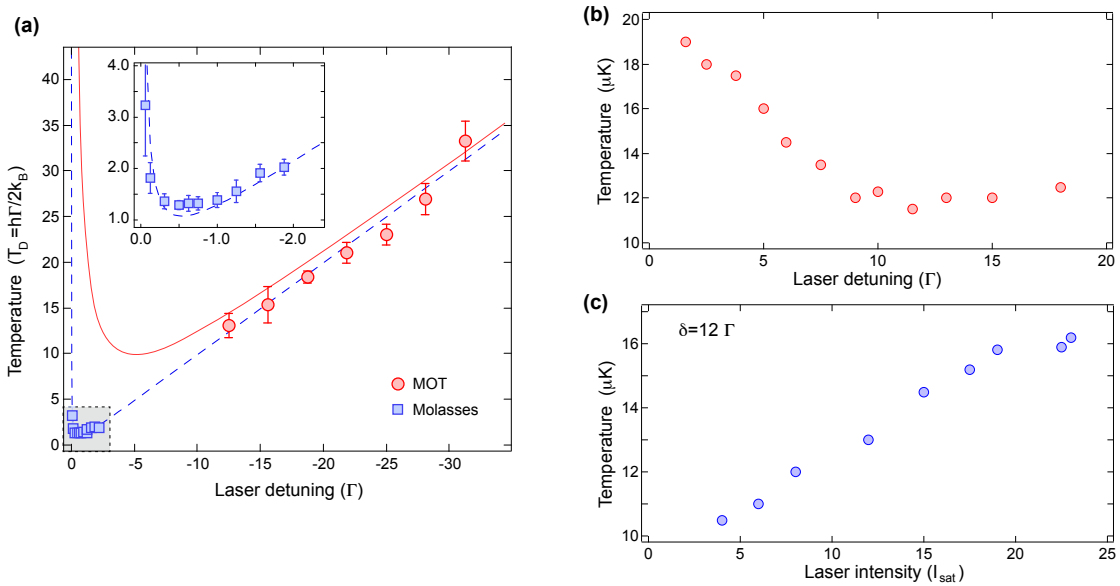

Figure 3.2: Equilibrium temperature in ^{4}He optical molasses. **(a)** Doppler molasses: equilibrium temperature (in unit of $T_D = 38\mu$K) as a function of the laser detuning δ on the $2^3S_1 \rightarrow 2^3P_2$ transition. **(b)**-**(c)** grey molasses on the $2^3S_1 \rightarrow 2^3P_1$ transition: equilibrium temperature as a function of the laser detuning (b) and laser intensity (c).

Another striking feature associated with the Doppler laser cooling mechanism is the sensibility of the molasses center-of-mass to power imbalance between counter-propagating laser beams. The radiation pressure at the origin of the Doppler force is indeed non-zero for an atom at rest as soon as the optical power in counter-propagating beams is not balanced. The force is null in a frame moving at the so-called drift velocity. This is in contrast with sub-Doppler laser cooling mechanisms where the force exerted on an atom results from the modulation (AC-stark shift) of the internal energy levels of the atom and is thus always null for an atom at rest in the lab frame. We have measured the drift velocity in our molasses and found excellent agreement with the predictions associated with the two-level model [45].

At small intensities and low atom numbers, we were able to cool the molasses ($T \simeq 40\mu$K) down to the Doppler temperature ($T_{\mathrm{D}} = 38\mu$K). But the experimental cycle to reach quantum degeneracy requires working with a large atom number, and thus a higher intensity – and accordingly a higher temperature – in the red-molasses (100μK). In addition to the relatively high temperatures of Helium molasses, the atomic density ($\simeq 2\times10^{10}$ atoms/cm^{-3}) is also relatively low compared to other species (due to the presence of large Penning collisions in a non-polarized gas of metastable atoms). Red-molasses of metastable Helium thus have a low phase-space density ($\mathcal{D} \simeq 2 \times 10^{-5}$). In order to further laser-cool the gas

before loading it into a trap, we have attempted with success the implementation of a grey molasses stage.

Grey molasses cooling Sub-Doppler laser cooling refers to techniques of laser cooling that involve more than two internal energy levels of an atom, allowing to reach equilibrium temperatures below the Doppler limit T_D. The celebrated sub-Doppler cooling mechanism of Sisyphus cooling in red-detuned optical molasses first emerged [60]. A few years later, in the quest towards quantum degeneracy, blue-detuned sub-Doppler molasses were implemented to increase further the atomic density, limited by light-induced phenomena in red-detuned molasses [223, 25, 24, 69]. The point here was to implement a Sysiphus cooling scheme between a bright and a dark state (with motional coupling between the two states) in order to accumulate slow atoms in the dark state that is not coupled to the laser beams. But the first implementation of these grey molasses [223, 25, 24, 69] coincided with the observation of Bose-Einstein condensation without the use of grey molasses [4]. Since quantum degeneracy was reached by directly loading red-detuned molasses into magnetic traps, grey molasses were somehow abandoned.

It is only recently that grey molasses were investigated and used again, to satisfy the needs associated with loading optical dipole traps. The requirements in atomic density and temperature to load the small trapping volume defined by a crossed optical dipole trap are indeed much more stringent than those associated to loading a magnetic trap. By further decreasing the temperature, grey molasses are a mean to optimize the ODT trap loading. In the past decade, grey molasses were implemented in ^{85}Rb [67], ^{40}K [75, 202], ^{7}Li [92], ^{39}K [187, 153], ^{6}Li [32], ^{23}Na [57], ^{87}Rb [185], ^{52}Cr [81] and metastable ^{4}He [28]. Thanks to the absence of an hyperfine coupling (the nuclear spin $I \simeq 0$), metastable Helium-4 atoms exhibit a perfect lambda-like atomic structure on the $2^3S_1 \rightarrow 2^3P_1$ transition. This configuration is particularly well suited to efficiently create long-lived dark states, as demonstrated by the observation of Velocity Selective Coherent Population Trapping with ^{4}He in the 80's-90's [8, 128]. VSCPT relies on peculiar atom trajectories that bring them into the dark state, and as a result only a few hundred atoms were detected in the VSCPT peaks. On the contrary, in grey molasses we are interested in having a large number of atoms at thermal equilibrium. We have thus investigated a regime rather different than that described for VSCPT in [8, 128].

In Fig. 3.2(b)-(c) we plot the dependency of the molasses temperature with laser detuning and intensity. Similarly to the observations with other atomic species, we find a close to linear dependency of the temperature with the molasses intensity and a large range of blue detunings over which the grey molasses are efficient. We note that the temperature we observe with a relatively large atom number (1×10^8) is $T_{\mathrm{GM}} = 10\mu\mathrm{K} \simeq 5T_{\mathrm{R}}$ with $k_{\mathrm{B}}T_{\mathrm{R}} = \hbar^2k_{\mathrm{R}}^2/2m$ and $k_{\mathrm{R}} = 2\pi/\lambda$. The ratio $T_{\mathrm{GM}}/T_{\mathrm{R}}$ we measure is the lowest reported one among the atomic species, a feature that may be attributed to the perfect lambda-like structure of ^{4}He. We note that we do not observe a minimum temperature as a function of decreasing intensities but we rather lose atoms as we lower this intensity. It suggests that we can further reduce the temperature at the cost of atom losses. Proceeding along this direction, we should indeed end in the VSCPT regime, but as explained earlier it is not our objective.

At the end of the grey molasses phase, we have $N \simeq 1.8\times10^9$ atoms at $\sim 15\mu$K. The phase space density has increased to $\mathcal{D} \simeq 5\times10^{-4}$ but the atomic density is too low to efficiently load an optical dipole trap at this stage of the experimental cycle.

3.1.3 Production of Bose-Einstein condensates in a crossed optical trap

A magnetic quadrupole stage. When we planned the experimental apparatus, we wanted to benefit from the advantages associated with Optical Dipole Traps (ODT) mentioned in the introduction to this chapter. With typical numbers (an optical power of several Watts and a waist of some dozens of micrometers) the trapping frequencies in a single beam ODT are relatively large in the direction transverse to the beam propagation. Adding a second beam crossing the first one thus allows one to obtain large trapping frequencies in 3D, leading to fast thermalization and good evaporation. As a result, the possibility to reach quantum degeneracy in a crossed ODT mainly rely on the initial number of loaded atoms, as subsequent evaporation is very efficient.

The loading of a crossed ODT from a gas strongly depends on the gas temperature and atomic density prior to loading, in particular an efficient loading requires these quantities to match the ODT volume and depth. Penning collisions between metastable Helium atoms are playing against an efficient loading when one aims at starting from a laser-cooled gas. On the one hand the laser-cooled gas is not spin-polarized and it has a low atomic density limited by Penning collisions [225]. One the other hand, when non-polarized atoms are transferred to the ODT the probability of Penning collision increases due to the tight confinement and the increase in the atomic density. We have made an attempt at loading the ODT directly from the grey molasses but we obtained a low atom number in the crossed ODT and Bose-Einstein condensation could not be reached in these conditions. In order to both increase the atomic density and spin-polarize the gas, we make use of a magnetic quadrupole trap in which radio-frequency evaporation could be performed. This approach was very much inspired by the work of our colleagues at NIST with Rubidium atoms [133] but with a difference. At NIST [133] the Bose-Einstein condensate is produced in a hybrid trap made of a single ODT and a magnetic quadrupole. In our work [28], the magnetic quadrupole is used to transfer the atoms in a crossed ODT and Bose-Einstein condensation is obtained in the crossed ODT once the magnetic quadrupole trap has been switched off.

The loading of the quadrupole trap from the grey molasses is performed after optically pumping the atoms into the $m_J = +1$ spin state. The initial gradient of the quadrupole (8 G/cm) is chosen to match the size and temperature of the grey molasses and minimize heating during the transfer. We typically load in the magnetic quadrupole about 85% of the atoms of the grey molasses with a negligible heating of the gas. Once loaded the gradient of the quadrupole is increased up to 40 G/cm, a value at which we perform a radio-frequency evaporation stage (linear ramp from 30 to 6 MHz over a duration of 3 seconds). The radio-frequency ramp is optimized to obtain a sufficiently cold and dense cloud to efficiently load the crossed dipole trap. At the end of the stage of radio-frequency evaporation, we have 10^8 atoms at 70μK corresponding to a density of 5×10^{11} cm^{-3} that is about 50 times larger than that of the grey molasses. We note that the presence of large Majorana losses (associated to the light mass of Helium) prevents from further increasing the atomic density and limits the lifetime of the gas in the quadrupole. We have measured the Majorana losses and the associated loss rate γ_M

$$\gamma_M = \chi \frac{\hbar}{m} \left(\frac{\mu B'}{k_B T} \right)^2 , \tag{3.2}$$

and investigated whether the geometrical factor χ is independent of the atomic species as

suggested previously [168, 96, 64]. We have measured $\chi = 0.17(2)$ [28], a value that is in agreement with reported studies with other atomic species.

Bose-Einstein condensation of ^{4}He* in a crossed optical dipole trap. The optical dipole trap (ODT) is made of two Gaussian shaped beams at 1550 nm (fiber laser source IPG ELR-30-1550-LP). The first beam has a power of 18 W, focused down to a waist of 133 μm. The second beam contains 8 W focused to a waist of 63 μm, and crosses the first beam at an angle of 40° in the horizontal plane. The resulting trap is roughly cylindrical with trap frequencies of 3.1 kHz radially and 624 Hz axially, and a trap depth of $U_0 = k_B \times 244\,\mu$K. The trap center is displaced roughly one beam waist below the quadrupole center to avoid accumulating atoms at the magnetic field zero. The transfer from the QMT to the ODT is performed by ramping down the field gradient to 3 G/cm over 0.5 s in the presence of the ODT. We load about 5×10^6 atoms in the ODT. In order to preserve spin polarization in the ODT, a bias field is switched on before the transfer to the ODT and kept all through the experimental cycle. We then ramp down the intensity of the ODT beams in the presence of a magnetic gradient that ensures to expel hot atoms from the crossed trap region (the effect of gravity on Helium atoms is not sufficient in the configuration where the crossed ODT is in the horizontal plane) [28]. A ramp of forced evaporation in the ODT (duration 0.5 s) allows us to produce (quasi-)pure ^{4}He* BECs with 5×10^5 atoms (see Fig. 3.3(a)).

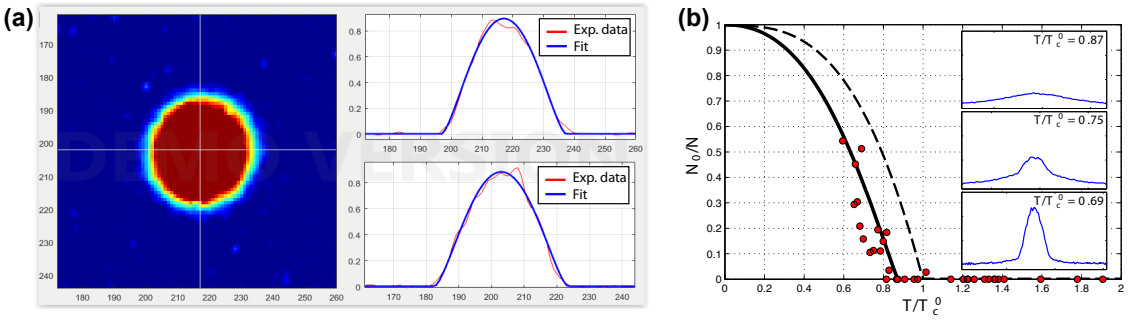

Figure 3.3: Bose-Einstein condensation probed by optical absorption imaging. **(a)** Two-dimensional absorption image of a (quasi-)pure Bose-Einstein condensate after a time-of-flight of 10 ms. On the side of the picture are shown cut in the 3D picture that are fitted by a Thomas-Fermi profile. **(b)** Condensed fraction as a function of temperature as measured by absorption imaging across the transition to Bose-Einstein condensation.

The total cycle duration to produce pure BECs is 6 seconds, a value significantly shorter than previously reported for ^{4}He* BECs. This difference stems from the choice we made to combine grey molasses with the loading of a crossed ODT from a magnetic quadrupole trap. Another practical advantage of the approach we implemented is related to the presence of large 3-body losses in the crossed ODT in the loading stage (thanks to a large number of atoms initially loaded into the ODT). These non-linear losses suppress a large part of the atom number fluctuations present in the previous stage of the experimental cycle. As a result, the atom number in the BEC is fluctuating by 5% or less when the experiment runs correctly. The approach we implemented has inspired our colleagues at the University of Amsterdam [79].

3.1.4 Absorption imaging

Parameters of the imaging pulse. In absorption imaging, a laser beam on the atomic resonance is shone through the gas on a camera. The gas absorbs photons and leaves a shadow on the camera from which two-dimensional picture of the gas is obtained. In order to extract quantities (*e.g.* density profile, sizes) from such an image, the pulse duration τ and the laser intensity $s \times I_{\text{sat}}$ of the imaging beam have to be chosen correctly, to avoid two possible drawbacks inherent to the technique.

On the one hand, after a few cycles of absorption-spontaneous emission an atom acquires a velocity along the direction of the imaging beam that can be sufficient to bring it out of resonance. The number of absorption cycles during the pulse duration τ is $N_{\text{cycle}} = \Gamma/2 \times s\tau/(1+s)$ leading to a Doppler shift $\Delta\omega_D = \hbar k^2 N_{\text{cycle}}/2m$. One can consider the atom to be at resonance as long as $\Delta\omega_D \leqslant \Gamma\sqrt{1+s}$, leading to the condition

$$\tau \leqslant \frac{\hbar k^2}{2m} \frac{s}{(1+s)^{3/2}}. \tag{3.3}$$

On the other hand, spontaneous emission induces a random walk of the atom in velocity space which may enlarge the gas during the imaging pulse. As long as this spatial broadening of the cloud is inferior to the effective pixel size L_{pix} in the imaging plane, one can safely extract the correct size from the two-dimensional image. A second condition relating the parameters of the imaging beam τ and s can be derived as well [101].

As illustrated by Eq. 3.3, these conditions are more stringent for light atoms than heavier ones, because of their larger recoil velocity. It happens that for atoms as light as Lithium and Helium the Doppler condition is stronger than that regarding spatial broadening. It is shown in Fig. 3.4 for the parameters of He_4^* atoms. Special care has thus to be taken when implementing absorption imaging with Helium or Lithium atoms, as shown by recent works investigating these issues in Li [101, 106]. In particular the imaging pulse should be short, of the order of a few μs.

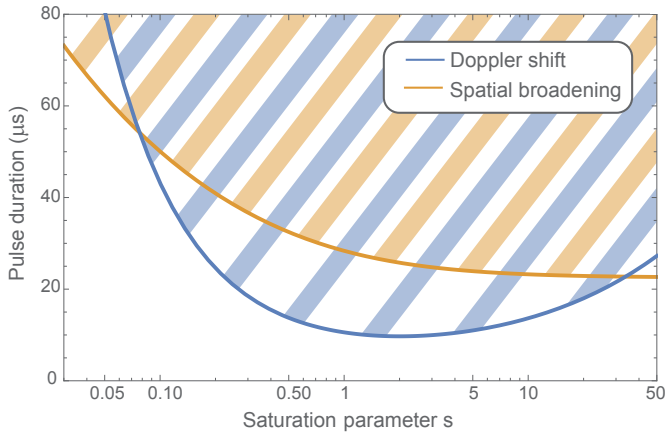

Figure 3.4: Experimental constrains for an adequate absorption imaging of ^{4}He* Bose-Einstein condensates. The quantitative analysis of absorption images can be affected by the effect associated to the recoil (Doppler shift of the atomic resonance) and by that associated to spatial diffusion during the pulse duration. Here we plot the pulse duration as a function of the intensity of the probe. In the shaded areas, one or both these drawbacks occur.

Absorption imaging setup for Helium. The most commonly used cameras in our community, Silicium EMCCD cameras, are not well adapted to image ^{4}He* and ^{3}He* since their quantum efficiency (QE) is ~0.1% at the wavelength (1083 nm) of both atomic transitions. Such a low QE indeed requires long pulses and larger intensities in order to have a signal than those set by the adequate conditions we have just mentioned. InGaAs cameras have a much higher QE at 1083 nm (~ 80%) but until recently their noise at room temperature have prevented one from using them to image quantum gases. For this reason, previous Helium experiments have used Silicium cameras with pulse durations of 50-200 μs and relatively large intensities [188, 219, 66, 123].

In our apparatus we use a new version of InGaAs camera (Xeva camera from the Xenics company) that is cooled to a temperature of -40°C thanks to Peltier elements. It became available on the market only a few years ago and we jumped onto this novel opportunity. It allows us to work with shorter pulse length and smaller saturation parameter for the imaging beam. We use pulse duration of $\tau = 25\mu$s with a saturation parameter $s \simeq 1.5$. With these parameters, the Doppler effect limits the measured number of atoms but the signal-to-noise ratio is better than that at $s \simeq 0.1$. Interestingly, the atom number calibration at $s \simeq 1.5$ (obtained by monitoring the size of the condensate after time-of-flight with the atom number and by measuring the critical temperature for Bose-Einstein condensation) yields a value which is equal to the bare atom number measured at $s \simeq 0.1$.

3.1.5 Losses and lifetime of ^{4}He* BECs

As mentioned previously, the major inelastic collisions present in a gas of metastable Helium atoms are called Penning collisions and take the form [200, 74]:

$$^4\mathrm{He}^*(2^3S) + {}^4\mathrm{He}^*(2^3S) \rightarrow \mathrm{He}(1S) + \mathrm{He}^+ + e^- \quad (3.4)$$

$$\rightarrow \mathrm{He}_2^+ + e^- \quad (3.5)$$

resulting in a net loss of the two colliding metastable atoms. In the early days of gaseous Bose-Einstein condensates, it was noted that these collisions should be drastically inhibited in a spin-polarized gas of metastable Helium since they do not allow to conserve the total spin ($S = 2$) of the colliding atoms. A reduction by 4 orders of magnitude of the associated inelastic loss rate β was predicted [200, 74], from $\beta_{\mathrm{nonpol}} \sim 10^{-10}$ cm^{-3}/s to $\beta_{\mathrm{pol}} \sim 10^{-14}$ cm^{-3}/s, suggesting that the realization of spin-polarized BECs of metastable Helium was possible. This prediction was confirmed by the observation of Bose-Einstein condensation in 2001 [182, 189]. The loss rate β_{pol} was measured in a magnetic trap [197] while β_{pol} was obtained for different thermal spin mixtures in an optical trap [165]. All these values are compatible with the theoretical predictions.

The lifetime of the BECs we produce in the crossed optical dipole trap happens to be limited by these inelastic Penning collisions. In the ODT the BEC lifetime is of the order of a few seconds, $\tau_{\mathrm{BEC}} \sim 5 - 10$s (see Fig. 3.5). The background pressure in our science chamber is 3×10^{-11} and provides a long lifetime (one-particle lifetime ~ 40 s measured in the quadrupole trap). As a matter of fact, the decay of the BEC atom number N_0 is non exponential[1]. On the contrary, $1/N_0^{2/5}$ increases almost linearly with the holding time (see inset in Fig. 3.5), as expected for two-body inelastic collisions for a BEC in the Thomas-Fermi regime [204]. Fitting the decay curve with two-body and three-body inelastic losses,

[1] We also note that no heating of the BECs is observed, suggesting that the spontaneous scattering induced by the far-detuned ODT is as expected negligible on the time scale of seconds.

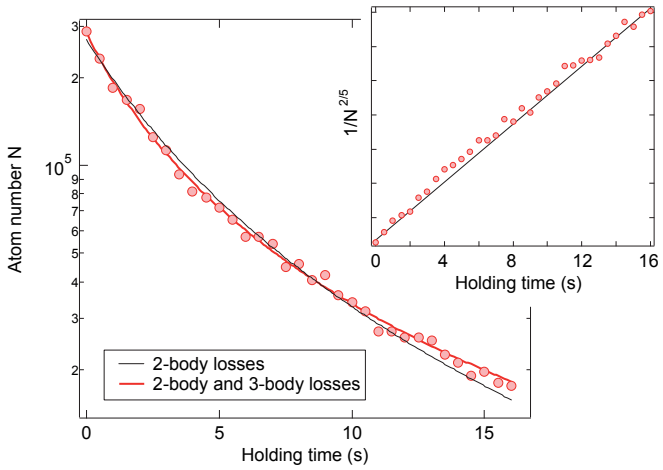

Figure 3.5: Lifetime of ^{4}He* Bose-Einstein condensates in the optical dipole trap. Measured atom number as a function of holding time in the ODT. The decay is mainly driven by two-body inelastic collisions (see the linear scaling of $1/N^{2/5}$ with the holding time in the inset) with a small contribution from three-body losses at short times.

we obtain values which are compatible with theoretical predictions: $\beta_2 = 1.6 \times 10^{-14}$ cm^{-3}/s and $\beta_3 = 0.8 \times 10^{-27}$ cm^{-6}/s.

3.2 Three-dimensional detection of individual atoms in momentum space

A strong scientific motivation to manipulate a gas of metastable Helium atoms (both ^{3}He* and ^{4}He* isotopes) is the possibility to detect individual atoms thanks to their large internal energy (19.8 eV). This original detection method, based on the use of Micro-Channel Plates (MCPs), was central in the choice I made to build an apparatus with metastable Helium. I will describe it briefly. Let us start by recalling that in the experiment we let the atoms fall on the MCP by gravity. As we shall see later, this fall time is long enough (~300 ms) to ensure that the position of the atom reflects only its velocity, or momentum.

The detection of energetic particles, such as UV and Xray photons or accelerated electrons and ions, with MCPs has shown to be crucial to many research areas ranging from time-of-flight mass spectrometry [19] and diffraction experiments [235, 26] to the monitoring of metastable atoms [225]. More detailed information that those provided below about the MCPs and delay lines, along with the analysis of the timing signal to reconstruct the position of individual atoms can be found in [23, 191, 203].

3.2.1 Working principle of the He* detector

From a single Helium atom to a shower of electrons. When impacting on a metallic surface, a metastable atom with sufficient internal energy (of the order of a few electron-volt or larger) can extract electrons from the metal [94]. In the specific case of metastable Helium in the 2^3S state, secondary electron ejection coefficients of about 70% were measured on different kind of metallic surfaces [65]. The first electron ejected from the metallic

surface has to be amplified to yield an electric signal that can be detected. Such an amplification is obtained by using Micro-Channel Plates, an ensemble of coated tubes of micron size [230]. The tubes are coated to maximize the probability of secondary electron ejection and are polarized with a high voltage (~ 1kV) in order to accelerate electrons and generate an avalanche process of electron emission. One MCP typically provides a gain of 10^3 – 10^4 electrons. Using a pair of MCPs on top of each other yields a sufficiently large gain to work in the gain-saturated regime where the distribution of pulse heights allows for discriminating most of the electronic noise from electron showers induced by an atom [230].

We have used several pairs of MCP. One pair is made of 25μm-diameter holes (spacing center-to-center 32 μm) at an angle of 8° with the surface of the plate (from Burle Industries Inc.). Their open-to-air ratio (OAR) is specified to be ~50% and their electronic gain to be larger than 10^4 at 1200 V. Another pair from the Hamamatsu company has 10μm-diameter holes at an angle of 20 ° and a OAR larger than 90%.

Coding the position of the Helium atoms. When a Helium atom hits the MCP surface, it starts the electronic avalanche process in a given channel and the electron shower exits the MCP output surface from the same channel. The information about the spatial position of the initial impact of the atom is conserved through the amplification process. By placing a phosphor screen behind the MCP, one can observe the position of the electron shower, *i.e.* the position of the impact on the input surface. While these screens are adapted to obtain a two-dimensional image of the positions of the impacts, the maximum refreshing rates one can achieve is way too low for our use. On the other hand, cross delay lines offer the possibility to reach high fluxes while maintaining a good spatial resolution in the plane of the MCP [201].

A sketch of the detection method is depicted in Fig. 3.6. It illustrate the principle of the delay lines to code the position of the electron shower. When crossing the delay lines, the electron shower couples charges to the wires and it generates two electronic pulses propagating in opposite directions along a given line[2]. The difference between the arrival times of the two pulses at the outputs of the line directly reflect the position of the impact along the line. A cross delay-line with orthogonal wiring thus provides the information about the two-dimensional position of the impact. These four arrival times also allow one to determine the time of the impact on the MCP surface, yielding the third coordinate of the impact. The detection method associating MCPs and delay-line is unique as it permits the reconstruction of the three-dimensional position of individual Helium atoms. The first implementation of this original probe was accomplished by my colleagues A. Aspect, D. Boiron and C. I. Westbrook at Institut d'Optique [192].

As mentioned previously, the propagation of electronic signal in the delay lines does not prevent from recording data at a high flux. Yet, as we shall discuss below, the transfer rates of digital times to the memory of a computer are the limiting factor in reaching high fluxes.

A FPGA Time-to-Digital Converter to reach a high flux of recorded data. The read-out electronics (amplifiers and Constant-Fraction Discriminators) have a bandwidth (a few hundred MHz) large compared to the typical rates of detected particles (10^5 – 10^6 particles per second). On the contrary, the electronics which digitize and store the timing signals are limiting the acquisition rates. As the amount of data increases, both when

[2]One delay line actually consists in two parallel wires that form an electronic guide.

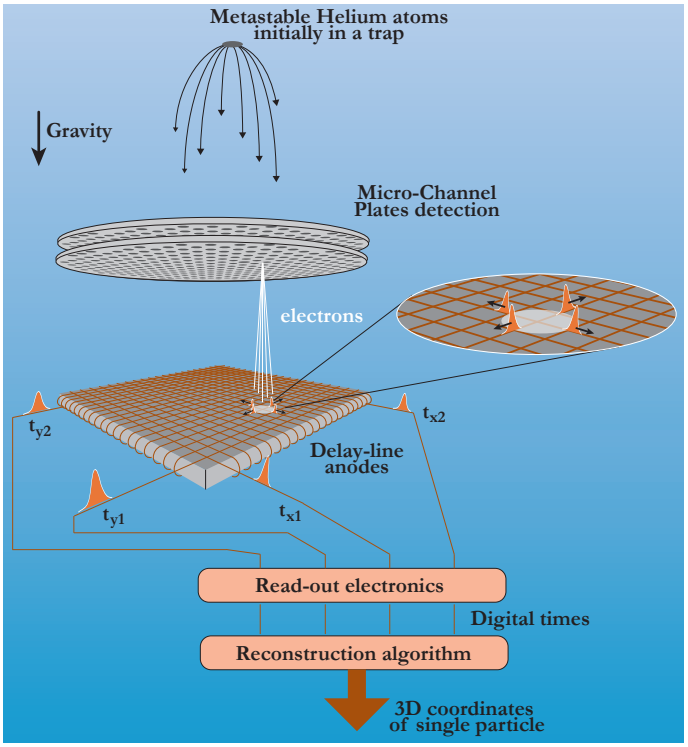

Figure 3.6: Sketch of the single-atom detection method. After release from the trap, metastable Helium atoms are falling onto a pair of MCPs. A single Helium atom extract one electron from the MCP surface which is amplified by the MCPs. The electron shower exiting the MCPs couples to a crossed delay-line yielding four arrival times at the end of the crossed lines. An electronics is used to measure the analog time and encode it digitally into a computer. From the digital times we run an algorithm that allows us to reconstruct the 3D positions of each atom.

lowering the time resolution to digitize the particle coordinates and when increasing the particle flux, the bottleneck in the detection chain is related to the digital data. This limitation is either due to the Time-to-Digital Converter (TDC) coding rate or due to the data transfer to a hard memory. In both the cases, the digital size associated to the coding of a single arrival time[3] is the issue. There are two options to deal with handling such large quantity of data: one can use large memories to store the data in the TDC itself and later transfer them at a low rate to a hard memory ; or one can attempt at transferring the data at a high rate all through the hard memory. The second option is better as the first one implies a maximum number of counts (size of the TDC memory) before a dead-time (transfer to the hard memory) takes place.

Prior to our work [154], the best rates of detected particles (with a three-dimensional reconstruction) that were reported are inferior to 1 MHz [109, 201, 59, 234, 97, 118]. Apart from our colleagues manipulating quantum gases of metastable Helium [97, 118], we should stress that there seemed not to be a strong scientific interest in reaching higher fluxes in nuclear and solid-state physics. Only recently, femtosecond electron diffraction techniques are enlarging their field of application and the use of MCPs working at high rate takes a lar-

[3]Consider a 32-bit word to code a single arrival time. A rate of 4×10^6 of particles per second corresponds to $4 \times 4 \times 10^6 \times 32$ bits per second, *i.e.* 64 MB/s. As a comparison, USB 2.0 transfer rate (~20MB/s) would not be sufficient and only USB 3.0 would make it (~100MB/s).

ger importance. In this context, we started a collaboration with R. Sellem and D. Heurteau from the DTPI (LUMAT federation) to develop a novel TDC from a FPGA chip (Spartan 6 from Xinlink). We chose to continuously transfer the digital data to the hard memory (SSD disk) by using the PCI bus of a computer into which the FPGA card is plugged. R. Sellem and D. Heurteau have built the TDC card and its interface while F. Nogrette have tested it using a source of UV photons (of energy 6-7 eV). After a first phase of tests and improvements, going back and forth between us and the LUMAT team, we have reached continuous detection and 3D reconstruction of $\sim 4 \times 10^6$ particles per second [154].

3.2.2 Characterization of the He* detector

Detection efficiency of metastable Helium. In the experiment, the MCPs are located 55 cm below the position where atoms are trapped (see Fig 3.7(a)). Atoms are released from the trap and let fall under gravity on the MCPs. Here special attention is paid to the spin-state of the atoms: as magnetic fields can hardly be uniformly cancelled over the 55 cm fall of the atoms, we transfer the atoms to an internal atomic state ($m_J = 0$) that is not sensitive to the magnetic field, to avoid any disturbances of the gas distribution during the fall. Bose condensates of metastable Helium atoms are obtained in a spin-polarized gas ($m_J = +1$ or $m_J = -1$) and we use a radio-frequency (rf) pulse to transfer a fraction to the $m_J = 0$ state. After the rf pulse, a magnetic field gradient ensures that the remaining atoms in both the $m_J = +1$ and $m_J = -1$ states are expelled from the MCP surface.

We have calibrated the rf frequency and the fraction of detected atoms on the MCPs by monitoring Rabi oscillations in the three-level system constituted by the states $m_J = -1, 0, +1$ for different rf powers (see Fig 3.7(b)-(c)). From the measured atom number, we obtain a detection efficiency of 25(3)% for the Burle detector and 35(3)% for the Hamamastu detector. Our colleagues in Palaiseau had put a lower bound of ~25% [136] while our Australian colleagues have estimated it to be in the range 10-40% from an indirect measurement [97].

Spatial resolution of the detector. The resolution of the He* detector may not be isotropic as it has different origin and limitation in the plane of the MCP and along the gravity axis, orthogonal to the MCP. We shall discuss them separately. Along the gravity axis, the position of the atom is given by the time at which it impacts the MCP. The coding step of the TDC is 120 ps and one could hope to obtain an extremely good resolution[4]. But the geometry of the MCP channels actually limits the resolution along the gravity axis (see Fig. 3.8). Take two atoms hitting the channel at the same time with a vertical separation. As a result of the initial vertical separation, the electronic pulses from the two atoms will hit the delay line at different times. In the reconstruction algorithm of the 3D position of an atom, the two atoms will thus have a vertical separation, despite the fact that they crossed the MCP surface at the same time[5]. From the characteristics of the Burle MCP, we obtain a vertical resolution of $\sigma_z \simeq 177$ μm, while we expect $\sigma_z \simeq 33\mu$m for the Hamamatsu pair. By investigating the size of two-atom bunching peak in a thermal gas with the Hamamatsu MCP, we have recently obtained results compatible with an isotropic resolution in 3D [41].

[4] Atoms hit the MPC at a velocity of $v \sim 3$m /s, giving $v \times 120 \times 10^{-12} \sim 0.36$ nm !

[5] The speed at which electrons travel throughout the MCPs exceeds by far that of the falling Helium atoms, and the travel time of electrons can be safely neglected.

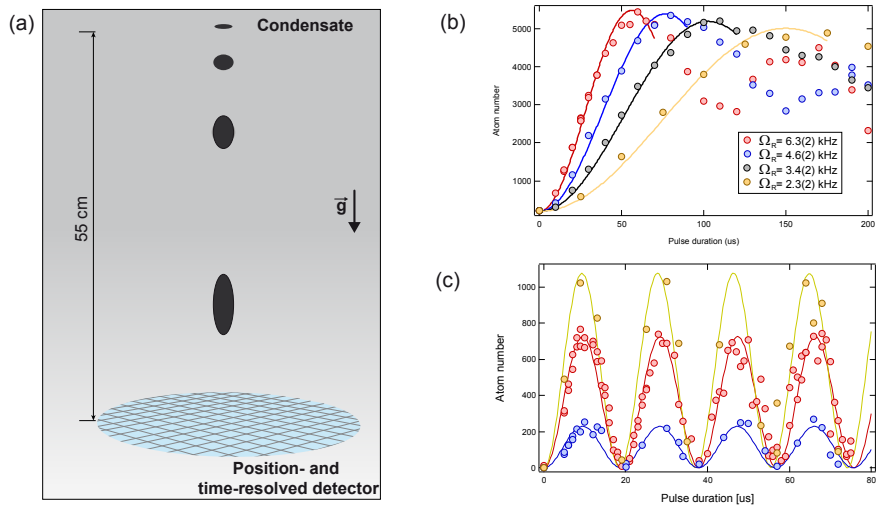

Figure 3.7: Radio-frequency coupling of atoms towards the MCPs. **(a)** The distance between the trap from which atoms are released and the MCP surface is about 55 cm. In order to avoid effects of spurious magnetic fields over this distance and to control the atom number falling on the MCPs we use a radio-frequency (rf) pulse at the time the trap is switched off. In the trap, atoms are polarized in the $m_J = +1$ state and the rf pulse transfer a fraction to the $m_J = 0$ state. Adding a strong magnetic field gradient after the rf pulse, we deviate the remaining atoms in $m_J = +1$ towards the science chamber and thus ensure that they are not falling onto the MCPs. Only the non-magnetic $m_J = 0$ atoms hit the detector. **(b)** Number of detected atoms from a thermal cloud ($N = 4 \times 10^4$ measured by absorption) as a function of the duration of the rf pulse. Rabi frequencies of a few kHz are measured, allowing us to transfer a large fraction of the trapped atoms to the $m_J = 0$ state within 20 μs. The absence of clean oscillations derives from the coupling of 3-levels ($m_J = 0, \pm 1$) and finite-temperature decoherence. **(c)** Out-of-resonance rf transfer of a Bose-Einstein condensate for which fast Rabi oscillations (set by the detuning to the resonance) can be monitored.

In the plane of the MCP, the position of an atom is given by the difference of arrival times at both end of the delay-line. The coding step of the TDC $\sigma_{\mathrm{TDC}} = 120$ ps provides a pixel size in the MCP plane of $\sigma_{\mathrm{TDC}}\, v_{\mathrm{DL}}/2 \simeq 60$ μm where $v_{\mathrm{DL}} \simeq 1$ mm/ns is the velocity of pulse propagation in the direction perpendicular to the delay line. In the absence of any type of noise, one could hope to obtain a resolution even lower than this value. But in practice, any electronic jitter and delay which is of the order of, or larger than, σ_{TDC} would worsen drastically affect the in-plane resolution. In our work [154] we have shown that the resolution was larger than σ_{TDC} and attributed it to electronic noise in the amplifiers, CFD and TDC. With this in mind, we have demonstrated an easy approach to estimate the in-plane resolution without the need of inserting physical masks under vacuum [154]. Recently we have acquired a better electronics for the amplifier and CFD parts. We have obtained a much better resolution, close to the value of the TDC coding step, as we now have an in-plane resolution (RMS size of the distribution) equals to $\sigma_{x,y} \simeq 70$ μm. This value is smaller than that reported by our colleagues in Palaiseau, Amsterdam and Vienna but it is larger than that reported by the Australian group [97]. We note that the Australian group is using a TDC with a coding step of 25 ps, which may explain their smaller resolution if

one assumes that their electronic noise is low enough. Decreasing the TDC coding step with our new electronics may be sufficient to reach lower values for $\sigma_{x,y}$ with our detector in the future.

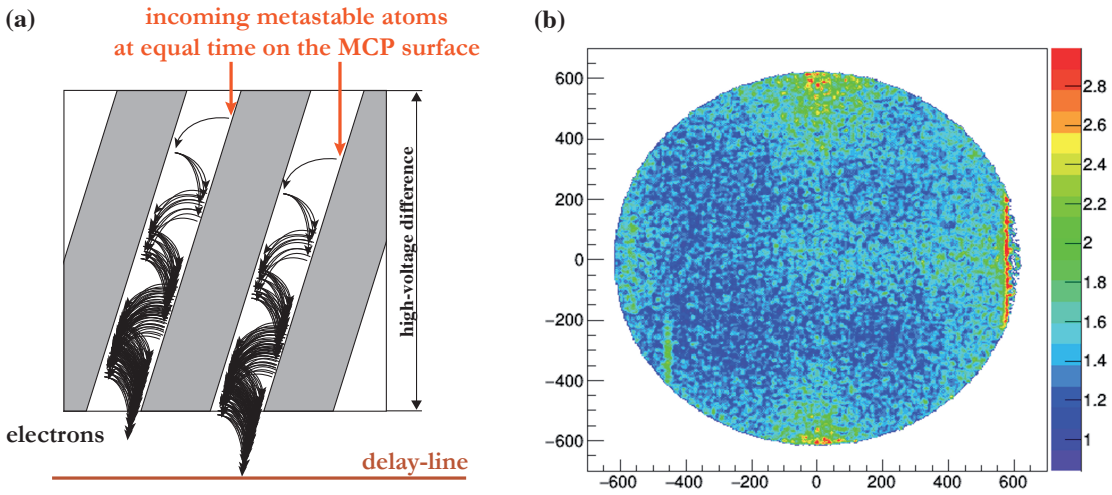

Figure 3.8: Spatial resolution of the MCP detector. **(a)** Vertical resolution - Along the vertical axis (gravity), two incoming atoms falling at an equal time may lead to a time difference detected on the delay-line due to geometrical considerations. Thus the position of an incoming atom can not be reconstructed to better than the vertical distance an atom can penetrate into one channel. **(b)** In-plane resolution - Two-dimensional map of the quantity σ_D which we associate to an RMS resolution in the plane of the MCP. The color scale is given in units of the effective pixel (60μm).

Local saturation of the MCP at high flux. One of important drawback of the MCP detector is the saturation of the detection efficiency at high flux of particles arriving within a small area of the MCP surface (typically 10^5 particles/s/cm^{-2} [191]). When an electron shower is created by the impact of a metastable atom on the MCP surface, a local depletion of charges occurs, which in turn diminishes the local gain of the MCP until charges are brought back to equilibrium by the power supply. During the time interval for which charges are not at equilibrium, the probability to detect a second Helium atom can be drastically reduced. When detecting Bose condensates, this local saturation effect is visible as soon as one transfers (with the rf pulse) more than a few percent of the atoms towards the MCP. In the past, we have attempted at reducing this saturation effect by using different coatings of the input surface [99]. In particular, one idea was to use coating with a lower electric resistance that would allow for a faster replenishing of the charges by the power supply. Yet, we have not been able to conclude clearly, most probably because we were using UV photons that were uniformly illuminating the MCP surface, thus rather leading to a saturation linked with the speed of the TDC and digital data transfer (see previously). I believe it would be worth performing similar measurements with Bose condensates instead.

3.2.3 Observing ^{4}He* gases with the He* detector

Bose-Einstein condensates revealed by the He* detector. A example of the measured 3D distribution of atoms is shown in Fig. 3.9. Here we have produced a Bose-Einstein condensate of metastable Helium ^{4}He* atoms in the ODT (*i.e.* a harmonic trap) and let it fall on the the He* detector. Each red dots correspond to a single atom and 2D projections of the 3D distribution are shown in each plane. Note here that we have transformed the measured positions $\mathbf{r}$ after a time-of-flight t_{TOF} of every atom into a momentum by using the ballistic relation, $\mathbf{k} = m\mathbf{r}/\hbar t_{\mathrm{TOF}}$. A discussion of the validity of the ballistic relation will be presented in Chapter 4.

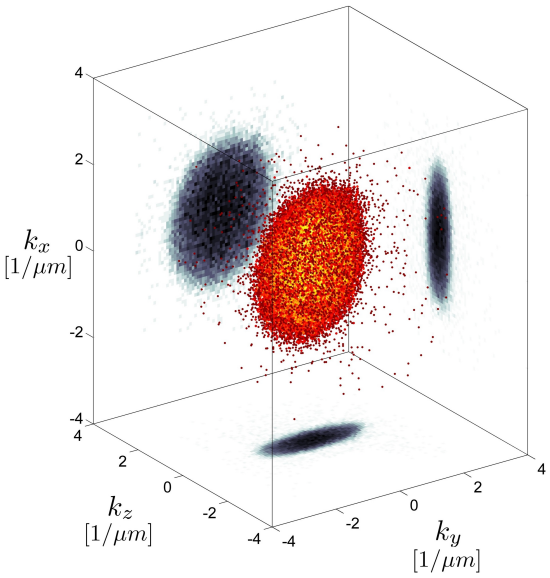

Figure 3.9: 3D distribution of a Bose-Einstein condensate after a 330ms-long expansion. Each dot is a single atom detected in 3D with a momentum $\mathbf{k}$ obtained from the measured position $\mathbf{r}$ and the ballistic relation. The 2D projections of the distribution are shown in black on each panel, illustrating the pancake shape of the BEC released from the elongated ODT trap (trapping frequencies $\omega_x/2\pi \sim 100$ Hz, $\omega_y/2\pi \simeq \omega_z/2\pi \sim 450$ Hz).

Second-order correlation in a thermal gas. A test of the correct behavior of the MCP detector and the 3D reconstruction algorithm can be made by reproducing an early experiment where the celebrated Hanbury-Brown and Twiss (HBT) effect was observed with metastable Helium [192]. The bunching associated to the HBT indeed relies on the possibility to detect and reconstruct correctly the 3D positions of single atoms. In addition, the amplitude and the width of the bunching in a thermal Bose gas depends on a few parameters that can be evaluated separately: the trap frequencies and the temperature of the gas. Investigating the HBT effect thus allows us to quantitatively test our detection method. In Fig. 3.10, we show a measurement of the local second-order correlation $g_2(\Delta x)$ as a function of the separation Δx between two detected atoms[6]. It illustrates the presence of the bunching effect at small Δx in a thermal gas, in opposition to the case of a (quasi-

[6]The spatial distance Δx is that measured on the detector and it is not the in-trap separation between the two atoms.

)pure BEC. By fitting $g_2(\Delta x)$ in Fig. 3.10(a) with a Gaussian function we extract amplitude and width of the bunching that can be compared to quantitative expectations.

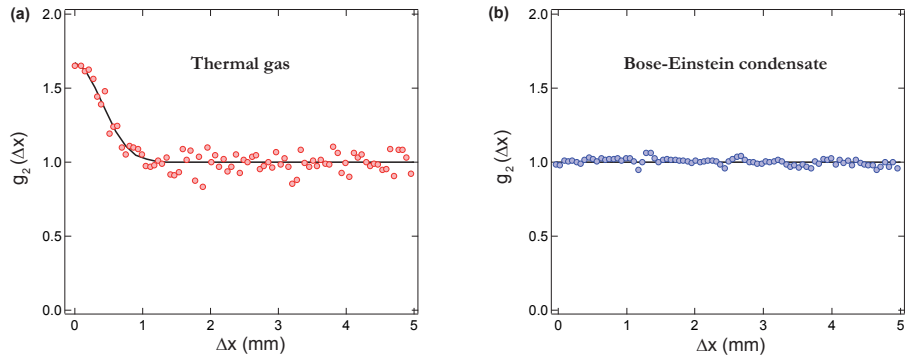

Figure 3.10: Hanbury-Brown and Twiss effect with atoms. Measurement of the second-order correlation $g_2(\Delta x)$ between two atoms separated by a distance Δx on the detector. **(a)** $g_2(\Delta x)$ in a thermal gas. The excess of $g_2(\Delta x)$ at small Δx is a direct signature of the bosonic bunching as introduced by Hanbury-Brown and Twiss. **(b)** $g_2(\Delta x)$ in a (quasi-) pure Bose-Einstein condensate. No bunching is present in the BEC as a single quantum state is populated.

3.3 Associated peer-reviewed publications

[1] *"An oscillator circuit to produce a rf discharge and application to metastable helium saturated absorption spectroscopy"*
F. Moron, A. L. Hoendevanger, M. Bonneau, Q. Bouton, A. Aspect, D. Boiron, D. Clément, C. I. Westbrook
Rev. Scient. Instrum. 83 044705 (2012)

[2] *"Influence of Gold Coating and Interplate Voltage on the Performance of Chevron Micro-Channel Plates for the Time and Space Resolved Single Particle Detection"*
A. L. Hoendervanger, D. Clément, A. Aspect, C. I. Westbrook, D. Dowek, Y. Picard and D. Boiron
Rev. Scient. Instrum. 84 023307 (2013)

[3] *"Three-dimensional laser cooling at the Doppler limit"*
R. Chang, A. L. Hoendervanger, Q. Bouton, Y. Fang, T. Klafka, K. Audo, A. Aspect, C. I. Westbrook and D. Clément
Phys. Rev. A, 90 063407 (2014)

[4] *"Characterization of a detector chain using a FPGA-based Time-to-Digital Converter to reconstruct the three-dimensional coordinates of single particles at high flux"*
F. Nogrette, D. Heurteau, R. Chang, Q. Bouton, C. I. Westbrook, R. Sellem and D. Clément
Rev. Scient. Instrum. 86 113105 (2015)

[5] *"Fast production of Bose-Einstein condensates of metastable Helium"*
Q. Bouton, R. Chang, A. L. Hoendervanger, F. Nogrette, A. Aspect, C. I. Westbrook and D. Clément
Phys. Rev. A 91 061402 (R) (2015)

Chapter 4

Investigations of interacting Bose gases in the momentum space

In this section we present three experimental works performed with the newly built Helium apparatus. The first topic is centered on the momentum tails of expanding BECs from a 3D harmonic trap. The second work concerns lattice Bose superfluids and the BEC transition in a 3D optical lattice. In the third work, we investigate the atom correlations in a Mott insulating state.

4.1 Algebraic momentum tails in the expansion of weakly-interacting BECs

Soon after the installation of the He^* detector, intrigued by the new possibility to detect atoms one by one, we played with the detection of BECs. This was motivated by the fact that there are hardly dark counts on the He^* detector, thus allowing one to measure extremely dilute atomic densities from averaging the experimental runs. The absence of dark counts derives simply from the presence of a threshold in the detection that is chosen in order to remove efficiently the dark counts. In looking for deviations to the bi-modal distributions – associated to the presence of a Bose-Einstein condensate and a thermal component – usually observed in TOF experiments, we had in mind to attempt at finding signatures of the quantum depletion in the TOF distributions [169].

4.1.1 Quantum depletion and Tan's contact

The physics associated with the quantum depletion was introduced in the XXth century to describe the properties of liquid Helium. After superfluidity of liquid ^{4}He was discovered in 1937 [114, 1], its connection to Bose-Einstein condensation was posited by F. London [134] and L. Tisza [217]. However, while at zero temperature liquid helium is 100% superfluid, less than 10% of the atoms are actually in the Bose-Einstein condensate [149]; most particles are coherently expelled from the condensate by strong interactions, and spread over a wide range of momenta. Quantum depletion refers to the presence of bosons outside the condensate wave-function, *i.e.* outside the one-particle ground-state, at zero temperature. It occurs in the presence of interaction that modifies the ground-state of

the system (ideal bosons are all in the condensate wave-function at zero temperature): the many-body ground-state wave-function is an admixture of the condensate wave-function and of one-particle states of higher-energy. Treating interactions at the mean-field level is not sufficient to describe the quantum depletion. Indeed the shape of the ground-state wave-function in the mean-field approximation is modified by the presence of interaction but one-particle excited states are not populated (see Fig. 4.1). In 1947 N. N. Bogoliubov developed a theory that explains the microscopic origin of such interaction-driven, quantum depletion of a BEC [22]. This theory has become a cornerstone of our conceptual understanding of quantum fluids, but is quantitatively valid only for relatively weak interactions, and could not be tested with liquid helium. The realization of Bose-Einstein condensation in dilute and weakly-interacting gases paved the way to the investigation of these predictions.

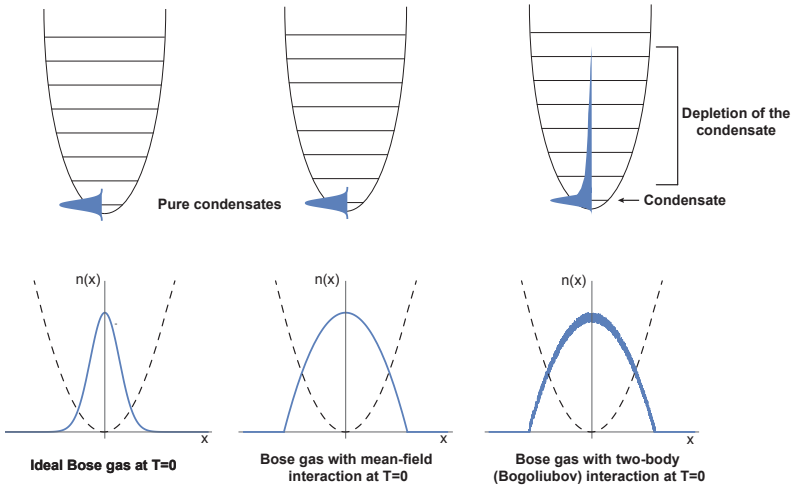

Figure 4.1: Ground-state of ideal and interacting trapped bosons at zero temperature. Top row: illustration of the population of single-particle states. Bottom row: illustration of the in-trap density distribution.

Quantum depletion in the Bogoliubov approximation. The Bogoliubov approach consists in writing the Hamiltonian of bosons with contact interaction by retaining only quadratic terms in the particle operators $\hat{a}_{\mathbf{k}}$ and writing the operator of the condensate as a complex number, $\hat{a}_0 = \sqrt{N_0}$ [169]. It thus assumes that the many-body problem can be solved by retaining in the interacting Hamiltonian three types of two-body interaction: two particles of the condensate remaining in the condensate, two particles of the condensate being promoted to one-particle states with opposite non-zero momenta k and two particles with opposite non-zero momenta k falling back into the condensate. This approximation is valid as long as $\rho a_s^3 \ll 1$ with ρ the density of the gas and a_s the scattering length. Under these approximations, the interacting Hamiltonian can be diagonalized by introducing the quasi-particles operators $\hat{b}_{\mathbf{k}}$ of the Bogoliubov transformation, $\hat{a}_{\mathbf{k}} = u_{\mathbf{k}}\hat{b}_{\mathbf{k}} + v^*_{-\mathbf{k}}\hat{b}^\dagger_{-\mathbf{k}}$ and $\hat{a}^\dagger_{\mathbf{k}} = u^*_{\mathbf{k}}\hat{b}^\dagger_{\mathbf{k}} + v_{-\mathbf{k}}\hat{b}_{-\mathbf{k}}$. The ground-state $|\psi_0\rangle$ of the interacting system at zero temperature then simply corresponds to the vacuum of the quasi-particles, *i.e.* $\hat{b}_{\mathbf{k}}|\psi_0\rangle = 0$ for any $k \neq 0$. Using the Bogoliubov transformation, the many-body ground-state can be written as an admixture of particle states and the particle momentum distribution is

$$\rho(\mathbf{k}) = \langle \hat{a}^\dagger_{\mathbf{k}}\hat{a}_{\mathbf{k}}\rangle = |v_{-\mathbf{k}}|^2. \tag{4.1}$$

We note that the population of non-zero momentum states in the many-body ground-state of an interacting Bose gas is necessary to create a Bogoliubov excitation: the creation operator $\hat{b}^\dagger_{\mathbf{k}}$ indeed contains an annihilation operator of a single-particle momentum state with $k \neq 0$!

In a homogeneous system, the fraction of quantum depletion is $(\rho-\rho_0)/n = 8/3\sqrt{\pi}\sqrt{\rho a_s^3} \simeq 1.5\sqrt{\rho a_s^3}$. In bulk 3D gaseous BECs, this fraction is small (since $\rho a_s^3 \ll 1$) and the quantum depletion typically amounts to 0.1% of the total atom number. It is obviously difficult to identify such a small fraction from fluorescence or absorption images. In order to enlarge the depleted fraction, a first experiment used a 3D optical lattice to increase the strength of the effective interaction [231]. But the identification of the quantum depletion from a bi-modal fit of the distributions suffers from some drawbacks. On the one hand, it is now well established that distinguishing the finite temperature contribution from the quantum depletion in the time-of-flight distribution of lattice bosons is rather difficult [117]. Our recent results on a system similar to that of [231] (see next section) confirm that a simple bi-modal fit (within the first Brillouin zone) yields a depleted fraction largely dominated by the thermal depletion [42]. On the other hand, the presence of the trap and the lattice does not allow for a quantitative comparison with the expected fraction from the Bogoliubov theory of homogeneous systems.

Another experiment was recently performed with a gas with tunable interaction in a box potential, permitting a direct quantitative comparison with the Bogoliubov prediction [135]. In this work, which I was involved in, the total depleted fraction was measured by coherently removing the atoms of the condensate with Bragg spectroscopy and the scaling of the depleted fraction with $\sqrt{na_s^3}$ was quantitatively verified. Importantly, it was demonstrated that the tuning of the scattering length (via a magnetic Feshbach resonance) is adiabatic within the precision of the implemented Bragg technique. This allowed establishing a limit on the finite-temperature contribution to the measured depletion and confirming that the larger part of the measured depletion was coming from the quantum depletion.

Momentum distribution associated to the quantum depletion and Tan's constant. In both the works [231, 135] there was no distinction between the contribution from finite temperature (thermal depletion) and that at zero temperature (quantum depletion). A possible way to distinguish thermal from quantum depletion is to look at the momentum distribution: the population of one-particle states yields different scalings with momentum $\mathbf{k}$ depending upon the type of fluctuations from which it originates (on the link between quantum depletion and quantum fluctuations, see the enlightening paper [170]). This can be seen easily by calculating the momentum distribution from Bogoliubov theory at finite temperature,

$$\rho(\mathbf{k}) = |v_{-\mathbf{k}}|^2 + (|u_{\mathbf{k}}|^2 + |v_{-\mathbf{k}}|^2)\langle \hat{b}^\dagger_{\mathbf{k}}\hat{b}_{\mathbf{k}}\rangle \tag{4.2}$$

with $\langle \hat{b}^\dagger_{\mathbf{k}}\hat{b}_{\mathbf{k}}\rangle = 1/[e^{\beta\varepsilon(\mathbf{k})} - 1]$ corresponds to the population of quasi-particles induced by the finite temperature. The finite temperature contribution contains a term $\langle \hat{b}^\dagger_{\mathbf{k}}\hat{b}_{\mathbf{k}}\rangle$ that adds a momentum dependence which modifies the scaling with momentum $\mathbf{k}$. At low momenta, the population associated with the quantum depletion $\propto 1/k$ while that induced by the temperature scales as $1/k^2$. At large momentum, the finite temperature contribution decays exponentially with $\mathbf{k}$ while the zero-temperature population scales as $1/k^4$. If one would measure the in-trap momentum distribution $\rho(\mathbf{k})$ over a few decades in density, it

would thus be possible to unambiguously identify the thermal and the quantum depletion through scalings with momentum k.

The $1/k^4$ scaling at large momentum k obtained in the Bogoliubov picture is identical to that predicted by S. Tan from considering two-body contact interaction in the s-wave channel [214, 213]. As a matter of fact, both the quantum depletion and the Tan prediction originates from the presence of two-body contact interaction and they are describing the same physics at large momenta! The Tan contact C is defined as

$$\lim_{k\to\infty} \rho(k) \times k^4 = \frac{C}{(2\pi)^3}. \tag{4.3}$$

While the k^{-4} scaling at large momentum is simply related the presence of contact interactions (the two-body wave-function decreases as $1/r$ at short inter-particle distances r), the value of C depends upon the many-body system under consideration. In addition, S. Tan demonstrated that the contact C is an important thermodynamical quantity entering universal relations. The Tan contact has thus become central in the many-body description of quantum gases and it is the object of experimental investigations with diverse many-body gaseous systems [208, 228, 186, 138, 78, 127]. We note that calculating the contact in weakly-interacting BECs from the Bogoliubov theory yields the same results as when using Tan's approach.

4.1.2 Observation of $1/k^4$-tails in the time-of-flight distribution of interacting BECs

After observing some first signals in the experiment, we accumulated thousands of atom distributions of 3D Bose-Einstein condensates released from the harmonic trap. The density profile after a time-of-flight $t_{\mathrm{TOF}} = 330$ ms is plotted in figure Fig. 4.2. A large dynamical in atomic density is obtained, yielding an unprecedented access to the extremely dilute tails at large momenta. We can identify three distinct contributions [44]:

- a central region of high density with anisotropic parabolic density profiles: the BEC;
- an intermediate region with spherical symmetry, a profile correctly fitted by a thermal Bose distribution and a total population and a width increasing when heating the gas, in agreement with the Hartree-Fock predictions: the thermal depletion;
- a high-momenta region with spherically symmetric trails decaying algebraically as $1/k^4$.

We made several observations related to the large momentum tails [44]. Numerically we have shown that they can not be explain at the mean-field level, even taking into account the full time-of-flight dynamics beyond the scaling solution for the expanding BEC [38, 113]. In the experiment we have found the presence of similar $1/k^4$-tails at different temperatures, suggesting that they are not originating from a finite-temperature effect. We have verified that the measured contact per particle increases with the in-trap condensate density. Unfortunately we could explore a range of condensate densities ρ_0 too small to be in the position of verifying the scaling of C with ρ_0. In addition, we have performed many tests with the He^* detector to rule out as many technical or spurious origin we came up with. We are not listing them here but we would like to mention two of them which we find important. Firstly, increasing the in-trap condensate density, we have observed $1/k^4$-tails with a larger amplitude while the detected condensate density on the He^* detector was decreasing. This observation rules out spurious effects of the He^* detector that

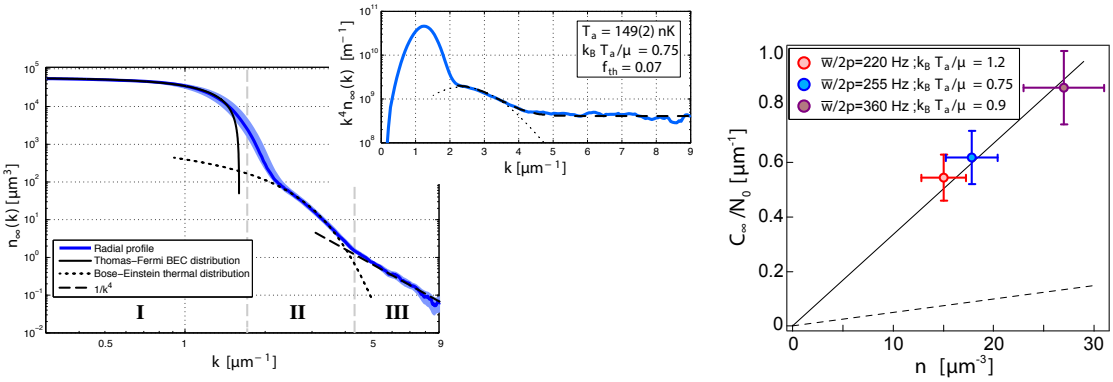

Figure 4.2: Observation of $1/k^4$-tails in the time-of-flight distribution of interacting BECs. Left: log-log plot of the asymptotic momentum distribution ρ_∞ measured in the experiment where 3 distinct regions can be identified: BEC (I), thermal cloud (II) and large momentum tails algebraically decaying. Center: plot of $\rho_\infty(k) \times k^4$. Right: measured amplitude C_∞ of the k^{-4}-tails per condensed particle N_0 as a function of the in-trap BEC density n_0.

would vary linearly with the detected density. Secondly, we have observed time-of-flight distributions of purely thermal gases decaying much faster than $1/k^4$, demonstrating the detector is capable of monitoring atomic densities decaying faster than $1/k^4$.

4.1.3 Origin of the observed tails: an open question

Quantum depletion. A central point in the discussion about the observed $1/k^4$-tails is the fact that we do not measure the in-trap momentum distribution when releasing a BEC from a 3D harmonic trap. When repulsive interaction are present during the time-of-flight, it is indeed well established that the central region of the atomic distribution is described by the scaling solution [38, 113], drastically differing from $\rho(\mathbf{k})$. Associating the $1/k^4$-tails to the quantum depletion requires that the tails of the TOF distribution reflect the in-trap momentum distribution. Unfortunately there is no beyond mean-field theory for the expansion of an interacting BECs. As a consequence, although many features were pointing towards associating the measured tails to the quantum depletion we have been cautious in our early paper [44]. Interestingly, our work has motived theory colleagues to consider the problem of the TOF dynamics from the point of view of the two-body contact.

Time-of-flight evolution of the contact. While the time-of-flight dynamics of a beyond mean-field BEC has yet not been solved, a theoretical work describing the TOF of the contact was published soon after we reported our measurement [175]. The Trento group demonstrated that the contact associated with two interacting particles adiabatically decreases to negligible values after a long time-of-flight. They also concluded that the contact in an interacting BEC should also decrease with the condensate density ρ_0 during the time-of-flight. The physical picture here is that the large momentum components in the many-body wave-function are evolving on a time scale much faster than that associated to the condensate density and are thus adiabatically following the decrease of ρ_0 during the time-of-flight. This work suggests that the $1/k^4$-tails we observed can not be directly related to the in-trap momentum distribution.

Prior to our work, it was shown that the contact in a unitary Fermi gas decreases after expansion when interactions are not tuned to zero during the time-of-flight [208]. This experiment corresponds to a regime different from ours: the interaction strength is extremely large and the population in the $1/k^4$-tails is almost 100 times larger. Nevertheless, this experiment also suggests that we can not relate the measured contact after time-of-flight with that expected in the trap. Therefore, associating the observed $1/k^4$-tails to the presence of in-trap two-body interaction would necessitate a violation of the condition of adiabatic following of the condensate density. We have been thinking along this line but we have not been able to find out a plausible scenario. We have thus kept performing some additional measures to further investigate the origin of the observed tails.

An effect associated to having a spin mixture. Early 2018 we have identified a novel signal in the experiment: the presence of a small fraction ($\leq 1\%$) of atoms in the $m_J = 0$ state in the optical dipole trap. This cloud of $m_J = 0$ atoms is extremely dilute and impossible to detect by absorption imaging. With the set of MCPs used in the work of [44] it could not be detected either because of a central region with a detection efficiency close to zero. The observation of $m_J = 0$ atoms became possible with a new pair of MCPs working properly. We have performed experiments aiming at identifying the contribution of the $m_J = 0$ cloud to the tails that we attributed initially to the $m_J = +1$ BECs. This identification turned out difficult but we made some observations that should lead us to a better understanding of the physical phenomenon from which the tails originate.

Detecting only the atoms in $m_J = 0$ with the He* detector is rather straightforward with the new MCPs: we do not apply a radio-frequency pulse after switching off the optical trap but use only a strong magnetic field gradient that displaces the $m_J = +1$ atoms away from the detector. Doing so we could establish that:

(i) in the presence of a BEC (in the $m_J = +1$ state), the $m_J = 0$ cloud exhibits large momentum tails compatible with a k^{-4} decay;

(ii) in the absence of a BEC, the $m_J = 0$ cloud does not have large momentum tails and it is well fitted with the distribution expected for a thermal gas;

(iii) the amplitude of the tails increases (close to linearly) with the atom number in $m_J = 0$ while it hardly changes with the BEC atom number [1].

In figure 4.3, we have reproduced the analysis performed in [44] for the new set of data for which the fraction of atoms $m_J = 0$ was reduced to 0.05%. Both the amplitude of the tails and its scaling with the BEC density are not compatible with the prediction for the in-trap quantum depletion of the BEC, clearly ruling out the possibility to associate the observed tails with the quantum depletion. We also note that the new set of data can be considered as an experimental verification of the prediction from our colleagues in Trento [175]: the measured amplitude of the tails is smaller than that expected in the trap for the quantum depletion of the BEC, which implies that the amplitude of the tails associated to the quantum depletion indeed decreases during the TOF dynamics.

These recent observations suggest that the large momentum tails are related to the simultaneous presence of a BEC of $m_J = +1$ atoms and of impurities of $m_J = 0$ atoms. In the

[1] In the first experiment [44], we modified the condensate density by varying the optical dipole trap depth. But we now have evidence that varying the ODT trap depth also varies the trapped atom number in $m_J = 0$. The variation of the tails amplitude observed in [44] was thus not deriving from modifying the BEC density but from actually varying the atom number in $m_J = 0$!

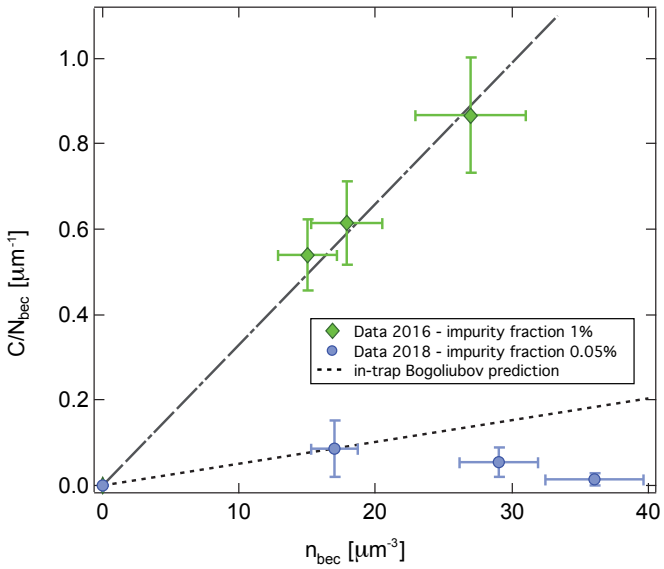

Figure 4.3: Amplitude of $1/k^4$-tails in the time-of-flight distribution of interacting BECs. Measured amplitude C_∞ of the k^{-4}-tails per condensed particle N_{bec} as a function of the in-trap BEC density n_{bec}. The two sets of data correspond respectively to that published in [44] where the fraction of the impurities was $\sim 1\%$ and to the new set of data taken with a lower fraction of impurities, $\sim 0.05\%$. The new data rules out the possibility to associate the observed tails with the in-trap quantum depletion of the BEC (majority atoms).

regime of our experiment, the mean-field potential of the BEC on the impurities is dominating the interaction and is expected to compensate the trapping potential for the $m_J = 0$ atoms, resulting in a flat potential for the impurities. Whether the $m_J = 0$ atoms may have algebraically decaying momentum tails in these conditions is yet not probable. Another origin for the presence of the tails is the TOF dynamics as atoms in $m_J = 0$ and $m_J = +1$ interact during the TOF. In particular, the $m_J = 0$ atoms will be accelerated by the mean-field potential created by the BEC. These different scenarios are under investigation as I write this manuscript.

4.1.4 Perspectives

A direction to go beyond the investigation of 3D BECs consists in investigating low dimensional gases. On the one hand, the physics of the s-wave contact interaction is predicted to produce k^{-4}-tails in low-dimensional gases as well [157]. For instance, we have recently investigated theoretically the contact in 1D Bose gases and predicted an interesting behavior of the contact with temperature: the contact exhibits a maximum value that provides an unequivocal signature of fermionization [232]. Measuring the contact of 1D bosons as a function of temperature would therefore be very interesting!

On the other hand, the time-of-flight dynamics of low dimensional gases drastically differs from that of 3D BECs and it is reasonable to think that the adiabatic decrease of the contact with the time-of-flight predicted in the 3D case will not occur [175]. Indeed, a new energy scale associated to the trapping frequency where the motion is frozen in low dimensional gases is present and exceeds by far any other energy scales. As a consequence, the TOF dynamics is not governed by interaction (as in the scaling solution for 3D BECs

[38, 113]) and the in-trap momentum distribution along the axis of the system can be accessed in a TOF experiment. Under these conditions, the observation of k^{-4}-tails could be related to a measurement of the in-trap contact. When successful, the measurement of the contact in 1D Bose gases could be the starting point to investigate out-of-equilibrium dynamics, for instance performing an interaction quench (by modifying the transverse trapping frequency) as suggested in [37].

4.2 Single-atom-resolved probing of lattice gases in momentum space

In this section, we discuss the first measurements we performed with lattice gases. The central objective here is to validate the possibility to measure the momentum-space distribution of lattice gases with our approach. Although one can often read that time-of-flight images of quantum gases provide access to the momentum distribution, this is often not strictly the case, especially in three-dimensions, as the requirements to be met are difficult to reach in practice. The effect of the presence of interaction during the time-of-flight may also strongly affect the TOF dynamics, as in the case of a 3D harmonically-trapped BEC (see section 4.1). We will first discuss the conditions necessary to obtain the in-trap momentum distribution in a time-of-flight experiment. We will then present the benchmarking we performed of our apparatus with lattice superfluids, demonstrating to access the momentum-space distribution. Finally we will illustrate the capabilities offered by our technique.

4.2.1 Accessing the momentum space in time-of-flight experiments

A ballistic expansion. The basic idea of time-of-flight experiments is to map the final position of the atoms (the quantity that is measured!) onto their momentum in the trap. Assuming (i) that the trap is switched off on a time scale much shorter those associated to the energies in the problem and (ii) that interaction are negligible during the time-of-flight dynamics, one can use the ballistic relation

$$\hbar\mathbf{k} = \frac{m}{t_{\mathrm{TOF}}}\mathbf{r}(t_{\mathrm{TOF}}) \tag{4.4}$$

to associate an initial momentum $\mathbf{k}$ to a given measured position $\mathbf{r}$ after a time-of-flight t_{TOF}. When atoms are released from optical potentials, the switching off takes place on the order of one micro-second (or less) ensuring the first condition to be fulfilled. In our apparatus, both the crossed dipole trap and the optical lattices are switched off within one micro-second. The second condition – negligible interaction during the time-of-flight – is less obviously to fulfil, except if one deals with a non-interacting gas. The following paragraphs describe situations where the interaction are non-zero instead.

One possibility to avoid the effect of interactions on the TOF dynamics is to tune the interacting strength a_s to zero when the atoms are released from the trap. In principle, a_s should be instantaneously set to zero but since a_s is (often) tuned with a magnetic field, one implements a (fast) ramp of finite duration in the magnetic field [208, 142, 78]. This results in the presence of some corrections to in-trap momentum distributions (for instance the value of the contact measured in [208] was corrected by 10%). Although not perfect, this

technique has shown to work relatively well. On the other hand, there exist atomic species for which Feshbach resonances are not accessible to tune the scattering length before the time-of-flight. This is the case of metastable Helium ^{4}He*. In order for the ballistic to hold when interaction are not switched off, one can rely on the presence of trapping frequencies whose associated energies largely exceed the mean-field interaction energy. When a trapping frequency $\omega_T/2\pi$ is much larger than the chemical potential μ, $\hbar\omega_T \gg \mu$, the wave-function along this axis expands on a time scale $\sim 1/\omega_T$. As a consequence the gas dilutes on a time scale much shorter than that associated to the interaction-driven dynamics. To a good approximation, the rapid expansion along the strong trapping axis thus amounts to an effective suppression of the interaction. This situation is met when low-dimensional (1D and 2D) gases are created but also when atoms are released from an optical lattice of sufficiently large amplitude (and low lattice filling) so that the trapping frequency of a single site is large enough [84].

Even in the situation where the time-of-flight dynamics is driven by the single-particle expansion of the wave-function, the presence of an interaction energy in the trap implies, by conservation of the total energy, a modification of the time-of-flight distribution with respect to the in-trap momentum distribution. In low dimensional systems (1D or 2D), the interaction energy is distributed in the confined direction(s). In a 3D lattice, the on-site interaction energy is smoothly varying along the trap in the superfluid phase. When the trap is switched off, the wave-function of each lattice site expand freely (see previous arguments) before it overlaps with the wave-function of adjacent sites. A different filling factor from one site to the other leads to a phase difference between the wave-functions of the different sites when they overlap. In turn, this phase difference accumulated during the early time of the expansion reflects itself in the long time distribution as a modification of the interference pattern. For typical scattering lengths, a low filling factor condition ensures that the associated modification of the time-of-flight distribution with respect to $\rho(\mathbf{k})$ is extremely small, as shown in [126].

Finally, we should mention that the above reasoning based on energy scales applies at the mean-field level. In turn, it does not allow one to exclude that collisions between two particles are negligible. Moreover, when a BEC is released from an optical lattice, several copies of the BEC – corresponding to the different peaks of the interference pattern observed in TOF – are separating with a large relative velocity, of the order of the recoil associated to the lattice. It is thus probable that two-body collisions occur in this situation. When present, two-body collisions between ultra-cold bosons manifest by the presence of a scattering halo in the TOF distributions, as a result of elastic s-wave scattering. These scattering spheres were observed in different experiments (see for instance [48, 215, 167]). The large dynamical range in density that the He* detector probes is well adapted to reveal faint halos if present. As we shall present later in this chapter, we have recently characterized the presence of two-body scattering in our experiment.

The far-field condition. Assuming that the gas expands ballistically, the in-trap momentum distribution $\rho(\mathbf{k})$ can be measured if the time-of-flight is long enough to have all the momentum components fully developed. To illustrate this statement, let us first recall that the free propagation of the atomic wave-function ψ writes [169]

$$\psi(\mathbf{r},t) = \mathrm{e}^{-3i\pi/4}\left(\frac{m}{2\pi\hbar t}\right)^{3/2}\int d\mathbf{r}'\ \mathrm{e}^{im(\mathbf{r}-\mathbf{r}')^2/2\hbar t}\ \psi(\mathbf{r}',t=0) \tag{4.5}$$

This formulation with the Feynman propagator is in close analogy with the propagation in optics within the paraxial approximation,

$$E(\boldsymbol{\rho},z) \simeq \frac{1}{4\pi z}\int d\boldsymbol{\rho}'\, e^{ik(\boldsymbol{\rho}-\boldsymbol{\rho}')^2/2z}\, E(\boldsymbol{\rho}',z=0) \tag{4.6}$$

where the the atomic wave-function is replaced by the electric field and the time of expansion t by the distance z that light has propagated. For instance, in both integrals the phase term quadratic in r' decays with the propagation (like $1/t$ or $1/z$) faster than the phase term linear in r'. As a result, one can distinguish two regimes of propagation. At short time t (or distance z) the phase in the integral depends on both the linear and quadratic terms in r': this is the Fresnel regime of propagation. At long time t (or distance z) the phase is linear in r' and the integral yields the Fourier transform of the field $\psi(\mathbf{r},t=0)$ (or $E(\boldsymbol{\rho},z=0)$): this is the Fraunhofer regime of propagation. The Fourier transform appears explicitly noting that the phase term linear in r' writes $e^{-i2m\,\mathbf{r}.\mathbf{r}'/2\hbar t} = e^{-i\,\mathbf{k}.\mathbf{r}'}$, introducing the momentum $\mathbf{k}$ associated to the position $\mathbf{r}$ after a time-of-flight t.

In close analogy with the Fresnel number in optics, one can introduce a far-field time t_{FF} such that when $t/t_{\mathrm{FF}} > 1$ the atomic distribution is, to an excellent approximation, equal to the initial momentum distribution. The passage from the Fresnel to the far-field (Fraunhofer) regime of propagation is continuous but one can define the far-field time as

$$t_{\mathrm{FF}} = \frac{mr_0^2}{2\hbar} \tag{4.7}$$

which ensures that the time-of-flight distribution $\rho(\mathbf{r},t_{\mathrm{tof}})$ differs from $\rho(\mathbf{k})$ (using the ballistic relation) by less than 10^{-3} for $t > t_{\mathrm{FF}}$. We illustrate this aspect in figure Fig. 4.4 for a coherent atomic matter-wave released from an optical lattice of spacing a.

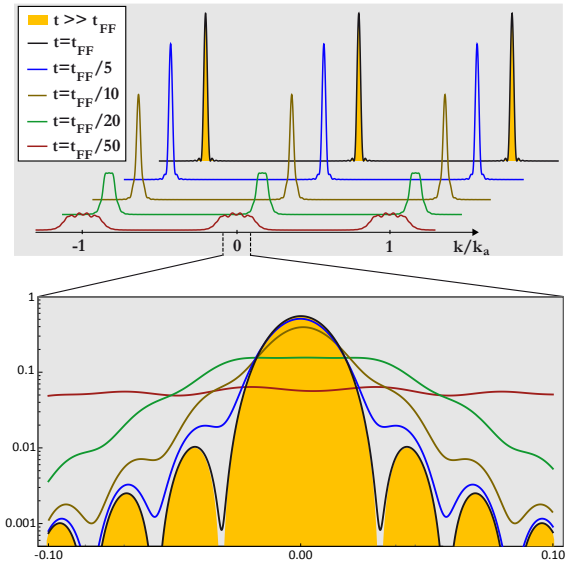

Figure 4.4: Illustration of the condition to reach the far-field regime in TOF. Top: Time-of-flight distributions of a coherent matter-wave released from an optical lattice in the absence of interaction. When $t \simeq t_{\mathrm{FF}}$, the TOF distribution matches the in-trap momentum distribution at the 0.1% level of accuracy.

In practice, the far-field condition given by Eq. 4.7 exceeds the capabilities of most of the existing experimental apparatus because it requires probing the gas when it is extremely

dilute, a situation for which optical imaging techniques are not well suited. Assuming that one aims at measuring the momentum distribution (between $-1.5k_a$ and $+1.5k_a$) of a 3D bosonic lattice superfluid extending over 60 sites, the following far-field time and field of view are required:

Species	λ (μm)	t_{FF} (ms)	Field of view (cm)
^{4}He	1.55	68	2.6
^{7}Li	1.064	56	1.8
^{39}K	1.064	310	1.8
^{87}Rb	1.064	691	1.8

Apart from the long time-of-flight required when using heavy atomic species, the most stringent difficulty for 3D lattice gases lies in the large volume (of centimeter distances) one needs to probe. The diluteness of the gas under these conditions renders extremely difficult the use of optical imaging. For instance, a large time-of-flight can be obtained even with massive atoms like Rubidium thanks to a 3D levitation as demonstrated in the group of V. Josse at Laboratoire Charles Fabry [111]. But an accurate imaging of the density is obtained for ultra-cold gases which extends over 0.5 mm only (even after a 0.5 s time-of-flight). On the contrary the possibility to probe metastable Helium gases over centimeter distances thanks to the electronic detection (see chapter 3) is perfectly suited for the purposes of detection in the far-field. In [42] we have shown the evolution of the measured density profiles during time-of-flight which indicates that we reach the far-field regime of expansion with the He* detector.

Probing 3D lattice gases in 3D. In our experiment, we have measured the far-field distribution of metastable Helium atoms loaded into a 3D optical lattice [42]. An example of such a distribution is shown in figure 4.5. The number of lattice sites populated is typically 50 along each direction, yielding an initial size $r_0 = 50a = 50\lambda_L/2 \simeq 38.75$ μm where the lattice wavelength is $\lambda_L = 1550$ nm. The associated far-field time is $t_{\mathrm{FF}} \simeq 50$ ms, much shorter than the time-of-flight we used, $t_{\mathrm{TOF}} = 330$ ms, thus ensuring that the distributions we measure are deep in the far-field regime of propagation. To our knowledge, our measurement is the first one performed with $t_{\mathrm{TOF}} \gg t_{\mathrm{FF}}$. This allows us to compare the density profile with QMC calculations over 4 orders of magnitude.

Finally we should stress that in the regime of moderate (or higher) lattice amplitude and low filling (<2 atoms per site) we do not observe any scattering halo over this large range of densities. This implies that the number of scattering event is extremely small, in other words that two-body collisions seem negligible within the experimental uncertainties. To be more quantitative here, we have recently conducted a series of experiment in the regime of large lattice filling (up to 7 atoms/site) in order to observe the scattering spheres associated with two-body collisions. We have observe the scattering spheres and extracted from their analysis the number of collisions. In addition we have introduced a classical model of colliding clouds to predict this number of collisions, as first introduced in [237, 236], and we obtained a good quantitative agreement with the measured values (see Fig. 4.6). From extrapolating the measured number of collisions at large filling using the predictions of the classical model, we conclude that the number of collision per atom in the regime of unity filling is as low as 10^{-4}, confirming that it can be safely neglected.

Apart from probing the far-field, the use of the He* detector is also of particular interest for lattice gases because it allows us to reconstruct the 3D atom distributions. Since

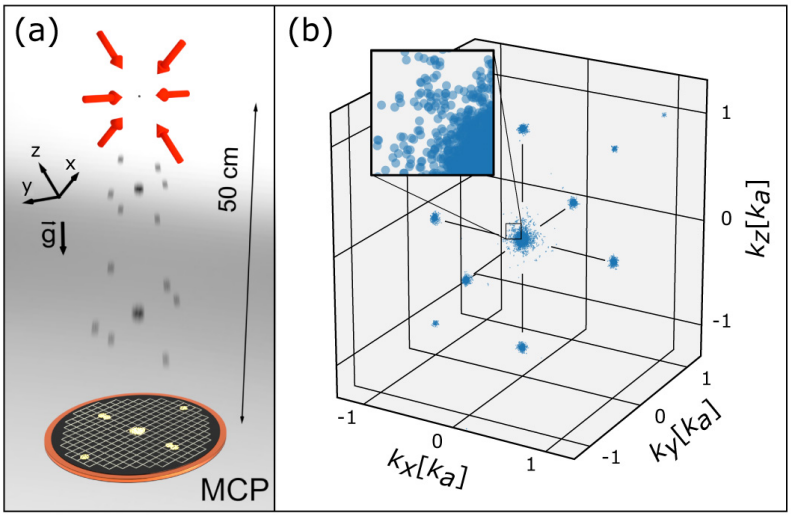

Figure 4.5: 3D atom distributions of lattice gases after a long time-of-flight. **(a)** Sketch of the experiment. A ^{4}He* BEC is loaded into a 3D optical lattice (red arrows). When the lattice is abruptly switched off, the gas falls under gravity and hits the He* detector after 50 cm of free fall. The diffraction peaks of the lattice superfluids can be seen on the detector. **(b)** 3D atom distribution of metastable Helium lattice gases as reconstructed in the experiment. Each blue dot is a single atom.

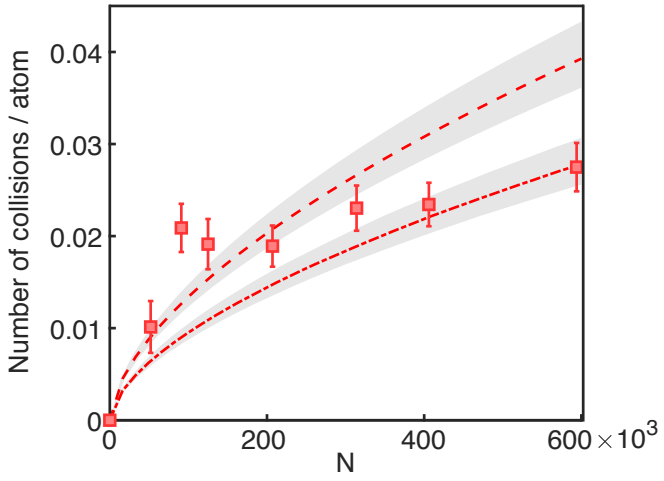

Figure 4.6: Two-body collisions during the TOF dynamics of lattice superfluids. Measured number of collisions per atom during the expansion of lattice superfluid with a large lattice filling, as a function of the total number of atoms in the 3D lattice. The dashed (*resp.* dotted-dashed) line is the expectation from an ab-initio classical model of colliding atoms without (*resp.* with) taking into the mean-field effects during the TOF dynamics.

the time-of-flight distribution from the lattice does not have a symmetry permitting to use inverse Abel transforms, column-integrated 2D distributions as obtained from optical imaging goes with loosing information about the 3D distribution that cannot be obtained by post-processing the data.

4.2.2 Benchmarking the experiment with the Bose-Hubbard hamiltonian

Comparing the experimental data with in-trap momentum distributions. In the previous paragraph we have put forward a series of arguments to justify the possibility of measuring the 3D momentum distribution of lattice gases. Here we would like to actually verify with the measured experimental data the validity of these statements. Since we aim at investigating strongly correlated quantum matter in optical lattice, we have to validate our approach in a regime where correlations are large enough but where theoretical models are beyond doubt. Note that there exists no analytical solution for 3D correlated lattice models and one has to rely on numerical calculations. We thus decided to build upon the seminal work of Trotzky et al. [222] where it was demonstrated that ultra-cold bosons loaded into a 3D cubic optical lattice realize the Bose-Hubbard hamiltonian H_{BH} which can be solved thanks to ab-initio Quantum Monte-Carlo (QMC) approaches, with

$$H_{\mathrm{BH}} = -J\sum_{j,l}(b_j^\dagger b_l + \mathrm{h.c.}) + \sum_j \frac{U}{2} n_j(n_j-1) + \sum_j \frac{m\omega_{\mathrm{T}}^2 a^2 j^2}{2} n_j \tag{4.8}$$

where b_j is the annihilation operator associated with site labelled j and $n_j = b_j^\dagger b_j$.

Our starting point is to assume that our experiment is described by the Bose-Hubbard hamiltonian. Then the benchmarking of the atom distributions measured with the He* detector relies on the comparison between the experimental data $\rho(\mathbf{r},t_{\mathrm{TOF}})$ and ab-initio QMC calculations of the in-trap momentum distribution $\rho(\mathbf{k})$. It is of primary importance to stress that we compare the experiments with calculations of the in-trap momentum distributions $\rho(\mathbf{k})$. We thus make no assumptions about the time-of-flight dynamics, in particular regarding the role of interaction or the duration of the time-of-flight. Our approach is different in nature from that used by Trotzky et al. [222] where the authors calculated the in-trap density distribution $\rho(\mathbf{r},t=0)$ with QMC and simulate a small time-of-flight (15 ms) assuming that interactions are negligible in the TOF dynamics.

The BEC transition in the QMC calculations. The ab-initio QMC calculations were performed by our colleague G. Carleo (ETH Zurich). They are based on the Worm algorithm introduced by Pollet et al. [173] and adapted to our objectives (see Supplementary material of [42]). We will not detail the principle of these numerics here. The calculations take into account the presence of the trap as well as the finite temperature. They are performed with the parameters calibrated on the experimental apparatus (atom number, lattice parameters, trap frequencies), except for the temperature – not measured in the experiment – which is the only adjustable parameter in the comparison with the numerics. It is interesting to mention that the atoms occupy about $50 \times 50 \times 50$ lattice sites in our experimental conditions and that running the calculations for one set of parameters (atom number, trap frequencies, ..) with a varying temperature T (about 10 values of T) takes 50 years of CPU time... which fortunately turns into a few hours on the ETH cluster in Zurich!

In figure Fig. 4.7 we plot the QMC distributions across the BEC transition with all experimental parameters but the temperature being fixed. The momentum distribution evolves from a low-temperature situation where the diffraction peaks associated to the condensate are extremely visible (note that Fig. 4.7(a) is in log scale) to the high-temperature regime where the distribution is rather flat. While the opposite regimes $T \ll T_c$ and $T \gg T_c$ can be obviously identified, the critical temperature T_c can not simply be extracted from

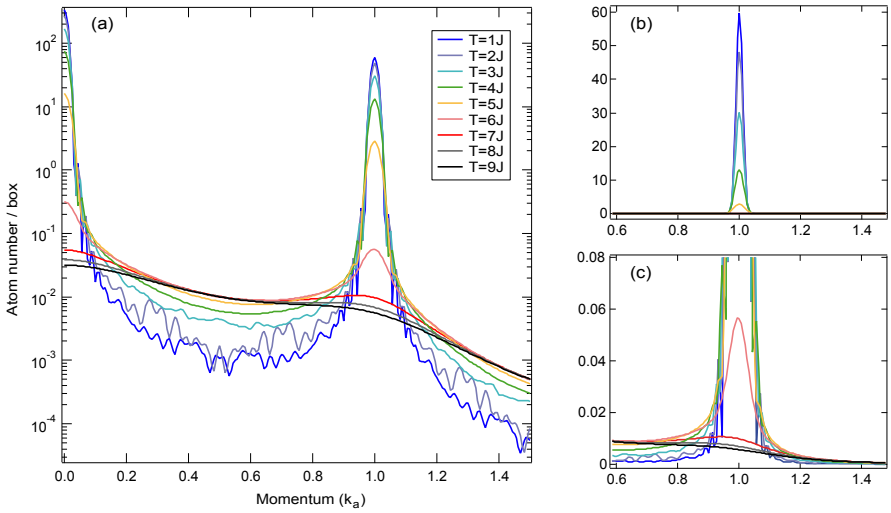

Figure 4.7: n(k) across the condensation transition calculated by the Quantum-Monte Carlo approach. 1D cut through the 3D momentum distributions obtained from ab-initio QMC calculations. All the parameters but the temepature T are fixed. The different panels correspond to different plots of the same quantity.

the presence of diffraction peaks. It was indeed shown in [117] that some phase coherence present above T_c leads to the presence of diffraction peaks also above T_c. On the contrary, the presence of a condensate (below T_c) signals itself by a sharp increase of $n(\mathbf{k})$ while a normal fluid exhibits a smooth distribution, as we illustrate in Fig. 4.8. We would like to stress here that the sharpness of the diffraction peaks that signals the presence of a condensate can be identified only from the 3D in-trap momentum distribution. If one considers two of the main drawbacks associated to time-of-flight distributions as measured prior to our work, namely a too short time-of-flight and the use of column-integrated 2D images, the sharpness is washed out close to T_c: on the one hand, the diffraction peaks slowly develop during t_{TOF} as we explained before and sharp features can only be observed in the far-field regime (see Fig. 4.4); on the other hand, the integration along of a line of sight obviously leads to some averaging that smoothes the 3D distributions.

Comparison between experiments and QMC distributions. In both the experiment and the QMC numerics we obtain 3D atom distributions. We compare 1D cuts through these distributions in figure 4.9. To take into account the efficiency of the detection process, we rescale the experimental data by matching the height of the first-order diffraction peak obtained from the QMC calculations. We find a temperature T (here $T = 3.9J$) that allows us to match the experimental and QMC profiles over 4 orders of magnitude in density. In particular, the width of the diffraction peaks are in excellent agreement, demonstrating that we probe the gases in the far-field regime of expansion. In addition, this confirms that interaction are not playing a significant role in the time-of-flight dynamics. We conclude from this comparison that the 3D atom distributions we measure with the He^* detector are equal to the in-trap momentum distributions to an excellent approximation. In the comparison with QMC calculations, the temperature T is the only adjustable parameter. The other quantities (atom number, trap frequencies, ..) were calibrated on the apparatus and their average value was used in the numerics. We have investigated whether modifying the calibrated parameters within their error bars could

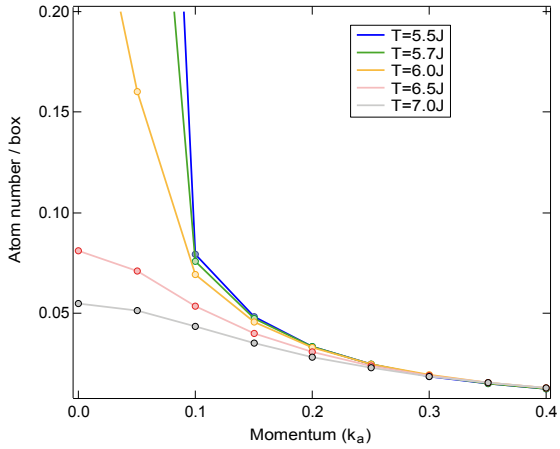

Figure 4.8: Observation of the critical temperature in the QMC distributions $n(\mathbf{k})$. As introduced in [117], the presence of diffraction peaks is not a sign of the transition by itself as some phase coherence is present above T_c. But the presence of sharp diffraction peaks as opposed to a smooth distribution signals the critical temperature of the BEC transition. Here the critical temperature lies between $T = 6J$ and $T = 6.5J$.

significantly modify the comparison and we found that they hardly affect the measured signals as compared with the effect of the temperature.

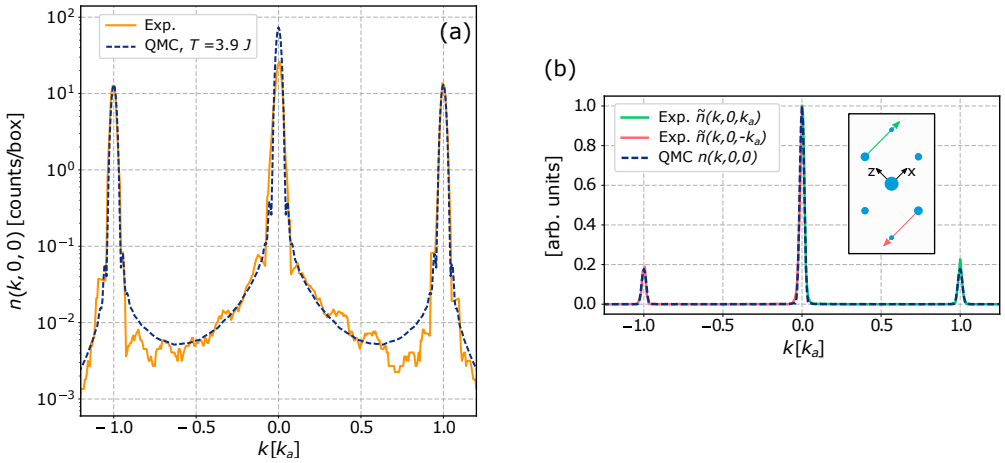

Figure 4.9: Comparison between experimental and QMC profiles. **(a)** Log-plot of 1D cuts $n(k,0,0)$ through the measured 3D distribution $n(\mathbf{k})$ (orange), and through the QMC momentum distribution (dashed line). The temperature T is the only adjustable parameter. The measured amplitude of the central peak is slightly affected by a saturation of the He* detector. **(b)** 1D cuts $\tilde{n}(k,0,\pm k_a)$ compared to the QMC profile $n(k,0,0)$. The height of the central peak of these distributions has been normalized to one. Saturation effects are not present on the first- and second-order peaks of diffraction.

One could question our approach that leaves the temperature as a fitting parameter. It would be obviously better to measure the temperature by other means in the experiment and perform a fully ab-initio comparison with QMC calculations. The choice we made derives from two facts. Firstly, to our knowledge there exists no technique which allows to measure the temperature of lattice superfluids. Quantum gas microscopes have permitted

to monitor the atom number fluctuations per lattice site and extract the entropy (and, in turn, the temperature) in the Mott state [199]. This approach is adapted to a Mott state where the fluctuations of atom per site is given by the finite temperature of the gas but it can not be used in the superfluid regime. Secondly, one can evaluate the temperature of the lattice gas by measuring T prior to loading the atoms into the lattice and assuming the loading to be adiabatic. This approach was used in [222]. But while it provides the correct range of temperature, relatively large error bars of ~30% were found when comparing to the QMC calculations. The authors of [222] could attribute a part of the discrepancy to heating mechanisms present in the lattice but it is also clear that it would be extremely difficult to evaluate the temperature in the lattice within a 10% error. For this reason, we considered that using this approach would allow us to be quantitative at a sufficiently good level of precision.

4.2.3 Condensed fraction across the BEC transition in a cubic lattice

Momentum distribution of lattice superfluids. In the correlated superfluid phase, two distinct contributions can be identified in the momentum distribution [117], that of the condensate $\rho_0(\mathbf{k})$ and that of the depleted atoms $\rho_{\mathrm{NC}}(\mathbf{k})$ (both quantum and thermal depletion),

$$\rho(\mathbf{k}) = \rho_0(\mathbf{k}) + \rho_{\mathrm{NC}}(\mathbf{k}). \tag{4.9}$$

The condensate has long-range phase coherence and $\rho_0(\mathbf{k})$ has a Fourier-limited width $\sim 1/L$. On the other hand, $\rho_{\mathrm{NC}}(\mathbf{k})$ is a smoothly varying distribution with a typical momentum width $\sim 1/a$ given by the lattice density of state. This results from the population of all quasi-momentum states by the quantum depletion at $U/J = 9.5$ and by the thermal depletion at non-vanishing temperatures. For large trapped systems $L \gg a$, n_0 and ρ_{NC} thus clearly separate in the momentum space with the condensate manifesting as sharp peaks on top of the broad distribution of depleted atoms [117]. For the first time we are in the position to exploit quantitatively this separation of scales in momentum space. Previous experiments have indeed observed this separation but the measurements were not performed in the 3D momentum space which is required for a quantitative analysis. From the original signals we monitor, we have calibrated the temperature and measured the condensed fraction. In the following we should explain how we proceeded.

Our thermometry method. To determine the temperature of the lattice gases, we use the comparison with QMC, inspired by the pioneering work of [222]. We have chosen to introduce a single parameter,

$$r_T = \rho(k_a, 0, 0)/\rho(k_a/2, 0, 0) \tag{4.10}$$

to be matched with QMC numerics. The choice of the quantity r_T derives from the fact that the population of finite momentum states strongly depends on the temperature T (see Fig. 4.7). In the regime of the experiment, r_T varies by 4 orders of magnitude when T increases only by a factor 3, yielding an unprecedented precision in the calibration of the temperature. Using a controlled heating sequence, we have varied the temperature in the experiment at a fixed $U/J = 9.5$. By comparing the measured r_T with the thermometry curve we obtain T with a 5% uncertainty, limited by the experimental uncertainty on the atom number. In Fig. 4.10 we also show comparisons of the measured 1D cuts $\rho(k, 0, 0)$

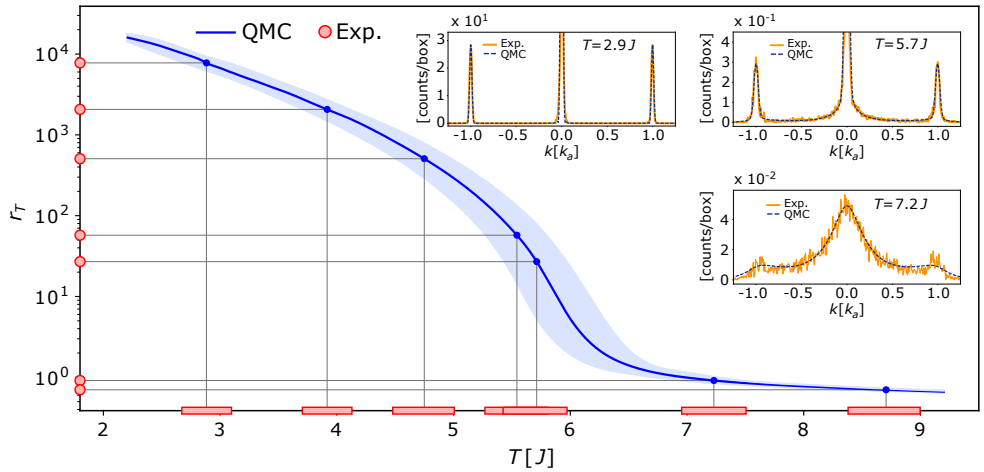

Figure 4.10: Thermometry of lattice superfluids. Plot of the ratio $r_T = \rho(k_a, 0, 0)/\rho(k_a/2, 0, 0)$ as a function of the temperature T as extracted from the QMC calculations (solid blue lines). The measured r_T (red dots) are compared with the thermometry curve to extract the temperature in the experiment (red rectangles on the temperature axis). The blue shaded area takes into account the uncertainty in the experimental atom number. The width of the rectangles depicts the corresponding error in determining the temperature. Three experimental 1D cuts $n(k, 0, 0)$ corresponding to $T = 2.9J, 5.7J$ and $7.2J$ are also shown along with the QMC calculations.

with QMC calculations performed at the temperature obtained from the measurement of r_T. The excellent agreement over the entire range of temperatures validates the thermometry method. The thermometry curve plotted in Fig. 4.10 applies to the Bose-Hubbard hamiltonian (with our parameters) and is model-dependent. But the central idea of the method – probing low-energy excitations, the population of which strongly varies with the temperature – can be generalized to a large variety of Hamiltonians.

Extracting the condensed fraction. The condensed fraction f_c is a central quantity to investigate finite-temperature phase diagrams [77]. But measuring f_c in many-body systems is notoriously challenging as the strong interactions make it difficult to probe the population of single-particle states and access $\rho(\mathbf{k})$. Techniques like neutron scattering in liquid Helium indeed fail to separate the condensate from the depleted atoms [130] while Bragg spectroscopy in strongly interacting bulk gases necessitates switching off the interactions [135]. In lattice systems, the time-of-flight dynamics driven by the single-particle expansion from each lattice site should allow to access $\rho(\mathbf{k})$. As discussed previously, the appearance of the condensate is associated with a sharp peak (of width $\sim 1/L$) appearing on top of a smooth distribution (with a peak of width $\sim 1/a$) [117]. In large systems where $L \gg a$, this distinction can be clearly identified. In Fig. 4.11(a) we show the occurrence of a sharp peak around $k \simeq 0$ that is associated with the condensate. Measuring the condensed fraction f_c thus amounts to measuring the atom number N_{peak} in the condensate peaks with respect to the total atom number N, $f_c = N_{\text{peak}}/N$. Here we make the assumption that $N_{\text{peak}} \simeq N_0$ with N_0 the number of condensed atoms and $N = N_0 + N_{\text{NC}}$. This assumption relies on the inequality $L \gg a$ which ensures that the fraction of depleted atoms contained in the sharp peaks of size $1/L$ is extremely low, of order $(a/L)^3$. We note that in the critical

region of the Mott transition this approach may fail as the condensate peak is not expected to be very sharp in k-space as a result of strong correlations.

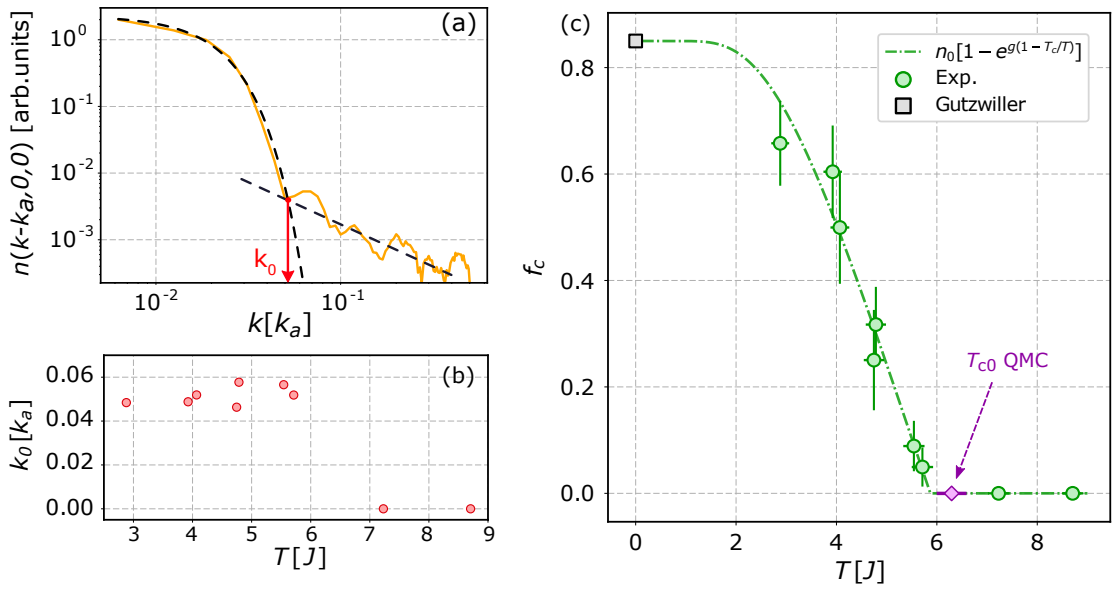

Figure 4.11: Condensed fraction of lattice gases across the BEC transition. (a) Extracting the momentum k_0 associated to the edge of the condensate mode in momentum space. (b). Momentum k_0 as a function of the temperature T calibrated from the comparison with QMC calculations. (c) Condensed fraction f_c measured in the experiment as a function of T/J.

In the experiment, the large dynamical range in density provided by the He* detector allows us to fit the tails associated to the depletion of the condensate and identify k_0 accurately. A similar approach would result difficult from column-integrated images as obtained when probing quantum gases with absorption imaging. The variation of the extracted k_0 with T is plotted in Fig. 4.11(b). We then use the full 3D distribution to count the fraction f_c of atoms of the first Brillouin zone contained in a sphere of radius k0 centered on $\mathbf{k} \simeq 0$. We plot f_c as a function of T in Fig. 4.11(c). In the absence of a theoretical model, we extract the critical temperature using an empirical function [176], obtaining $T_c = 5.9(2)J$. This approach allows us to observe the onset of BEC in a deep lattice with unprecedented resolution. We note that the ab-initio QMC calculation of the condensed fraction in a trap is possible and it would be interesting to compare the numerical results to our measurements [172]. But these calculations require using special techniques [176] to efficiently solve the problem in a system as large as that of our experiment ($50 \times 50 \times 50$ lattice sites) and we have not done it. On the contrary we have compared the extracted T_c to the thermodynamic limit of a homogeneous system with a chemical potential identical to that at our trap center. It is interesting that the two temperatures are matching within error bars, showing that the BEC transition first occurs at the trap center and that the trapping frequency is small enough not to affect too much the critical temperature (in our experiment $m\omega^2 a^2/2 \simeq 0.02J$).

Two-particle momentum correlations in lattice superfluids. We have mentioned the celebrated atomic analog of the Hanbury-Brown and Twiss effect where a bunching phenomenon was observed in the TOF distribution of a thermal gas, *i.e.* an incoherent

source [192]. In the previous chapter (see Chap. 3, we have shown HBT signals observed with our apparatus when the gas was released from a harmonic trap. We recall that in the absence of interaction, the physical picture is rather simple [87]. In a thermal gas, several eigenstates are populated by the finite temperature and these modes interfere during the TOF expansion to give rise to a bosonic bunching, similarly to the celebrated Hanbury-Brown and Twiss experiment. In a pure ideal BEC, a single momentum state is populated and no interference can occur, leading to a flat two-particle correlation function. This difference between a thermal population of bosonic modes above the critical temperature T_c and that of a Bose-Einstein condensate below T_c has been observed in many cold atom experiments [192, 161, 62, 166, 61] and also in similar regimes with light beams [6], polaritons [115, 9] and photonic condensates [194]. All these measurements have been conducted in a regime where interactions are weak, or even zero in the case of photons. Interestingly, our observation of the condensation phenomenon in the 3D lattice permits to investigate the HBT phenomenology in the presence of strong interactions ($U > T$).

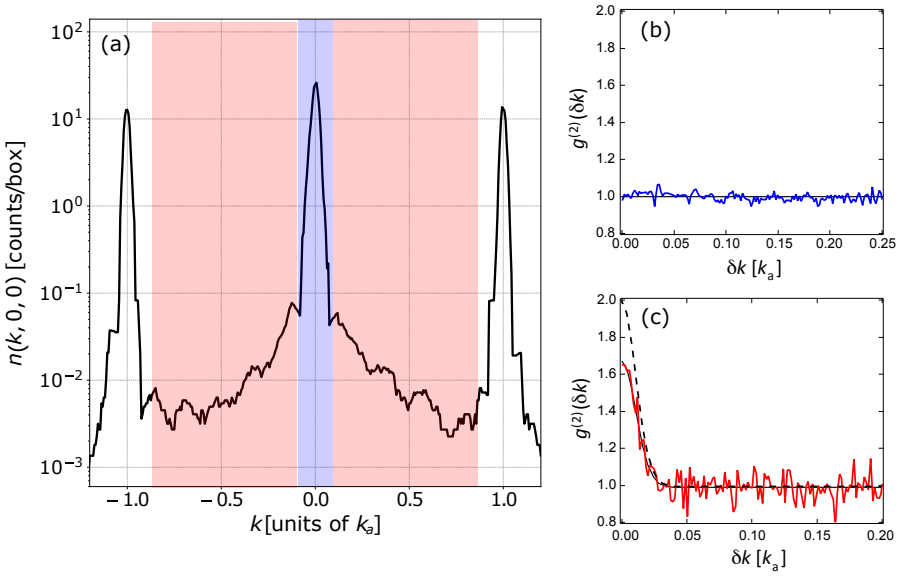

Figure 4.12: Two-particle momentum correlations in lattice superfluids. (a) 1D cut through the 3D momentum distribution of lattice superfliuds. The blue area corresponds to the condensate mode while the red area to the other modes populated by the quantum and thermal depletion. (b) Second-order correlation function $g^{(2)}$ in the condensate as a function of particle distance δk (blue area in (a)). (c) Second-order correlation function $g^{(2)}$ in the depleted cloud as a function of particle distance δk (red area in (a)).

From the measured atom distributions, we have extracted the two-body correlation function $g^{(2)}(k, k') = g^{(2)}(\delta k)$ of finding two particles distant by δk. In addition, measuring the in-trap momentum distribution – as opposite to the TOF distributions of harmonically-trapped BECs – allows us to separate the mode of the condensate from the other modes as they hardly overlap spatially. As introduced earlier, this permits a measurement of the condensed fraction. For the two-body correlations, it allows us to calculate $g^{(2)}$ in the condensate mode and in the other modes separately, as illustrated in Fig. 4.12. One interesting feature is that such a measurement can be conducted down to extremely low temperature where the condensed fraction is very large. For similar condensed fraction (say more than 70%), the TOF distribution of a 3D harmonically-trapped BEC extends over the thermal cloud almost entirely as a result of the mean-field interaction during the TOF, prohibiting

the access to calculating $g^{(2)}$ in the thermal component. This is similar to the situation above laser threshold where the correlation between the few spontaneous photons is hidden by the laser mode.

As expected, we find that there is no bunching in the condensate while bunching is observed in the depleted cloud where many modes contribute. Fitting the measured two-body correlation function with a Gaussian, we extract the two-body correlation length l_c defined as $g^{(2)}(\delta k) = 1 + \exp[-\delta k^2/l_c^2]$. This two-body correlation length l_c of the depleted cloud can be compared with existing HBT predictions for a thermal gas of bosons [87]. In the case of ideal bosons for which the Wick theorem applies (because the Hamiltonian $H = \sum_k \hbar\omega(k)a^\dagger(k)a(k)$ is quadratic in the momentum degree of freedom), one expects $g^{(2)}(\delta k) = 1 + |g^{(1)}(\delta k)|^2$. In addition, the phase coherence of a thermal gas at sufficiently large temperature ($T > T_c$) is short-range and the gas can be considered as incoherent. Under these assumptions (non-interacting and phase-incoherent bosons), ideal thermal bosons in a harmonic trap have $l_c = 1/\sigma$ where σ is the RMS size of the gas in the trap [192, 87, 61]. Interestingly we find in our experiment that the measured l_c lies systematically below $1/\sigma$, even when to estimate σ we use the in-trap density profile calculated from QMC which takes into account the modification of the in-trap profile as a result of interaction. This deviation from the usual HBT picture for ideal thermal particles is currently the object of investigation. We do not yet have an explanation of the measured l_c in the interacting depleted cloud but two comments are due here. Firstly, all the measurements are performed with the on-site interaction U being larger than the temperature k_BT. This is the case even for the data sets above the critical temperature for BEC, $U > k_BT > k_BT_c$. It appears then reasonable that interactions should be accounted for and that the assumption of ideal bosons is not correct in the regime of the experiment. Secondly, to account for interactions and to recover Wick theorem, one can use the Bogoliubov approximation: the Hamiltonian becomes quadratic in the quasi-particle operators and Wick theorem applies for these quasi-particle operators. The validity of the Bogoliubov approximation to make quantitative predictions may be questioned at $U/J \simeq 10$ where the quantum depletion is of the order of $\sim 15\%$. If one assumes nonetheless that it is a valid approximation, it suggests that the depleted cloud mainly consists in phononic excitations, even for the states populated by thermal fluctuations. As a consequence, the coherence properties of the excitations differ from that of single-particle excitations and this may be at the origin of our observation.

4.3 Many-body correlations deep in the Mott regime

In this section we present recent experiments performed throughout the phase diagram of the Bose-Hubbard hamiltonian. Firstly we discuss the observation of the superfluid-to-Mott crossover with metastable Helium atoms. Secondly we discuss the measurement of multi-particle correlations deep in the Mott insulator regime.

4.3.1 Observation of the Mott transition with metastable Helium ^{4}He* atoms

Regarding many-body quantum phase transitions, a landmark experiment with quantum gases is the observation of the Superfluid-to-Mott transition in an optical lattice [91]. Validating the theoretical proposal of [110], this piece of work doubtlessly paved the way to

decades of an intensive international effort towards the implementation and investigation of many-body lattice Hamiltonians, mostly inspired from condensed-matter physics. The recent observation of anti-ferromagnetism in the low temperature sector of the phase diagram of the Fermi-Hubbard is one of the most impressive outcome along this line of research [146]. The Superfluid-to-Mott transition is a zero temperature phase transition of the Bose-Hubbard Hamiltonian [77]. At low ratio $U/J \ll 1$ (and $T = 0$) the ground-state of H_{BH} is a superfluid while at large ratio $U/J \gg 1$ it is an insulator state named Mott state after Sir. N. Mott [151]. The ratio U/J can be simply tuned in lattice gas experiments by changing the amplitude of the lattice (*i.e.* the intensity of the laser).

In the experiment at Institut d'Optique, we have measured momentum distributions of lattice gases at different ratio U/J, typically ranging from $U/J = 1$ to $U/J = 100$, observing distributions whose features are compatible with those associated to the Mott transition (Fig. 4.13). Indeed the Mott transition is expected to take place at the critical ratio $(U/J)_c = 29.34$ in a 3D square lattice [35, 172]. To our knowledge, it is the first observation of the Mott transition with a gas of metastable atoms and it may open some perspective to investigate the interplay of unitary and dissipative dynamics as we shall briefly exposed in the perspective section.

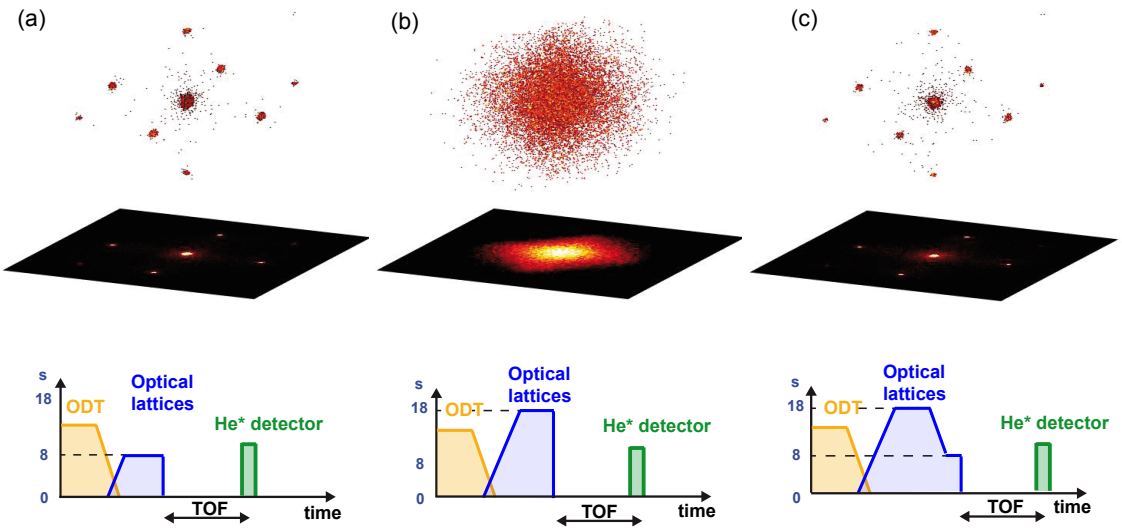

Figure 4.13: Mott transition in a 3D optical lattice. Illustration of the Mott transition in our experiment with the 3D momentum distributions measured at various ratio U/J. The sketches below the 3D distributions depict the condition of the experiment: (a) below the Mott transition, (b) above the Mott transition, and (c) finally ramping back the lattice amplitude below the transition.

From using the thermometry method associated to a comparison of the measured momentum densities with ab-initio QMC calculations (see section 4.2.3), we are able to identify the position of the experimental realisations in the finite-temperature phase diagram of the Bose-Hubbard Hamiltonian. A sketch of the phase diagram for a homogeneous lattice gas is shown in Fig. 4.14 as a function of the ratio U/J and T/J. Here we consider a unity occupation of the lattice sites, which is ensured in the experiment by working with a total atom number $N \sim 5000$ in the trap. The QMC calculations for the experimental data set labelled #2 have been performed by our colleague T. Roscilde (ENS Lyon). We note that the temperature obtained deep in the Mott regime (for $U/J = 100$), $T/U \sim 0.05$, is similar

to that obtained from measuring the on-site atom number fluctuations with quantum gas microscopes [199, 10].

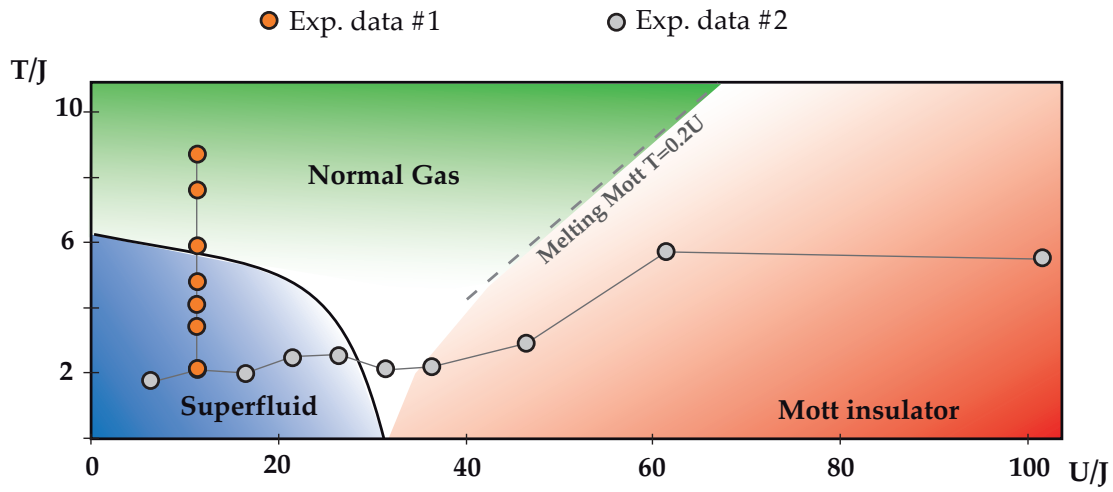

Figure 4.14: Sketch of the finite-temperature phase diagram of the Bose-Hubbard Hamiltonian. Dots represent the different data sets we have used in this thesis. The Hubbard parameters U and J are obtained from the calibration of the amplitude of the optical lattice. The temperature T is extracted from comparing the measured momentum densities $\rho(k)$ with ab-initio QMC calculations.

The phase diagram shown in Fig. 4.14 sets the stage for the investigation of the critical region in the vicinity of the appearance of the Mott plateau. In particular, an interesting question that we will investigate in the future is whether the temperature is low enough and the system large enough to be in the position of observing some quantum critical phenomenon. Of course, in the inhomogeneous trap induced by the lattice beams, we have to deal with a crossover (and not a phase transition) and with the co-existence of several phases. This situation complicates the understanding of the role of thermal fluctuations and their interplay with quantum fluctuations. From monitoring usual quantities like the condensed fraction or the visibility, it is not obvious to provide a quantitative answer to this question.

4.3.2 Two and three-body correlations deep in a Mott insulator

Before proceeding with the intricate regime of the critical region, we have investigated the Mott ground-state deep in the insulating regime. As it can be seen from Fig. 4.13, the momentum density deep in the Mott state does not exhibit diffraction peaks. This derives from the fact that atoms are pinned to the sites of the lattice and the coherence length of the phase (associated to $g^{(1)}(r,r')$) is smaller than the lattice spacing. The momentum density thus results from the expansion of a large number of point-like sources (one atom from a single site being one such source) with random phase relations. This situation is similar to that of a thermal gas well above the critical temperature for Bose-Einstein condensation and to that of a diffuser imprinting random phases on a beam of light. As a result, one expect to observe after propagation a phenomenon similar to that of optical speckle and

the Hanbury-Brown and Twiss (HBT) effect [88, 192]. This picture was confirmed in a pioneering experiment by measuring the noise correlation in the absorption images of a bosonic Mott insulator [80]. More specifically, a bunching phenomenon was reported which exhibits a periodicity reminiscent of that of the lattice. But, due to technical limitations associated with absorption imaging (line of sight integration, limited momentum resolution and absence of single-atom sensitivity), the measured normalised quantity $g^{(2)}(0)-1$ was a bit less than 10^{-3}, much smaller than the expected value of 1, and the two-body correlation length could not be measured. Using the capabilities of the He* detector should permit to overcome these limitations.

Momentum-space correlations deep in the Mott insulator regime. To describe the momentum-space correlations of a Mott insulator, we would like to present an alternative picture to that of Hanbury-Brown and Twiss type of experiments, which is commonly used in Optics and in our community. To this aim we introduce the momentum-space operators

$$\hat{a}(\mathbf{k}) = \frac{1}{\sqrt{V}} \sum_{l=1}^{N_{\text{site}}} e^{i\mathbf{k}.\mathbf{r}_l} \hat{b}_l, \tag{4.11}$$

where the volume of quantization V is chosen as the in-trap volume of the gas. As a consequence of the crystalline structure of the lattice, all momentum-space quantities are periodic with the period of the reciprocal lattice $k_d = 2\pi/d$ where d is the lattice spacing, *e.g.* $\hat{a}(\mathbf{k}+\mathbf{K}) = \hat{a}(\mathbf{k})$ with $\mathbf{K} = k_d(n_x\mathbf{u}_x + n_y\mathbf{u}_y + n_z\mathbf{u}_z)$ where $\{\mathbf{u}_j\}_{x,y,z}$ are the orthonormal vectors associated to the lattice and $\{n_j\}_{x,y,z}$ are integers.

Deep in the Mott phase at large amplitude of the lattice potential, the tunnelling becomes vanishingly small and it is standard to approximate the many-body ground-state by a "perfect" Mott insulator, *i.e.*, a Mott insulator with no coupling between the sites, $J = 0$. The perfect Mott insulator for the Hubbard Hamiltonian with unity occupation of the lattice site is then $|\psi\rangle_{J=0} = \Pi_l \hat{b}_l^\dagger |0\rangle$. The absence of phase coherence between the lattice sites, $\langle\psi|\hat{b}_l^\dagger \hat{b}_{l'}|\psi\rangle_{J=0} = \langle \hat{b}_l^\dagger \hat{b}_{l'}\rangle_{J=0} = \delta_{l,l'}$, has important consequences on the momentum-space properties. Under these conditions, the correlations between two momentum operators takes the form

$$\langle \hat{a}^\dagger(\mathbf{k})\hat{a}(\mathbf{k}')\rangle_{J=0} = \frac{1}{V} \sum_{l=1}^{N_{\text{site}}} \langle \hat{n}_l \rangle \, e^{-i(\mathbf{k}-\mathbf{k}').\mathbf{r}_l}. \tag{4.12}$$

The momentum density of a perfect Mott insulator is thus constant, $\rho(\mathbf{k}) = \langle \hat{a}^\dagger(\mathbf{k})\hat{a}(\mathbf{k})\rangle_{J=0} = \rho(0)$. In addition, the correlations between momentum components separated by more than the inverse of the system size L are vanishingly small. On the contrary, the sum in Eq. 4.12 is non zero for $|\mathbf{k}-\mathbf{k}'| < 2\pi/L$, which implies that some correlations are present in momentum-space even if there are no position-space correlations, a situation similar to that described by the Van Cittert-Zernike theorem in Optics. Eq. 4.12 defines the one-particle volume of coherence, *i.e.*, the volume over which the first-order correlation function $g^{(1)}(\mathbf{k},\mathbf{k}') = \langle \hat{a}^\dagger(\mathbf{k})\hat{a}(\mathbf{k}')\rangle / \sqrt{\rho(\mathbf{k})\rho(\mathbf{k}')}$ is non-zero. This momentum-space volume of coherence reflects the distribution of atoms $\{\langle \hat{n}_l \rangle\}_l$ in the lattice.

As pointed out in [3], higher-order momentum-space correlations can reveal some properties of many-body ground-states even when the momentum density is featureless. For instance, bosonic bunching is expected in the two-body correlations $g^{(2)}(\mathbf{k},\mathbf{k}')$ associated with finding one particle with a momentum $\mathbf{k}$ and a second one with a momentum $\mathbf{k}'$. In the case of the perfect Mott state, that is to say when the tunnelling is zero, the amplitude and the width of the bunching effect can be predicted accurately. Indeed, the atom

number per lattice site is then fixed. For a unity occupation of the lattice $n_l = 1$, the Bose-Hubbard Hamiltonian reduces to that of non-interacting particles and is diagonal in the momentum-space basis. As a result, the many-body momentum-space correlations are those of uncorrelated bosons with a Gaussian density operator [82]. For such a Gaussian many-body ground-state, the Wick decomposition yields $g^{(2)}(\mathbf{k},\mathbf{k}') = 1 + |g^{(1)}(\mathbf{k},\mathbf{k}')|^2$. In particular, the amplitude of the two-body correlation at zero particle distance is twice that found for non-correlated particles, $g^{(2)}(\mathbf{k},\mathbf{k}) = 2$. In addition, the shape of the bunching peak provides a quantitative information about the in-trap profile. Its exact shape is set by the term $|g^{(1)}(\mathbf{k},\mathbf{k}')|^2$, *i.e.*, the volume of coherence. Interestingly, higher-order correlation functions can also be derived from the first-order correlation function $g^{(1)}(\mathbf{k},\mathbf{k}')$ when Wick theorem applies (see [61] for instance).

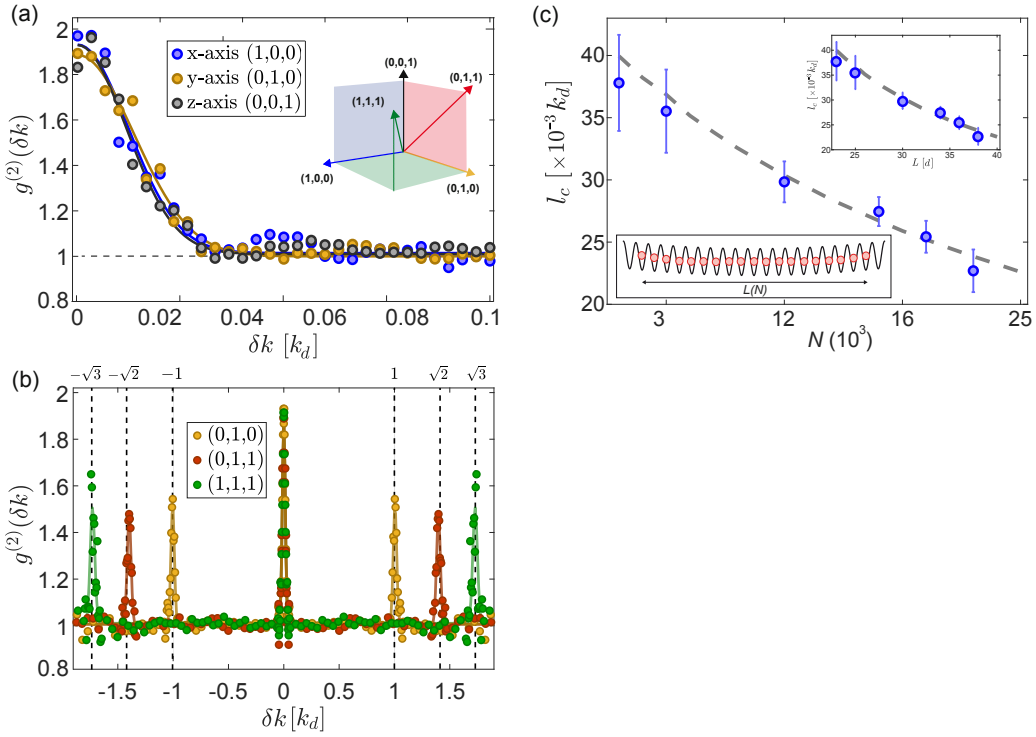

Figure 4.15: Two-particle momentum correlation in the Mott state. (a) Two-body correlation function $g^{(2)}(\delta k)$ plotted as a function of the momentum difference between two particles along a given axis $\mathbf{u}$, $\delta k = (\mathbf{k} - \mathbf{k}').\mathbf{u}$. The different colours correspond to the three axis of the reciprocal lattice. (b) $g^{(2)}(\delta k)$ plotted as a function of δk along the different axis through the 3D reciprocal lattice and illustrating its cubic structure. (c) Two-body correlation length l_c as a function of the total atom number N. The dashed line is the ab-initio prediction for a Gaussian many-body ground-state whose atoms are distributed in the lattice according to the Gutzwiller ansatz for the experimental parameters. Inset: l_c as a function of the in-trap size L.

Measurement of many-body correlations in the Mott. In the experiment, we have extracted the normalized second-order correlation function $g^{(2)}(\delta k)$ from the 3D atom distributions, where δk is the momentum difference between two particles along a given axis $\mathbf{u}$, $\delta k = (\mathbf{k} - \mathbf{k}').\mathbf{u}$. In Fig. 4.15(a)-(b), $g^{(2)}(\delta k)$ is plotted as a function of δk along different axis of the reciprocal lattice. The measured bunching amplitude $g^{(2)}(0)$ is com-

patible with 2, *i.e.* a perfect contrast of the two-particle correlations. Note that we also observe the periodicity associated to the lattice in $g^{(2)}(\delta k)$ in 3D, with periods k_a, $\sqrt{2}k_a$ and $\sqrt{3}k_a$. In addition, we measured the two-body correlation length l_c as a function of the total atom number N, finding a perfect agreement with an ab-initio model which uses the Gutzwiller ansatz to calculate the in-trap density profile, see Fig. 4.15(c). The decrease of l_c with N derives from the fact that bunching occurs within one momentum-space eigenstate, the volume of which is given by $1/L$, and from the incompressibility of the Mott state: when N increases, L increases (in a trapped ideal thermal gas as in [192, 61], L is independent of N). Our findings demonstrate quantitatively that the many-body ground-state deep in the insulating regime is well described by considering a Gaussian density operator in momentum-space.

From the single-atom-resolved distributions, one can also calculate higher-order correlations than $g^{(2)}$. To illustrate this possibility, we have extracted the three-body correlations as well. The third-order correlation function $g^{(3)}$ is plotted in Fig. 4.16 as a function of the momentum differences δk_1 and δk_2 between the two pairs of detected atoms. We observe that the pattern is periodic with the period k_d of the reciprocal lattice, similarly to the two-body correlations. The blue background corresponding to non-correlated atoms has an amplitude equal to 1, as expected from a correct normalisation of the correlation function $g^{(3)}$. One can distinguish lines with some correlation, corresponding respectively to $\delta k_1 = \delta k_2$, $\delta k_1 = 0$ and $\delta k_2 = 0$. The correlation along this line is the two-body bunching effect previously described, whose amplitude is about twice that of the background. Finally, at $\delta k_1 = \delta k_2 = 0$ (modulo the reciprocal lattice period k_d) one observe an even larger correlation, whose amplitude is compatible with $3! = 6$ as expected for indistinguishable ideal bosonic particles. This peak located at $\delta k_1 = \delta k_2 = 0$ is the intrinsic three-body correlation signal. These qualitative observation on the correlation between three atoms in momentum states further illustrates the outstanding capabilities of the He* detector to provide signals of correlations between individual particles in 3D !

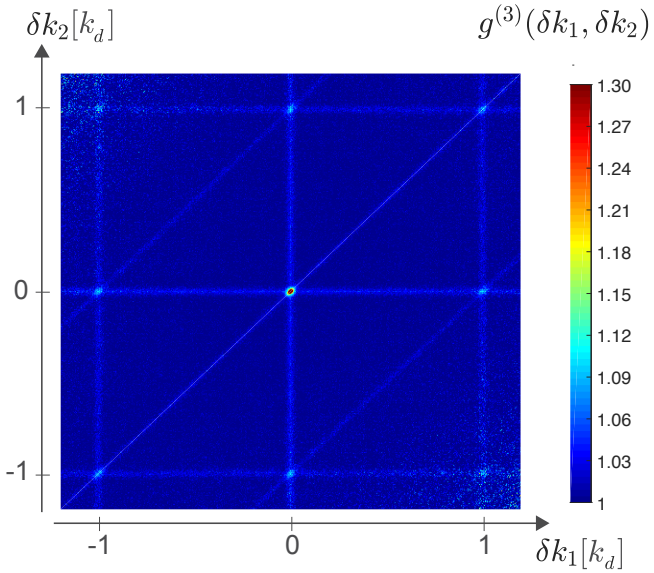

Figure 4.16: Three-particle momentum correlation in the Mott state. Three-body correlation $g^{(3)}(\delta k_1, \delta k_2)$ plotted as a function of the momentum differences δk_1 and δk_2 between the two pairs of detected atoms.

4.3.3 Perspectives

As illustrated in the Mott regime, the He* detector provides access to physical quantities that could not be measured at the quantitative level so far. We are currently revisiting the phase diagram of the Bose-Hubbard Hamiltonian with this novel detection method. This includes measuring the condensed fraction across the Mott crossover to identify the location of the appearance of the first Mott plateau. Previous experiments in 3D lattice gases – by monitoring the presence of superfluid currents [152] or the momentum properties [144] – have found a critical ratio U/J for the Mott transition compatible with mean-field predictions and different from the most advanced Quantum Monte-Carlo calculations. Since QMC calculations are expected to better describe (and locate) the Mott transition than mean-field approaches, this experimental result is somewhat puzzling and calls for an alternative approach to establishing the location of the Mott transition.

The He* detector could also allow us to calibrate the temperature of the lattice gas from the monitoring of adequate fluctuations in momentum space. It was indeed suggested that the fluctuation/dissipation theorem provides a mean to perform a thermometry from an accurate measure of the momentum distributions [184]. When successful this approach would yield a temperature calibration from the experiment, independent of the QMC calculation as obtained so far, and the result of which could be compared with the QMC predictions.

By revealing the 3D momenta of individual atoms, the He* detector also provides the unique opportunity to investigate momentum correlations in lattice gases. We have shown first signals of many-particle correlations in various regimes far from the critical region of the Mott transition: pure condensates, interacting thermal clouds and deep in the Mott state. It demonstrates the capabilities our the single-atom He* detector to resolve the correlation volumes associated to several particles in 3D, in striking contrast with the techniques such as the light sheet [31, 166] or the noise-correlation [80]. In the future, we will look for correlation signals associated with the presence of quantum correlations in the vicinity of the Mott transition. It includes the signature of the quantum depletion through correlated atom pairs at opposite momenta $(k, -k)$ [220], the presence of particle-hole coherence [220] and correlations in the quantum critical regime of the Mott transition.

When looking for the quantum critical region of the Mott transition, the presence of a trap on top of the lattice potential is a nuisance as it effectively realises an average over different regimes of criticality [226, 35]. A future perspective for the experiment would consist in implementing box potentials to work with (close to) constant densities (see for instance [83]). This is an appealing approach but it will also require some involved manipulation of optical potentials to obtain a given filling of the lattice (see for instance [50]). Another perspective would consist in investigating finite-size scaling in trapped systems as proposed theoretically [33, 34].

4.4 Associated peer-reviewed publications

[1] *"Momentum-resolved observation of thermal and quantum depletion in an interacting Bose gas"*

R. Chang, Q. Bouton, H. Cayla, C. Qu, A. Aspect, C. I. Westbrook, D. Clément
Phys. Rev. Lett. 117, 235303 (2016)

[2] *"Quantum depletion of a homogeneous Bose-Einstein condensate"*
R. Lopes, C. Eigen, N. Navon, D. Clément, R. P. Smith, Z. Hadzibabic
Phys. Rev. Lett. 119, 190404 (2017)

[3] *"Single-atom-resolved probing of lattice gases in momentum space"*
H. Cayla, C. Carcy, Q. Bouton, R. Chang, G. Carleo, M. Mancini and D. Clément
Phys. Rev. A 97, 061609(R) (2018)

[4] *"Tan's Contact for Trapped Lieb-Liniger Bosons at Finite Temperature"*
H. Yao, D. Clément, A. Minguzzi, P. Vignolo and L. Sanchez-Palencia
Phys. Rev. Lett. 121, 220402 (2018)

[5] *"Momentum-space atom correlations in a Mott insulator"*
C. Carcy, H. Cayla, A. Tenart, A. Aspect, M. Mancini and D. Clément
Phys. Rev. X 9, 041028 (2019)

[6] *"Two-body collisions in the time-of-flight dynamics of lattice Bose superfluids"*
A. Tenart, C. Carcy, H. Cayla, T. Bourdel, M. Mancini and D. Clément
Phys. Rev. Research 2, 013017 (2020)

Chapter 5

Conclusion

This thesis mainly describes the experimental work I have initiated after joining the Institut d'Optique in Palaiseau. The first years after my arrival were devoted to the building of a new experimental apparatus capable of producing Bose-Einstein condensates with the metastable species ^{4}He*. With respect to the state-of-the-art for cooling ^{4}He*, we implemented several technical innovations and reached the following objectives: a short cycle duration ($\sim$ 7 seconds); an excellent stability (atom number fluctuations in the BEC $\sim$ 10%); a large optical access to the atoms; the use of an optical trap to leave the possibility of tuning magnetic fields; an upgraded version of the He* detector with a better resolution and a higher detection rate. These achievements lay the floor for a systematic investigation of the research questions we are interested in. I must say that there is a real difference between the level of stability and reproducibility obtained on this apparatus – thanks to the dedicated work of my young collaborators! – and that of the experiments I worked with previously. I believe that this highlights the maturity of our research field and signals the technical skills accumulated and widespread within our community. The effort we put to reach such a level of control and reproducibility is also justified by our scientific objectives. On the one hand, we are looking for beyond mean-field effects the characterisation of which often requires a fine tuning of the experimental parameters. On the other hand, extracting correlations between individual particles requires, on top of the capability to detect single atoms, to average the experimental signals over many runs of the experiment before reaching a good signal-to-noise level. This requirement sets stringent conditions on the level of reproducibility of the apparatus!

The first experiments on the new apparatus were performed over the past years. Firstly, we have dedicated quite some time and energy to investigate the large momentum tails observed in expanding BECs. We have recently revealed the presence of spin impurities and found they are central to understand the origin of algebraic tails. Although we started working on this topic several years ago, the picture is yet not clear, especially because we have found the presence of the spin impurities only recently. Coming back to the same topic every now and then may seem annoying but it also happens to be very stimulating, in particular to envision novel explanations to the first observations that were initially misunderstood. In this context, I acknowledge many fruitful discussions with colleagues from around the world, thus enjoying one fascinating aspect of doing basic research. Secondly, we have installed optical lattices and investigated the phase diagram of the Bose-Hubbard hamiltonian. In my perspective, we have achieved two milestones: on the one hand we

benchmarked our capability to reconstruct momentum-space distributions of lattice gases atom-by-atom with unprecedented precision; on the other hand we have shown the interest of our approach to measure atom correlations in the momentum-space, obtaining perfectly contrasted signals of correlation in the Mott state. These milestones demonstrate that the outstanding capabilities of the He* detector, previously illustrated with analogs of quantum optics experiments [225], are also relevant to investigate strongly interacting quantum systems in the momentum-space. In addition, they pave the way to investigating correlations in more complex quantum states, where the correlation signals may be of small amplitude.

In the coming years, we will pursue the investigation of many-body quantum states and dynamics of interacting bosons with the existing apparatus, looking for signatures of quantum correlations. My opinion is that we have hardly started playing with the opportunities that the approach we have implemented is providing us with. The information contained in the full distribution of the atom momenta of a gas is indeed large and many physical quantities of interest may be found when investigating those distributions. In principle, we can look into any statistical properties and correlations of high-order, a situation for which there may not even exist theoretical predictions because of the difficulty to account for multi-particle correlations (and entanglement). The main drawback we have to face in this direction is the low detection efficiency α of the He* detector that increases the uncertainty on the measured fluctuations. For a single-atom-resolved detector with no dark counts (as the He* detector), the fluctuations on the detected atom number in a small 3D box (of the momentum-space in our case) is enhanced above the shot-noise limit by a factor $\sim 1/\sqrt{\alpha}$. This implies that any signal of fluctuations below this limit can hardly be observed in the experiment. To give an example, one could think that the He* detector is perfectly suited to measure the atom number fluctuations in the condensate mode across a BEC phase transitions, as observed in a recent experiment [124]. For the specific case of Bose-Einstein condensation at finite temperature [124], the condensate atom number fluctuations close to the critical temperature ($\sim \sqrt{N}$ where N is the total atom number) can be observed provided that $\alpha > 0.15$ (we are now able to reach this value on our He* apparatus). Having in mind these considerations on the role of the detection is important to proceed with the practical implementation of future experiments. Nevertheless, it does certainly not preclude the measurement of multi-particle correlations in strongly interacting quantum systems!

In the near future, moving towards new directions should be envisioned and I would like to briefly cite three of them. Firstly, we should consider implementing flat potentials as the effect of a harmonic trap is notoriously annoying in situations of interest to us, *e.g.* to investigate critical phenomena at quantum phase transitions or to study one-dimensional gases. The inhomogeneous potential associated with parabolic traps affects quantum coherences and correlations. For instance, it further limits the divergence of correlation lengths across phase transitions, as compared to a homogeneous system with similar finite size effects. There are several technical solutions to obtain flat potentials for the bulk and we are oriented towards the implementation of optical potentials controlled with SLM [83, 155] or DMD [238] devices.

Another future direction consists in adding the fermionic species ^{3}He* to open a new playground for experiments. We have recently started designing the additional systems required by working with ^{3}He* atoms. One central objective of this direction is to reveal

the momentum-space two-particle correlations expected in the presence of Cooper pairing, *i.e.* two fermions with opposite momenta. Before being in the position to observe these correlations, we need to establish the possibility of using a Feshbach resonance and explore the BEC-BCS crossover with ^{3}He* atoms. We note that the short lifetime of spin mixtures due to Penning collisions suggests to consider spin-polarized gases. With the current knowledge on the interaction potentials [89], it is not possible to predict whether p-wave Feshbach resonances are accessible to experiments. In the hope of a positive outcome, we will investigate this possibility with our apparatus. In the longer term, observing momentum correlations in a spin-polarized ^{3}He* gas would provide a direct signal to study the stability of the p-wave Cooper pairs, a pre-requisite to cool the pairs.

Finally, the presence of Penning collisions could be used as a resource in optical lattices. Penning collisions result in the loss of the two colliding metastable atoms, thus realising one type of dissipation, *i.e.* losses. Changing the atomic spin states, the rate of Penning collisions on a lattice site can be varied by several orders of magnitude between two regimes of losses. On the one hand, when the losses are much greater than any other energy scale in the problem, quantum Zeno effects should be observable, similarly to the pioneering work of [212] with molecules. These effects could be used to tailor the atom distribution in the lattice, like to ensure a uniform unit filling over the entire lattice. On the other hand, when the losses are comparable to the tunnelling rate, interesting dissipative Hamiltonians can be realised to investigate the interplay between unitary and dissipative dynamics in optical lattices. For instance it may open a window to study metastable states and the emergence of correlations [171, 18].

Chapter 6

Personal information

6.1 Short Curriculum Vitae

CLEMENT David
Date of birth: 04/03/1979
Nationality: french
Personal webpage: hyperlink
ResearcherID: A-1915-2009

- **EDUCATION**

2008	**PhD thesis** with Highest Honors - Université Pierre et Marie Curie, France *Title:* Bose-Einstein condensates in random potentials - *Dir.:* A. Aspect
2004	**Agrégation in Physics-Chemistry**
2003	Selective exam to join the Ecole Normale Supérieure de Cachan, France
2003	**Master in Quantum Physics** - Ecole Normale Supérieure de Paris, France

- **CURRENT POSITION**

2010-present	**Assistant Professor - Maître de Conférence** at Institut d'Optique **Coordinator of the "Lattice gas" team** - Atom Optics group, France
2016-present	Junior member of the **Institut Universitaire de France** (5 years duration)

- **PREVIOUS POSITIONS**

2007-2010	**Postdoctoral fellow** - Group of M. Inguscio (LENS), Florence (Italy)
2002	**Undergraduate** - Group of H. Levine - University of San Diego (USA)

- **FELLOWSHIPS AND AWARDS**

2018	Prize from the **Fondation iXCore pour la recherche**
2017	**Jeune chercheuse-jeune chercheur (JCJC)** grant from ANR (4 years)
2016	**Junior member** of the Institut Universitaire de France (5 years)
2011	**Junior chair** from the network Triangle de la Physique (3 years)
2010	**Chair of Excellence** from the CNRS (5 years)
2009	**Marie Curie Fellowship** from the European Research Council (2 years)
2004	**Research PhD Grant** from Ministry of Education (3 years)

- **AREA OF EXPERTISE AND KNOWLEDGE**

  - Cutting-edge technologies for quantum gases (laser, vacuum and electronics).

  - Manipulation and detection of metastable Helium gases.

  - Many-body physics in optical lattices and realization of low-dimensional gases.

  - Probing response functions of correlated quantum matter with light scattering.

  - Physics with disorder: experimental implementation (speckle) and theoretical approaches.

6.2 Scientific publications and communications

Author of 28 peer-review publications and 8 proceedings.

Peer-reviewed publications

[28] *"Two-body collisions in the time-of-flight dynamics of lattice Bose superfluids"*
A. Tenart, C. Carcy, H. Cayla, T. Bourdel, M. Mancini and D. Clément
Phys. Rev. Research 2, 013017 (2020)

[27] *"Momentum-space atom correlations in a Mott insulator"*
C. Carcy, H. Cayla, A. Tenart, A. Aspect, M. Mancini and D. Clément
Phys. Rev. X 9, 041028 (2019)

[26] *"Tan's Contact for Trapped Lieb-Liniger Bosons at Finite Temperature"*
H. Yao, D. Clément, A. Minguzzi, P. Vignolo and L. Sanchez-Palencia
Phys. Rev. Lett. 121, 220402 (2018)

[25] *"Single-atom-resolved probing of lattice gases in momentum space"*
H. Cayla, C. Carcy, Q. Bouton, R. Chang, G. Carleo, M. Mancini and D. Clément
Phys. Rev. A 97, 061609(R) (2018)

[24] *"Quantum depletion of a homogeneous Bose-Einstein condensate"*
R. Lopes, C. Eigen, N. Navon, D. Clément, R. P. Smith and Z. Hadzibabic
Phys. Rev. Lett. 119, 190404 (2017)

[23] *"Momentum-resolved observation of thermal and quantum depletion in an interacting Bose gas"*
R. Chang, Q. Bouton, H. Cayla, C. Qu, A. Aspect, C. I. Westbrook and D. Clément
Phys. Rev. Lett. 117, 235303 (2016)

[22] *"Characterization of a detector chain using a FPGA-based Time-to-Digital Converter to reconstruct the three-dimensional coordinates of single particles at high flux"*
F. Nogrette, D. Heurteau, R. Chang, Q. Bouton, C. I. Westbrook, R. Sellem and D. Clément
Rev. Scient. Instrum. 86 113105 (2015)

[21] *"Fast production of Bose-Einstein condensates of metastable Helium"*
Q. Bouton, R. Chang, A. L. Hoendervanger, F. Nogrette, A. Aspect, C. I. Westbrook and D. Clément
Phys. Rev. A 91 061402 (R) (2015)

[20] *"Three-dimensional laser cooling at the Doppler limit"*
R. Chang, A. L. Hoendervanger, Q. Bouton, Y. Fang, T. Klafka, K. Audo, A. Aspect, C. I. Westbrook and D. Clément
Phys. Rev. A, 90 063407 (2014) - Editor's suggestion

[19] *"Dynamical structure factor of one-dimensional Bose gases: experimental signatures of beyond-Luttinger liquid physics"*
N. Fabbri, M. Panfil, D. Clément, L. Fallani, M. Inguscio, C. Fort and J.-S. Caux
Phys. Rev. A 91 043617 (2015)

[18] *"Influence of Gold Coating and Interplate Voltage on the Performance of Chevron Micro-Channel Plates for the Time and Space Resolved Single Particle Detection"*
A. L. Hoendervanger, D. Clément, A. Aspect, C. I. Westbrook, D. Dowek, Y. Picard and D. Boiron
Rev. Scient. Instrum. 84 023307 (2013)

[17] *"Quasiparticle dynamics in a Bose insulator by inter-band Bragg spectroscopy"*
N. Fabbri, S. D. Huber, D. Clément, L. Fallani, C. Fort, M. Inguscio, E. Altman
Phys. Rev. Lett. 109 055301 (2012)

[16] *"An oscillator circuit to produce a rf discharge and application to metastable helium saturated absorption spectroscopy"*
F. Moron, A. L. Hoendevanger, M. Bonneau, Q. Bouton, A. Aspect, D. Boiron, D. Clément, C. I. Westbrook
Rev. Scient. Instrum. 83 044705 (2012)

[15] *"Momentum-resolved study of an array of 1D strongly phase-fluctuating Bose gases"*
N. Fabbri, D. Clément, L. Fallani, C. Fort and M. Inguscio
Phys. Rev. A 83 031604(R) (2011)

[14] *"Bragg spectroscopy of strongly correlated bosons in optical lattices"*
D. Clément, N. Fabbri, L. Fallani, C. Fort and M. Inguscio
J. Low Temp. Phys. 158 5-15 (2010)

[13] *"Multi-band spectroscopy of inhomogeneous Mott insulator states of ultracold bosons"*
D. Clément, N. Fabbri, L. Fallani, C. Fort and M. Inguscio
New J. Phys. 11 103030 (2009) [in "NJP Best of 2009"]

[12] *"Static and dynamic properties of disordered Bose-Einstein condensates"*
D. Clément
Annales de Physique Fr. 33, n○ 4-5 (2008)

[11] *"Excitations of a Bose-Einstein condensate in a one-dimensional periodic potential"*
N. Fabbri, D. Clément, L. Fallani, C. Fort, M. Modugno, K. M. R. van der Stam and M. Inguscio
Phys. Rev. A 79 043623 (2009)

[10] *"Exploring correlated 1D Bose gases across from the superfluid to the Mott insulator state by inelastic light scattering"*
D. Clément, N. Fabbri, L. Fallani, C. Fort and M. Inguscio
Phys. Rev. Lett. 102 155301 (2009) [with Physics 2, 29 (2009)]

[9] *"Direct observation of Anderson localization of matterwaves in a controlled disorder"*
J. Billy, V. Josse, Z. Zuo, A. Bernard, B. Hambrecht, P. Lugan, D. Clément, L. Sanchez-Palencia, P. Bouyer and A. Aspect
Nature 453 891 (2008)

[8] *"Disorder-induced trapping versus Anderson localization in Bose-Einstein condensates expanding in disordered potentials"*
L. Sanchez-Palencia, D. Clément, P. Lugan, P. Bouyer and A. Aspect
New. J. Phys. 10 045019 (2008)

[7] *"Density Modulations in an Elongated BEC Released from a Disorder Potential"*
D. Clément, P. Bouyer, A. Aspect and L. Sanchez-Palencia
Phys. Rev. A 77 033631 (2008)

[6] *"Localization of Bogolyubov Quasiparticles in Interacting Bose-Einstein Condensates Subjected to Correlated Random Potentials"*
P. Lugan, D. Clément, P. Bouyer, A. Aspect and L. Sanchez-Palencia
Phys. Rev. Lett. 99 180402 (2007)

[5] *"Anderson Localization of Bose-Einstein Condensates in Random Potentials"*
L. Sanchez-Palencia, D. Clément, P. Lugan, P. Bouyer, G. V. Shlyapnikov and A. Aspect
Phys. Rev. Lett. 98 210401 (2007)

[4] *"Ultracold Bose Gases in 1D Random Potentials: From Lifshits Glasses to Bose-Einstein Condensates"*
P. Lugan, D. Clément, P. Bouyer, A. Aspect, M. Lewenstein and L. Sanchez-Palencia
Phys. Rev. Lett. 98 170403 (2007)

[3] *"Experimental study of the transport of coherent interacting matter-waves in a 1D random potential induced by laser speckle"*
D. Clément, A. F. Varon, J. A. Retter, L. Sanchez-Palencia, A. Aspect and P. Bouyer
New J. Phys. 8 165 (2006)

[2] *"Suppression of Transport of an Interacting Elongated Bose-Einstein Condensate in a 1D Random Potential"*
D. Clément, A. F. Varon, M. Hugbart, J. A. Retter, P. Bouyer, L. Sanchez-Palencia, D. Gangardt, G. V. Shlyapnikov, A. Aspect
Phys. Rev. Lett. 95 170409 (2005)

[1] *"Coherence length of an elongated condensate : a study by matterwave interferometry"*
M. Hugbart, J. A. Retter, F. Gerbier, A. F. Varon, S. Richard, J.H. Thywissen, D. Clément, P. Bouyer, A. Aspect
EPJD 35 155-163 (2005)

Oral communications

07/2019 Invited talk at **Congrès de la SFP**, Nantes (France)
"Momentum-space atom correlations in Mott insulators"

06/2019 Invited seminar at **Univ. Kaiserslautern**, Kaiserslautern (Germany)
"Momentum-space atom correlations in Mott insulators"

05/2019 Seminar at **UNAM**, Mexico DF (Mexico)
"Momentum-space atom correlations in Mott insulators"

10/2018 Invited talk at **ENIQMA workshop**, Lyon (France)
"One-body and two-body correlations in gaseous Mott insulators"

06/2018 Invited talk at **Conference on Frontiers in Laser Sciences**, Tel Aviv (Israel)
"Reconstructing the momentum distribution of lattice gas atom-by-atom"

05/2018 Invited talk at **DAMOP 2018**, Fort Lauderlade (USA)
"Probing lattice gas in momentum space with single atom sensitivity"

11/2017 Invited talk at **Entanglement Interacting Quantum Matter Workshop**, Lille (France)
"Probing lattice gas in momentum space with single atom sensitivity"

11/2017 Invited talk at **International Conference on Quantum Simulation**, Paris (France)
"Probing lattice gas in momentum space with single atom sensitivity"

09/2017 Hot-topic talk at **BEC 2017**, San Feliu (Spain)
"Probing lattice gas in momentum space with single atom sensitivity"

07/2017 Contributed talk at **EGAS conference**, Durham (UK)
"Probing lattice gas atom-by-atom in momentum space"

05/2017 Invited seminar at **Amsterdam V. University**, Amsterdam (Netherlands)
"Momentum-resolved investigation of the depletion in interacting bose condensates"

05/2017 Invited seminar at **Université Cergy-Pontoise**, Cergy (France)
"Single-atom- and momentum-resolved investigation of the depletion in interacting bose condensates"

02/2017 Invited seminar at **LENS**, Florence (Italy)
"Momentum-resolved investigation of the depletion in interacting Bose gases"

11/2016 Invited speaker at **journée du Labex PALM**, Orsay (France)
"Momentum-resolved observation of thermal and quantum depletion in an interacting Bose gas"

11/2016 Invited seminar at **Academia dei Lincei**, Roma (Italy)
"Observation of quantum depletion in an interacting Bose gas"

10/2016 Invited seminar at **Cavendish Laboratory**, University of Cambridge (UK)
"Momentum-resolved observation of quantum depletion in an interacting Bose gas"

02/2016 Invited seminar at **INO-BEC center**, Trento (Italy)
"Investigated many-body correlations in momentum space: An illustration on the quantum depletion"

10/2015 Contributed talk at **Quantum Manipulation of Atoms and Photons**, Shanghai (China)
"A momentum-space microscope of lattice gases"

06/2015 Contributed talk at **Quantum Technology VI**, Warsaw (Poland)
"A special atom to investigate correlated quantum matter"

06/2012 Invited speaker at **Journée LUMAT**, Orsay (France)
"Probing metastable Helium atoms with InGaAs camera and Micro-Channel Plates "

09/2010 Invited speaker at **Dynamics of quantum gases in one dimension**, Orsay (France)
"Probing correlated lattice 1D bosons by inelastic light scattering"

03/2010 Contributed talk at **New Perspectives In Quantum Statistics And Correlations**, Heidelberg (Germany)
"Probing correlated lattice bosons by inelastic light scattering"

09/2009 Invited speaker at the **BEC 2009 - Frontiers in Quantum Gases**, San Feliu (Spain)
"Bragg spectrsocopy of ultracold bosons in optical lattices"

08/2009 Invited speaker at the **International Symposium on Quantum Fluids and Solids**, Chicago (USA)
"Exploring correlated 1D Bose gases across from the superfluid to the Mott state by inelastic light scattering"

06/2008 Invited seminar of **INFM-BEC Laboratory**, Trento (Italy)
"Localization phenomena in disordered media : recent experiments with gaseous matter-waves"

04/2008 Invited teacher at the doctoral school **New Frontiers in Micro and Nano Photonics**, Florence (Italy)
"Atomic matterwaves in disordered media"

12/2007 Invited seminar of **Laboratoire de Physique Théorique et des Modèles Statistiques**, Orsay (France)
"Dipole oscillations of BEC in a 1D random potential"

06/2007 PhD students seminar of **Laboratoire de Physique Théorique et des Modèles Statistiques**, Orsay
"Transport of BECs in 1D random potentials"

07/2006 Invited seminar of **Institut d'Optique Graduate School**, Orsay (France)
"Transport properties of coherent interacting matter-waves in a 1D random potential"

03/2006 Contributed talk at the **Young Atomic Opticians Conference**, Paris (France)
"Trapping a coherent matter-wave of interacting particles in a true 1D random potential"

MAJOR COLLABORATIONS

Recent and on-going collaborations:

T. Roscilde - Lyon (France) - *Criticality at the Mott transition*

L. Sanchez-Palencia - Palaiseau (France) - *Contact in 1D Bose gases and disorder-induced transition in 1D dirty bosons* - 1 publication H. Yao et al. Phys. Rev. Lett. (2018)

P. Vignolo - Nice (France) - *Contact in 1D Bose gases* - 1 publication H. Yao et al. Phys. Rev. Lett. (2018)

A. Minguzzi - Grenoble (France) - *Contact in 1D Bose gases* - 1 publication H. Yao et al. Phys. Rev. Lett. (2018)

Z. Hadzibabic - Cambridge (UK) - *Quantum depletion in uniform BECs* - 1 publication: R. Lopes et al., Phys. Rev. Lett. (2017)

G. Carleo - New York (USA) - *Quantum Monte-Carlo calculation for the phase diagram of lattice bosons at finite temperature* - 1 publication: H. Cayla et al., Phys. Rev. A (2018)

Past collaborations:

D. Dowek and R. Sellem - Orsay (France) - *Micro-channel plate detectors and timing signals analysis* - 2 publications: L. Hoendervanger et al., Rev. Scient. Instrum. (2013) ; F. Nogrette et al. Rev. Scient. Instrum. (2015)

L. Pitaevskii and S. Stringari - Trento (Italy) - *Quantum depletion and many-body effect in interacting Bose condensates*

P. Cheinet - Orsay (France) - *Spatially resolved detection of Rydberg atoms with micro-channel plate detectors*

C. Fort and M. Inguscio - Florence (Italy) - *Probing strongly interacting one-dimensional Bose gases with light scattering* - 4 publications since in Palaiseau

J.-S. Caux - Amsterdam (Netherlands) - *Bethe-Ansatz calculations of the dynamical structure of one-dimensional Bose gases* - 1 publication: N. Fabbri et al., Phys. Rev. A (2015)

E. Altman - Tel-Aviv (Israel) - *Investigating Green functions of lattice Bose gases* - 1 publication: N. Fabbri et al., Phys. Rev. Lett. (2012)

G. V. Shlyapnikov - Orsay (France) - *Anderson localization* - 2 publications: D. Clément et al. Phys. Rev. Lett. (2005) ; L. Sanchez-Palencia et al. Phys. Rev. Lett. (2007)

M. Lewenstein - Barcelona (Spain) - *Phase diagram of weakly interacting disordered bosons* - 1 publication P. Lugan et al., Phys. Rev. Lett. (2007)

GRANT FUNDING

Acronym	Period	Agency	Coordination	Amount	Topic
Eclair	2017-2018	Labex PALM	D. Clément	20k€	Extended cavity laser source
Quorum	2017-2020	ANR JCJC	D. Clément	390k€	^{3}He* Fermi sea and correlated fermionic pairs
Princeps	2014-2015	Univ. Paris Saclay	M. Barbot - D. Clément	15 k€	Trans-disciplinary project about the notion of uncertainty
Balzan Prize to A. Aspect	2014-2017	Balzan Foundation	M. Cheneau - D. Clément	110k€	Single-atom detection of lattice gases in momentum space
Corum	2016-2017	Labex PALM	D. Clément	60k€	One-year post-doctoral grant for M. Mancini
CountRateResol	2016-2017	LUMAT federation	D. Clément	20k€	Fast electronics for MCP detector
Cyraqs	2013-2016	Labex PALM	P. Cheinet	20k€	Detection of Rydberg atoms with MCPs
NewSpade	2013-2015	C'Nano	D. Clément	40k€	MCP detector and electronics
Daisy	2011-2015	Ile-de-France	D. Clément - C. Westbrook	250k€	Building the ^{4}He* apparatus and optical lattices
Chaire d'excellence	2010-2015	CNRS	D. Clément	60k€	Building the ^{4}He* apparatus
Corsa	2011-2014	RTRA Network	D. Clément	130k€	Building the ^{4}He* apparatus

6.3 Supervision tasks

As Maître de conférence at Institut d'Optique Graduate School, I have coordinated the Lattice Gas team and guided undergraduates, PhD and post-doc students. Below is the list of the supervised students.

PhD students:

- Lynn A. Hoendervanger - 2010/2014 - Completed
  Title: *A New Metastable Helium Machine : An Investigation into the Attributes of Trapping, Cooling and Detecting Metastable Helium*
  3 peer-review articles

- Yami Fang - 2012/2014 - Completed
  Exchange student from East China Normal University in Shanghai (China) for 1,5 year
  Title: *Research on non-degenerate four-wave mixing in Rubidium vapor and 3D laser cooling at the Doppler limit in metastable Helium*
  1 peer-review article

- Quentin Bouton - 2013/2016 - Completed
  Title: *Étude microscopique de la distribution en impulsion des condensats de Bose-Einstein d'Hélium métastable*
  4 peer-review articles

- Hugo Cayla - 2015-2018 - Completed
  Title: *Measuring the momentum distribution of lattice gases at the single-atom level*
  4 peer-review articles ; 1 preprint

- Cécile Carcy - 2016-present (3rd year)
  3 peer-review articles ; 1 preprint

- Antoine Tenart - 2018-present (1st year)
  2 peer-review articles ; 1 preprint

Post-doc fellows:

- Marco Mancini - 2016-2018 (2 years)
  3 peer-review articles ; 1 preprint

- Rockson Chang - 2013-2016 (2 years)
  4 peer-review articles

Undergraduate students:

Name	Academic level	Year	Duration	Topic
Quentin Bouton	License 3	2011	1 month	*Laser lock with an AOM*
Robert George	License 3	2011	1 month	*Writing a software to clean absorption images*
Olivier Levecq	License 3	2012	1 month	*Electronics for 30GHz beatnote*
Antoine Petrucci	License 3	2012	1 month	*Electronics for 30GHz beatnote*
Baptiste Fix	License 3	2013	1 month	*Realizing a 30GHz beatnote*
Lucie Roujas	License 3	2013	1 month	*Realizing a 30GHz beatnote*
Arthur Genthon	License 3	2016	1 month	*Numerical simulation of loading an array of 1D Bose gases*
Nassim el Ayoubi	License 3	2017	4 months	*PyQTgraph interface for absorption/fluorescence imaging*
Kevin Silva	License 3	2018	1 month	*Building a PID module for intensity stabilization*
Aimrane Hamdou	License 3	2018	1 month	*Building a PID module for intensity stabilization*
Simon Murmann	Master 1	2011	2 months	*Testing CCD and InGaAs camera to image He* atoms*
Denis Savoie	Master 1	2012	4 months	*Control of the experimental cycle with NI cards*
Rajiv Boddeda	Master 1	2012	4 months	*Simulation of magnetic and optical dipole trapping*
Tobias Klafka	Master 1	2014	5 months	*Radio-frequency evaporation and imaging calibration*
Shivam Raval	Master 1	2016	4 months	*Building a fast PID for laser intensity stabilisation*
Chao Zhang	Master 1	2019	5 months	*Building an External cavity laser at 1083 nm*
Lynn Hoendervanger	Master 2	2011	6 months	*Investigating MCPs at high flux of detected particles*
Quentin Bouton	Master 2	2013	6 months	*An optical dipole trap for metastable Helium BECs*
Kevin Audo	Master 2	2014	5 months	*Optical setup for realizing 3D optical lattices*
Cécile Carcy	Master 2	2015	5 months	*Implementing 3D optical lattices for Helium BECs*
Hugo Cayla	Master 2	2015	5 months	*Implementing ROOT-based algorithm for atom correlations*
Antoine Tenart	Master 2	2018	6 months	*Desiging the laser cooling system for $^3He^*$*
Gaetan Hercé	Master 2	2019	5 months	*Investigating Tan's contact in 1D bosons*

6.4 Teaching activities

As a Maître de conférence, my teaching duty is taking place at the Institut d'Optique Graduate School in Palaiseau. Over the period 2010-2019, my teaching load was reduced to 1/3 of the total teaching load of a Maître de conférence (except for the academic school year 2015-2016). This low teaching duty was associated with a chair d'excellence from CNRS (2010-2015) and is now associated with being a member of the Institut Universitaire de France (2016-2021).

Here is a brief description of my teaching activities:

2013-present	Lectures of "Statistical Optics" and lectures of "Light-Atom Interaction" in **Master 2 Laser-Optics-Matter** from Institut d'Optique Graduate School / Polytechnique / University Paris XI
2010-2013	Tutorials (english-speaking class of "Statistical Optics") and laboratory classes (Laser) at the **Institut d'Optique Graduate School** (engineer school SupOptique, Orsay) *(Master level)*
2005-2007	**Talks for non-introduced people on superconductivity** in high-schools and university-level competitive classes

2005-2007	Tutorials and laboratory classes in optics and electronics, at the **Institut d'Optique Graduate School** (engineer school SupOptique, Orsay) *(64 hours a year)*
2004-2005	Tutorials in university-level competitive classes (Physics) at **Lycée Saint Louis** (Paris) *(2 hours a week)*

6.5 Managing of research

COMMISSIONS OF TRUST

2017 - present	Member of the **Commission Consultative de Spécialistes de l'Université (CCSU)**, Université Paris Saclay (France)
2017 - present	Member of the **scientific commitee of the conference COLOQ** (Société Française d'Optique)
2017	**Referee for PhD thesis** of A. S. Flores - University of Amsterdam, Netherlands
2016	**Referee for PhD thesis** of M. Mancini - University of Florence, Italy
2014	**Referee for PhD thesis** of L. Tanzi - University of Florence, Italy
2011 - present	**Reviewer of research projects** (FIRB and SIR) for the Italian Ministry for Research (MIUR)
2008 - present	**Referee for international journals**: Physical Review Letters, Physical Review A, Journal of Low Temperature Physics, New Journal of Physics, European Physical Letters, Science, Journal Physics B: Atomic, Molecular and Optical Physics

ORGANIZATION OF CONFERENCES

2016 Co-organizer with M. Barbot (Ecole Normale Supérieure, Cachan) and F. Favino (Univ. Sapienza, Rome) of the workshop PRINCEPS, an interdisciplinary workshop on the concept of uncertainty

2018 Co-organizer with P. Vignolo (Univ. Nice) and A. Minguzzi (Univ. Grenoble) of the cold-atom workshop during the "Journée de la matière condensée" in Grenoble

Bibliography

[1] J. F. Allen and A. D. Misener. 'Flow of Liquid Helium II'. In: *Nature* 141 (1938), p. 75.

[2] W. Alt et al. 'Single atoms in a standing-wave dipole trap'. In: *Phys Rev A* 67 (2003), p. 033403.

[3] Ehud Altman, Eugene Demler and Mikhail Lukin. 'Probing many-body states of ultracold atoms via noise correlations'. In: *Phys. Rev. A* 70.1 (2004), p. 013603.

[4] M. H. Anderson et al. 'Observation of Bose-Einstein Condensation in a Dilute Atomic Vapor'. In: *Science* 269 (1995), pp. 198–201.

[5] PW Anderson. 'Absence of diffusion in certain random lattices'. In: *Physica Phys Rev* 109 (1958), p. 1492.

[6] F. T. Arecchi, E. Gatti and A. Sona. 'TIME DISTRIBUTION OF PHOTONS FROM COHERENT AND GAUSSIAN SOURCES'. In: *Phys Rev Lett* 20 (1965), p. 27.

[7] A. Aspect et al. 'Cooling atoms with stimulated emission'. In: *Phys Rev Lett* 57 (1986), p. 1688.

[8] A. Aspect et al. 'Laser Cooling below the One-Photon Recoil Energy by Laser Cooling below the One-Photon Recoil Energy by Velocity-Selective Coherent Population Trapping'. In: *Phys. Rev. Lett.* 61 (1988), p. 826.

[9] M. Assmann et al. 'Higher-order photon bunching in a semiconductor microcavity'. In: *Science* 325 (2009), pp. 297–300.

[10] W. S. Bakr et al. 'Probing the superfluid-to-Mott insulator transition at the single atom level'. In: *Science* 329 (2010), pp. 547–550.

[11] Waseem S Bakr et al. 'A quantum gas microscope for detecting single atoms in a Hubbard-regime optical lattice'. In: *Nature* 462.7269 (2009), pp. 74–77.

[12] Gilad Barak et al. 'Interacting electrons in one dimension beyond the Luttinger-liquid limit'. In: *Nat Phys* 6 (2010), p. 489.

[13] F. Bardou et al. 'Magneto-Optical Trapping of Metastable Helium: Collisions in the Presence of Resonant Light'. In: *Europhys. Lett.* 20 (1992), p. 681.

[14] R. Barends et al. 'Digitized adiabatic quantum computing with a superconducting circuit'. In: *Nature* 534 (2016), p. 222.

[15] D. Barredo et al. 'An atom-by-atom assembler of defect-free arbitrary 2d atomic arrays'. In: *Science* 354 (2016), p. 1021.

[16] M. D. Barrett, J. A.Sauer and M. S. Chapman. 'All-Optical Formation of an Atomic Bose-Einstein Condensate'. In: *Phys. Rev. Lett.* 87 (2001), p. 010404.

[17] A. Bergschneider et al. 'Experimental characterization of two-particle entanglement through position and momentum correlations'. In: *Nature Physics* (2019).

[18] J. Bernier et al. 'Emergence of spatially extended pair coherence through incoherent local environmental coupling'. In: *Phys. Rev. A* 87 (2013), p. 063608.

[19] D. Blavette et al. 'An atom probe for three-dimensional tomography'. In: *Nature* 363 (1993), pp. 432–435.

[20] Immanuel Bloch, Jean Dalibard and Sylvain Nascimbene. *Quantum simulations with ultracold quantum gases*. English. In: *Nat Phys* vol. 8.4 (2012), pp. 267–276.
[21] Immanuel Bloch, Jean Dalibard and Wilhelm Zwerger. 'Many-body physics with ultracold gases'. In: *Rev. Mod. Phys.* 80.3 (2008), pp. 885–964.
[22] N. Bogoliubov. 'On the theory of superfluidity'. In: *Physical Review* 11 (1947), pp. 23–32.
[23] D. Boiron. *Optique atomique quantique sur des nuages ultra-froids d'helium metastable*. 2010.
[24] D. Boiron et al. 'Laser cooling of cesium atoms in gray optical molasses down to 1.1 microK'. In: *Phys. Rev. A* 53 (1996), R3734.
[25] D. Boiron et al. 'Three-dimensional cooling of cesium atoms in four-beam gray optical molasses'. In: *Phys. Rev. A* 52 (1995), R3425.
[26] R. Boll and et al. 'Imaging molecular structure through femtosecond photoelectron diffraction on aligned and oriented gas-phase molecules'. In: *Faraday Discuss* 171 (2014), p. 57.
[27] T. Bourdel et al. 'Experimental study of the BEC-BCS crossover region in lithium 6'. In: *Phys Rev Lett* 93 (2004), p. 040501.
[28] Q. Bouton et al. 'Fast production of Bose-Einstein condensates of metastable Helium'. In: *Phys Rev A* 91 (2015), 061402(R).
[29] J. Britton et al. 'Engineered two dimensional Ising interactions in a trapped-ion quantum simulator with hundreds of spins'. In: *Nature* 484 (2012), pp. 489–492.
[30] A. Browaeys et al. 'Two body loss rate in a magneto-optical trap of metastable He'. In: *Eur. Phys. J. D* 8 (2000), pp. 199–203.
[31] Robert Bücker et al. 'Single-particle-sensitive imaging of freely propagating ultracold atoms'. In: *New J. Phys.* 11.10 (2009), p. 103039.
[32] A. Burchianti et al. 'Efficient all-optical production of large 6Li quantum gases using D1 gray-molasses cooling'. In: *Phys Rev A* 90 (2014), p. 043408.
[33] M. Campostrini and E. Vicari. 'Critical Behavior and Scaling in Trapped Systems'. In: *Phys Rev Lett* 102 (2009), p. 240601.
[34] M. Campostrini et al. 'Finite-Size Scaling at First-Order Quantum Transitions'. In: *Phys Rev Lett* 113 (2014), p. 070402.
[35] B Capogrosso-Sansone, N Prokof'ev and B Svistunov. 'Phase diagram and thermodynamics of the three-dimensional Bose-Hubbard model'. In: *Phys. Rev. B* 75.13 (2007), p. 134302.
[36] C. Carcy et al. 'Momentum-space atom correlations in a Mott insulator'. In: *Arxiv preprint* 1904.10995 (2019).
[37] G. Carleo et al. 'Unitary Dynamics of Strongly Interacting Bose Gases with the Time-Dependent Variational Monte Carlo Method in Continuous Space'. In: *Phys. Rev. X* 7 (2017), p. 031026.
[38] Yvan Castin and R Dum. 'Bose-Einstein condensates in time dependent traps'. English. In: *Phys. Rev. Lett.* 77.27 (1996), pp. 5315–5319.
[39] Jean-Sébastien Caux and Pasquale Calabrese. 'Dynamical density-density correlations in the one-dimensional Bose gas'. In: *Phys. Rev. A* 74.3 (2006), pp. 1–4.
[40] Jean-Sébastien Caux, Pasquale Calabrese and Nikita A Slavnov. 'One-particle dynamical correlations in the one-dimensional Bose gas'. English. In: *J Stat Mech-Theory E* (2007), P01008.
[41] H. Cayla. 'Measuring the momentum distribution of a lattice gas at the single-atom level'. PhD thesis. Institut d'Optique Graduate School, 2018.

[42] H. Cayla et al. 'Single-atom-resolved probing of lattice gases in momentum space'. In: *Phys Rev A* 97 (2018), 061609(R).
[43] M. A. Cazalilla et al. 'One dimensional bosons: From condensed matter systems to ultracold gases'. In: *Rev. Mod. Phys.* 83 (2011), p. 1405.
[44] R. Chang et al. 'Momentum-resolved observation of thermal quantum depletion in an interacting Bose gas'. In: *Phys Rev Lett* 117 (2016), p. 235303.
[45] R. Chang et al. 'Three-dimensional laser cooling at the Doppler limit'. In: *Phys Rev A* 90 (2014), p. 063407.
[46] C. Y. Chen et al. In: *Rev. Sci. Instrum.* 72 (2001), p. 271.
[47] G. De Chiara and A. Sanpera. 'Genuine quantum correlations in quantum many-body systems: a review of recent progress'. In: *Rep Prog Phys* 81 (2018), p. 074002.
[48] A. P. Chikkatur et al. 'Suppression and Enhancement of Impurity Scattering in a Bose-Einstein Condensate'. In: *Phys Rev Lett* 85 (2000), p. 483.
[49] C. Chin et al. 'Observation of the pairing gap in a strongly interacting Fermi gas'. In: *Science* 305 (2004), pp. 1128–1130.
[50] C. S. Chiu et al. 'Quantum state engineering of a Hubbard system with ultracold fermions'. In: *Phys. Rev. Lett.* 120 (2018), p. 243201.
[51] J. Choi et al. 'Exploring the many-body localization transition in two dimensions'. In: *Science* 352 (2016), p. 1547.
[52] David Clément et al. 'Bragg Spectroscopy of Strongly Correlated Bosons in Optical Lattices'. In: *J Low Temp Phys* 158.1-2 (2010), pp. 5–15.
[53] David Clément et al. 'Multi-band spectroscopy of inhomogeneous Mott-insulator states of ultracold bosons'. English. In: *New J. Phys.* 11 (2009), p. 103030.
[54] D. Clément et al. 'Exploring Correlated 1D Bose Gases from the Superfluid to the Mott-Insulator State by Inelastic Light Scattering'. In: *Phys. Rev. Lett.* 102 (2009), p. 155301.
[55] A. E. Clifford and A. H. Wing. 'Electronic Circuits and Tubes'. McGraw- Hill, New York, 1947.
[56] CMS Collaboration. 'Observation of long-range, near-side angular correlations in proton-proton collisions at the LHC'. In: *J. High Energy Phys.* 09 (2010), p. 091.
[57] G. Colzi et al. 'Sub-Doppler cooling of sodium atoms in gray molasses'. In: *Phys Rev A* 93 (2016), p. 023421.
[58] Ph. Courteille et al. 'Observation of a Feshbach Resonance in Cold Atom Scattering'. In: *Phys Rev Lett* 81 (1998), p. 69.
[59] A. Czasch et al. 'Position and time sensitive photon counting detector with image charge delay-line readout'. In: *Proc. SPIE* 6771 (2007), p. 67710.
[60] J. Dalibard and C. Cohen-Tannoudji. 'Atomic motion in laser light: connection between semiclassical and quantum descriptions'. In: *J Phys B-At Mol Opt* 18 (1985), p. 1661.
[61] R G Dall et al. 'Ideal n-body correlations with massive particles'. In: *Nature Physics* 9 (2013), pp. 341–344.
[62] R G Dall et al. 'Observation of atomic speckle and Hanbury Brown–Twiss correlations in guided matter waves'. In: *Nature Communications* 2 (2011), pp. 291–5.
[63] A Damascelli, Z Hussain and ZX Shen. 'Angle-resolved photoemission studies of the cuprate superconductors'. In: *Rev. Mod. Phys.* 75.2 (2003), pp. 473–541.
[64] Romain Dubessy et al. 'Rubidium-87 Bose-Einstein condensate in an optically plugged quadrupole trap'. In: *Phys Rev A* 85 (2012), p. 013643.

[65] FB Dunning, RD Rundel and RF Stebbings. 'Determination of secondary electron ejection coefficients for rare gas metastable atoms'. In: *Review of Scientific Instruments* 46.6 (1975), pp. 697–701.
[66] M. Ebner. 'Development of a metastable helium BEC as a platform for experiments with EPR-entangled matter waves'. PhD thesis. 2012.
[67] V. Elman and A. Hemmerich. 'Near-resonant dark optical lattice with increased occupation'. In: *Phys Rev A* 72 (2005), p. 043410.
[68] Manuel Endres et al. 'The 'Higgs' Amplitude Mode at the Two-Dimensional Superfluid-Mott Insulator Transition'. In: *Nature* 487 (2012), pp. 454–458.
[69] T. Esslinger et al. 'Purely optical dark lattice'. In: *Opt Lett* 21 (1996), p. 991.
[70] Nicole Fabbri et al. 'Momentum-resolved study of an array of one-dimensional strongly phase-fluctuating Bose gases'. English. In: *Phys. Rev. A* 83.3 (2011), p. 031604.
[71] N. Fabbri et al. 'Dynamical structure factor of one-dimensional Bose gases: Experimental signatures of beyond-Luttinger-liquid physics'. In: *Phys Rev A* 91 (2015), p. 043617.
[72] N Fabbri et al. 'Quasiparticle Dynamics in a Bose Insulator Probed by Interband Bragg Spectroscopy'. In: *Phys. Rev. Lett.* 109.5 (2012), p. 055301.
[73] B. Fang et al. 'Momentum-Space Correlations of a One-Dimensional Bose Gas'. In: *Phys Rev Lett* 116 (2016), p. 050402.
[74] P. O. Fedichev, M. W. Reynolds and U. M. Rahmanovand G. V. Shlyapnikov. 'Inelastic decay processes in a gas of spin-polarized triplet helium'. In: *Phys Rev A* 53 (1996), p. 1447.
[75] D. Rio Fernandes et al. 'Sub-Doppler laser cooling of fermionic 40K atoms in three-dimensional gray optical molasses'. In: *Europhysics letters* (2012).
[76] R. P. Feynman. 'Simulating Physics with Computers'. In: *International Journal of Theoretical Physics* 21.6/7 (1982).
[77] M. P. A. Fisher et al. 'Boson localization and the superfluid-insulator transition'. In: *Phys Rev B* 40 (1989), pp. 546–570.
[78] R. J. Fletcher et al. 'Two- and Three-body Contacts in the Unitary Bose Gas'. In: *Science* 355 (2017), p. 377.
[79] A. S. Flores et al. 'Simple method for producing Bose-Einstein condensates of metastable helium using a single beam optical dipole trap'. In: *Appl. Phys. B* 121 (2015), p. 391.
[80] Simon Fölling et al. 'Spatial quantum noise interferometry in expanding ultracold atom clouds'. In: *Nature* 434.7032 (2005), pp. 481–484.
[81] L. Gabardos et al. 'Cooling all external degrees of freedom of optically trapped chromium atoms using gray molasses'. In: *Phys. Rev. A* 99 (2019), p. 023607.
[82] C. W. Gardiner et al. 'Evaluation of heating effects on atoms trapped in an optical trap'. In: *Phys Rev A* 61 (2000), p. 045801.
[83] Alexander L Gaunt et al. 'Bose-Einstein Condensation of Atoms in a Uniform Potential'. In: *Phys. Rev. Lett.* 110.20 (2013), p. 200406.
[84] F Gerbier et al. 'Expansion of a Quantum Gas Released from an Optical Lattice'. In: *Phys. Rev. Lett.* 101.15 (2008), p. 155303.
[85] Tatjana Gericke et al. 'High-resolution scanning electron microscopy of an ultracold quantum gas'. English. In: *Nat Phys* 4.12 (2008), pp. 949–953.
[86] T. Giamarchi. 'Quantum physics in one dimension'. Oxford University Press, 2003.
[87] J. Viana Gomes et al. 'Theory for a Hanbury Brown Twiss experiment with a ballistically expanding cloud of cold atoms'. In: *Phys Rev A* 74 (2006), p. 053607.
[88] JW Goodman. 'Speckle phenomena in optics: theory and applications'. 2006.

[89] M. R. Goosen et al. 'Feshbach resonances in 3He*-4He* mixtures'. In: *Phys. Rev. A* 84 (2010), p. 042713.
[90] Markus Greiner et al. 'Collapse and revival of the matter wave field of a Bose-Einstein condensate'. English. In: *Nature* 419.6902 (2002), pp. 51–54.
[91] Markus Greiner et al. 'Quantum phase transition from a superfluid to a Mott insulator in a gas of ultracold atoms'. In: *Nature* 415.6867 (2002), pp. 39–44.
[92] Andrew T. Grier et al. 'L-enhanced sub-Doppler cooling of lithium atoms in D1 gray molasses'. In: *Phys. Rev. A* 87 (2013), p. 063411.
[93] G. Grynberg, A. Aspect and C. Fabre. 'Introduction to Quantum Optics: From the Semiclassical Approach to Quantized Light'. Cambridge University Press, Cambridge, 2010.
[94] Y. Harada, S. Masuda and H. Ozaki. 'Electron spectroscopy using metastable atoms as probes for solid surfaces'. In: *Chem. Rev.* 97 (1997), p. 1897.
[95] S. Haroche. 'Nobel Lecture: Controlling photons in a box and exploring the quantum to classical boundary'. In: *Rev. Mod. Phys.* 85 (2013), p. 1083.
[96] M.-S. Heo, J.-Y. Choi and Y.-I. Shin. 'Fast production of large 23Na Bose-Einstein condensates in an optically plugged magnetic quadrupole trap'. In: *Phys Rev A* 83 (2011), p. 013622.
[97] S. S. Hodgman. 'Transition lifetime measurements and correlation experiments with ultra-cold metastable Helium'. PhD thesis. Australina National University, 2011.
[98] S. S. Hodgman et al. 'Solving the Quantum Many-Body Problem via Correlations Measured with a Momentum Microscope'. In: *Phys Rev Lett* 118 (2017), p. 240402.
[99] A. L. Hoendervanger et al. 'Influence of gold coating and interplate voltage on the performance of chevron micro-channel plates for temporally and spatially resolved single particle detection'. In: *Rev. Sci. Instrum.* 84.2, 023307 (2013), p. 023307.
[100] L. Hoendervanger. 'A New Metastable Helium Machine : An Investigation into the Attributes of Trapping, Cooling and Detecting Metastable Helium'. PhD thesis. Institut d'Optique Graduate School, 2015.
[101] M. Horikoshi et al. 'Accurate in situ acquisition of column density of a dense cloud of ultracold 6Li atoms using absorption imaging'. In: *Arxiv preprint* (2016), 1608:07152.
[102] R. Horodecki et al. 'Quantum entanglement'. In: *Rev Mod Phys* 81 (2009), p. 865.
[103] D. I. Hoult and C. M. Preston. 'INEXPENSIVE PLASMA DISCHARGE SOURCE FOR MOLECULAR EMISSION SPECTROSCOPY WITH APPLICATION TO 15N ANALYSIS'. In: *Rev Sci Instrum* 63.3 (1992), pp. 1927–1931.
[104] L. Van Hove. 'The Occurrence of Singularities in the Elastic Frequency Distribution of a Crystal'. In: *Phys. Rev.* 89 (1953), p. 189.
[105] Sebastian D Huber et al. 'Dynamical properties of ultracold bosons in an optical lattice'. In: *Phys. Rev. B* 75.8 (2007), pp. 1–12.
[106] K. Hueck et al. 'Calibrating high intensity absorption imaging of ultracold atoms'. In: *Opt Express* 25 (2017), p. 8670.
[107] Adilet Imambekov, Thomas L Schmidt and Leonid I Glazman. 'One-dimensional quantum liquids: Beyond the Luttinger liquid paradigm'. In: *Rev. Mod. Phys.* 84.3 (2012), pp. 1253–1306.
[108] S. Inouye et al. 'Observation of a Feshbach resonance in a Bose-Einstein condensate'. In: *Nature* 392 (1998), pp. 151–154.
[109] O. Jagutzki et al. 'A broad-application microchannel-plate detector system for advanced particle or photon detection tasks: large area imaging, precise multi-hit tim-

ing information and high detection rate'. In: *Nuclear Instruments and Methods in Physics Research A* 477 (2002), pp. 244–249.
[110] D. Jaksch et al. 'Cold Bosonic Atoms in Optical Lattices'. In: *Phys. Rev. Lett.* 81 (1998), pp. 3108–3111.
[111] Fred Jendrzejewski et al. 'Coherent Backscattering of Ultracold Atoms'. In: *Physical review letters* 109.19 (2012), p. 195302.
[112] Robert Jördens et al. 'A Mott insulator of fermionic atoms in an optical lattice'. In: *Nature* 455.7210 (2008), pp. 204–207.
[113] Yu. Kagan, E. L. Surkov and G. V. Shlyapnikov. 'Evolution of a Bose-condensed gas under variations of the confining potential'. In: *Phys Rev A* 54 (1996), 1753(R).
[114] P. Kapitza. 'Viscosity of Liquid Helium below the λ-Point'. In: *Nature* 141 (1938), p. 74.
[115] J. Kasprzak et al. 'Second-Order Time Correlations within a Polariton Bose-Einstein Condensate in a CdTe Microcavity'. In: *Phys Rev Lett* 100 (2008), p. 067402.
[116] S. Kato et al. 'Laser spectroscopic probing of coexisting superfluid and insulating states of an atomic Bose–Hubbard system'. In: *Nature Communications* 7 (2016), p. 11341.
[117] Yasuyuki Kato et al. 'Sharp peaks in the momentum distribution of bosons in optical lattices in the normal state'. In: *Nat Phys* 4.8 (2008), pp. 617–621.
[118] M. Keller et al. 'Bose-Einstein condensate of metastable helium for quantum correlation experiments'. In: *Phys Rev A* 90 (2014), p. 063607.
[119] W Ketterle, D. S Durfee and D. M Stamper-Kurn. 'Making, probing and understanding Bose-Einstein condensates'. In: *Proceedings of the International School of Physics "Enrico Fermi"* 140 (1999), pp. 67–176.
[120] K. V. Kheruntsyan et al. 'Finite-temperature correlations and density profiles of an inhomogeneous interacting one-dimensional Bose gas'. In: *Phys Rev A* 71 (2005), p. 053615.
[121] J. Kinast et al. 'Evidence for superfluidity in a resonantly interacting Fermi gas'. In: *Phys. Rev. Lett.* 92 (2004), p. 150402.
[122] T Kinoshita, T Wenger and David S Weiss. 'Observation of a one-dimensional Tonks-Girardeau gas'. English. In: *Science* 305.5687 (2004), pp. 1125–1128.
[123] M. Kotyrba. 'Bose-Einstein condensation of metastable helium-4 for quantum entanglement experiments'. PhD thesis. University of Vienna, 2015.
[124] M. A. Kristensen et al. 'Observation of Atom Number Fluctuations in a Bose-Einstein Condensate'. In: *Phys Rev Lett* 122 (2019), p. 163601.
[125] M. Kumakura. 'Laser Trapping of Metastable 3He Atoms: Isotopic Difference in Cold Penning Collisions'. In: *Physical Review Letters* 82.14 (1999), pp. 2848–2851.
[126] Joern Kupferschmidt and Erich Mueller. 'Role of interactions in time-of-flight expansion of atomic clouds from optical lattices'. In: *Phys. Rev. A* 82.2 (2010), p. 023618.
[127] S. Laurent et al. 'Connecting few-body inelastic decay to quantum correlations in a many-body system: A weakly coupled impurity in a resonant Fermi gas'. In: *Phys. Rev. Lett.* 118 (2017), p. 103403.
[128] J. Lawall et al. 'Three-Dimensional Laser Cooling of Helium Beyond the Single-Photon Recoil Limit'. In: *Phys. Rev. Lett.* 75.23 (1995), p. 4194.
[129] J.E Lawler et al. 'A hollow cathode for doppler-free spectroscopy'. In: *J Applied Phys.* 52 (1981), p. 4375.
[130] A. L. Leggett. 'Quantum Liquids: Bose Condensation and Cooper Pairing in Condensed-Matter Systems'. Oxford University Press, 2006.

[131] EH Lieb. 'Exact analysis of an interacting Bose gas. II. The excitation spectrum'. In: *Physical Review* 130.4 (1963), pp. 1616–1624.
[132] EH Lieb and W Liniger. 'Exact analysis of an interacting Bose gas. I. The general solution and the ground state'. In: *Physical Review* 130.4 (1963), pp. 1605–1616.
[133] Y. J. Lin et al. 'Rapid production of Rb-87 Bose-Einstein condensates in a combined magnetic and optical potential'. In: *Phys. Rev. A* 79.6 (2009), p. 063631.
[134] F. London. 'On the Bose-Einstein Condensation'. In: *Phys. Rev.* 54 (1938), p. 547.
[135] R. Lopes et al. 'Quantum Depletion of a Homogeneous Bose-Einstein Condensate'. In: *Phys Rev Lett* 119 (2017), p. 1904404.
[136] R. Lopes et al. 'Second-order coherence of superradiance from a Bose-Einstein condensate'. In: *Phys. Rev. A* 90 (2014), p. 013615.
[137] WJ Lu et al. 'A practical direct current discharge helium absorption cell for laser frequency locking at 1083 nm'. English. In: *Rev Sci Instrum* 67.9 (1996), pp. 3003–3004.
[138] C. Luciuk et al. 'Evidence for universal relations describing a gas with p-wave interactions'. In: *Nat Phys* 11 (2016), pp. 1–8.
[139] A. Lukin et al. 'Probing entanglement in a many-body-localized system'. In: *Science* 364 (2019), pp. 256–260.
[140] G. D. Mahan. 'Many-Particle Physics'. Kluwer Academic / Plenum Publishers, 1981.
[141] E. Majorana. 'Atomi orientati in campo magnetico variabile'. In: *Il Nuovo Cimento* 9 (1932), p. 43.
[142] P. Makotyn et al. 'Universal dynamics of a degenerate unitary Bose gas'. In: *Nature Physics* 10 (2014), pp. 116–119.
[143] L. Mandel and E. Wolf. 'Optical Coherence and Quantum Optics'. Cambridge University Press, Cambridge, 1995.
[144] M. J. Mark et al. 'Precision Measurements on a Tunable Mott Insulator of Ultracold Atoms'. In: *Phys Rev Lett* 107 (2011), p. 175301.
[145] H. C. Mastwijk et al. 'Optical Collisions of Cold, Metastable Helium Atoms'. In: *Phys. Rev. Lett.* 80 (1998), p. 5516.
[146] A. Mazurenko et al. 'A cold-atom Fermi–Hubbard antiferromagnet'. In: *Nature* 545 (2017), pp. 462–466.
[147] F. Meinert et al. 'Probing the Excitations of a Lieb-Liniger Gas from Weak to Strong Coupling'. In: *Phys Rev Lett* 115 (2015), p. 085301.
[148] C Menotti and N Trivedi. 'Spectral weight redistribution in strongly correlated bosons in optical lattices'. English. In: *Phys. Rev. B* 77.23 (2008), p. 235120.
[149] A. Miller, D. Pines and P. Nozieres. 'Elementary Excitations in Liquid Helium'. In: *Phys. Rev.* 127 (1962), p. 1452.
[150] F Moron et al. 'An oscillator circuit to produce a radio-frequency discharge and application to metastable helium saturated absorption spectroscopy'. In: *Rev. Sci. Instrum.* 83.4 (2012), p. 044705.
[151] N. F. Mott. 'The Basis of the Electron Theory of Metals, with Special Reference to the Transition Metals'. In: *Phys. Soc. (London)* A62 (1949), p. 416.
[152] J. Mun et al. 'Phase Diagram for a Bose-Einstein Condensate Moving in an Optical Lattice'. In: *Phys Rev Lett* 99 (2007), p. 150604.
[153] Dipankar Nath et al. 'Quantum-interference-enhanced deep sub-Doppler cooling of 39K atoms in gray molasses'. In: *Phys. Rev. A* 88 (2013), p. 053407.
[154] F. Nogrette et al. 'Characterization of a detector chain using a FPGA-based Time-to-Digital Converter to reconstruct the three-dimensional coordinates of single particles at high flux'. In: *Review of Scientific Instruments* 86 (2015), p. 113105.

[155] F. Nogrette et al. 'Single-Atom Trapping in Holographic 2D Arrays of Microtraps with Arbitrary Geometries'. In: *Phys. Rev. X* 4 (2014), p. 021034.
[156] M Olshanii. 'Atomic scattering in the presence of an external confinement and a gas of impenetrable bosons'. In: *Phys. Rev. Lett.* 81.5 (1998), pp. 938–941.
[157] M Olshanii and V Dunjko. 'Short-distance correlation properties of the Lieb-Liniger system and momentum distributions of trapped one-dimensional atomic gases'. English. In: *Phys. Rev. Lett.* 91.9 (2003), p. 090401.
[158] D Van Oosten et al. 'Inelastic light scattering from a Mott insulator'. English. In: *Phys. Rev. A* 71.2 (2005), p. 021601.
[159] A Osterloh et al. 'Scaling of entanglement close to a quantum phase transition'. English. In: *Nature* 416.6881 (2002), pp. 608–610.
[160] H. Ott. 'Single atom detection in ultracold quantum gases: a review of current progress'. In: *Rep. Prog. Phys.* 79 (2016), p. 054401.
[161] Anton Ottl et al. 'Correlations and Counting Statistics of an Atom Laser'. In: *Phys Rev Lett* 95 (2005), p. 090404.
[162] R Ozeri et al. 'Colloquium: Bulk bogoliubov excitations in a bose-einstein condensate'. English. In: *Rev. Mod. Phys.* 77.1 (2005), pp. 187–205.
[163] M. Panfil and J. S. Caux. 'Finite temperature correlations in the Lieb-Liniger 1D Bose gas'. In: *Phys Rev A* (2014).
[164] B Paredes et al. 'Tonks-Girardeau gas of ultracold atoms in an optical lattice'. English. In: *Nature* 429.6989 (2004), pp. 277–281.
[165] G. B Partridge et al. 'Bose-Einstein condensation and spin mixtures of optically trapped metastable helium'. In: *Phys. Rev. A* 81.5 (2010), p. 053631.
[166] A. Perrin et al. 'Hanbury Brown and Twiss correlations across the Bose–Einstein condensation threshold'. In: *Nature Physics* 8 (2012), p. 195.
[167] A. Perrin et al. 'Observation of Atom Pairs in Spontaneous Four-Wave Mixing of Two Colliding Bose-Einstein Condensates'. In: *Phys. Rev. Lett.* 99 (15 2007), p. 150405.
[168] W. Petrich et al. 'Stable, Tightly Confining Magnetic Trap for Evaporative Cooling of Neutral Atoms'. In: *Phys. Rev. Lett.* 74 (1995), p. 3352.
[169] L. Pitaevskii and S. Stringari. 'Bose-Einstein Condensation'. Oxford University Press, 2003.
[170] L. Pitaevskii and S. Stringari. 'Uncertainty Principle, Quantum Fluctuations, and Broken Symmetries'. In: *J Low Temp Phys* 85 (1991), p. 377.
[171] D. Poletti et al. 'Emergence of Glasslike Dynamics for Dissipative and Strongly Interacting Bosons'. In: *Phys Rev Lett* 111 (2013), p. 195301.
[172] L. Pollet. 'Recent developments in quantum Monte Carlo simulations with applications for cold gases'. In: *Rep. Prog. Phys.* 75 (2012), p. 094501.
[173] L. Pollet, K. V. Houcke and S. M. A. Rombouts. In: *Journal of Computational Physics* 225 (2007), pp. 2249–2266.
[174] Guido Pupillo, Ana Maria Rey and Ghassan George Batrouni. 'Bragg spectroscopy of trapped one-dimensional strongly interacting bosons in optical lattices: Probing the cake structure'. In: *Phys. Rev. A* 74.1 (2006), pp. 1–7.
[175] C. Qu, L. P. Pitaevskii and S.Stringari. 'Expansion of harmonically trapped interacting particles and time dependence of the contact'. In: *Phys Rev A* 94 (2016), p. 063635.
[176] Ushnish Ray and David M. Ceperley. 'Revealing the condensate and noncondensate distributions in the inhomogeneous Bose-Hubbard model'. In: *Phys. Rev. A* 87 (5 2013), p. 051603.

[177] C. A. Regal, M. Greiner and D. S. Jin. 'Observation of Resonance Condensation of Fermionic Atom Pairs'. In: *Phys Rev Lett* 92 (2004), p. 040403.
[178] J. Reichel and V. Vuletic. 'Atom Chips'. John Wiley and Sons, 2011.
[179] Ana Maria Rey et al. 'Bragg spectroscopy of ultracold atoms loaded in an optical lattice'. In: *Phys. Rev. A* 72.2 (2005), pp. 1–5.
[180] Simon Richard et al. 'Momentum spectroscopy of 1D phase fluctuations in Bose-Einstein condensates'. In: *Phys. Rev. Lett.* 91.1 (2003), p. 4357.
[181] Marcos Rigol et al. 'State diagrams for harmonically trapped bosons in optical lattices'. English. In: *Phys. Rev. A* 79.5 (2009), p. 053605.
[182] A. Robert et al. 'A Bose-Einstein Condensate of Metastable Atoms'. In: *Science* 292 (2001), pp. 461–464.
[183] W Rooijakkers, W Hogervorst and W Vassen. 'An intense collimated beam of metastable helium atoms by two-dimensional laser cooling'. In: *Opt Commun* 123.1 (1996), pp. 321–330.
[184] T. Roscilde. 'Thermometry of Cold Atoms in Optical Lattices via Artificial Gauge Fields'. In: *Phys Rev Lett* 112 (2014), p. 110403.
[185] S. Rosi et al. 'A-enhanced grey molasses on the D2 trnasition of Rubidium-87 atoms'. In: *Scientific reports* 8 (2018), p. 1301.
[186] Y. Sagi et al. 'Measurement of the homogeneous contact of a unitary Fermi gas'. In: *Phys Rev Lett* 109 (2012), p. 220402.
[187] G. Salomon et al. 'Gray-molasses cooling of 39K to a high phase-space density'. In: *Europhysics letters* 104 (2013), p. 63002.
[188] F Pereira Dos Santos. 'CONDENSATION DE BOSE-EINSTEIN DE L'HELIUM METASTABLE'. PhD thesis. 2002, pp. 1–161.
[189] F Pereira Dos Santos et al. 'Bose-Einstein condensation of metastable helium'. In: *Phys Rev Lett* 86 (2001), p. 3459.
[190] F. Pereira Dos Santos et al. 'Penning collisions of laser-cooled metastable helium atoms'. In: *Eur. Phys. J. D* 14 (2001), pp. 15–22.
[191] M Schellekens. 'L'EFFET HANBURY BROWN ET TWISS POUR LES ATOMES FROIDS'. PhD thesis. 2007, pp. 1–210.
[192] M. Schellekens et al. 'Hanbury Brown Twiss Effect for Ultracold Quantum Gases'. In: *Science* 310.5748 (2005), pp. 648–651. eprint: http://www.sciencemag.org/content/310/5748/648.full.pdf.
[193] N. Schlosser et al. 'Sub-poissonian loading of single atoms in a microscopic dipole trap'. In: *Nature* 411 (2001), pp. 1024–1027.
[194] J. Schmitt et al. 'Observation of Grand-Canonical Number Statistics in a Photon Bose-Einstein Condensate'. In: *Phys Rev Lett* 112 (2014), p. 030401.
[195] U Schneider et al. 'Metallic and Insulating Phases of Repulsively Interacting Fermions in a 3D Optical Lattice'. In: *Science* 322.5907 (2008), pp. 1520–1525.
[196] M. Schreiber et al. 'Observation of many-body localization of interacting fermions in a quasi-random optical lattice'. In: *Science* (2015).
[197] S. Seidelin et al. 'Getting the Elastic Scattering Length by Observing Inelastic Collisions in Ultracold Metastable Helium Atoms'. In: *Phys. Rev. Lett.* 93 (2004), p. 090409.
[198] K Sengupta and N Dupuis. 'Mott-insulator-to-superfluid transition in the Bose-Hubbard model: A strong-coupling approach'. English. In: *Phys. Rev. A* 71.3 (2005), p. 033629.
[199] Jacob F. Sherson et al. 'Single-atom-resolved fluorescence imaging of an atomic Mott insulator'. In: *Nature* 467.7311 (2010), pp. 68–72.

[200] G. V. Shlyapnikov et al. 'Decay Kinetics and Bose Condensation in a Gas of Spin-Polarized Triplet Helium'. In: *Phys Rev Lett* 73 (1994), p. 3247.
[201] O. Siegmund et al. 'Cross Delay Line Detectors for High Time Resolution Astronomical Polarimetry and Biological Fluorescence Imaging'. In: *IEEE Nuclear Science Symposium Conference Record N14* (2005).
[202] F. Sievers et al. 'Simultaneous sub-Doppler laser cooling of fermionic 6Li and 40K on the D1 line: Theory and Experiment'. In: *Phys Rev A* 91 (2015), p. 023426.
[203] O Sirjean. 'Collisions ionisantes: un nouveau diagnostic pour les condensats de Bose-Einstein d'hélium métastable'. PhD thesis. 2003, pp. 1–358.
[204] J. Söding et al. 'Three-body decay of a rubidium Bose–Einstein condensate'. In: *Appl Phys B* 69 (1999).
[205] I. B. Spielman, W. D. Phillips and J. V. Porto. 'Mott-Insulator Transition in a Two-Dimensional Atomic Bose Gas'. In: *Phys Rev Lett* 98 (2007), p. 080404.
[206] J Stenger et al. 'Bragg spectroscopy of a Bose-Einstein condensate'. English. In: *Phys. Rev. Lett.* 82.23 (1999), pp. 4569–4573.
[207] J. T Stewart, J. P Gaebler and D. S Jin. 'Using photoemission spectroscopy to probe a strongly interacting Fermi gas'. English. In: *Nature* 454.7205 (2008), pp. 744–747.
[208] J. T. Stewart et al. 'Verification of Universal Relations in a Strongly Interacting Fermi Gas'. In: *Phys Rev Lett* 104 (2010), p. 235301.
[209] T Stoferle et al. 'Transition from a strongly interacting 1D superfluid to a Mott insulator'. In: *Phys. Rev. Lett.* 92.13 (2004), p. 130403.
[210] CI Sukenik and HC Busch. 'A rf discharge cell for saturated absorption spectroscopy of metastable argon'. English. In: *Rev Sci Instrum* 73.2 (2002), pp. 493–494.
[211] JA Swansson et al. 'A high flux, liquid-helium cooled source of metastable rare gas atoms'. English. In: *Appl Phys B-Lasers O* 79.4 (2004), pp. 485–489.
[212] N. Syassen et al. 'Strong Dissipation Inhibits Losses and Induces Correlations in Cold Molecular Gases'. In: *Science* 320 (2008), pp. 1329–1331.
[213] S. Tan. 'Energetics of a strongly correlated Fermi gas'. In: *Annals of Physics* 323 (2008), pp. 2952–2970.
[214] S. Tan. 'Large momentum part of a strongly correlated Fermi gas'. In: *Annals of Physics* 323 (2008), pp. 2971–2986.
[215] N. R. Thomas et al. 'Imaging of s and d Partial-Wave Interference in Quantum Scattering of Identical Bosonic Atoms'. In: *Phys. Rev. Lett.* 93 (2004), p. 173201.
[216] M. Tinkham. 'Introduction to Superconductivity'. Dover Publications, 1996.
[217] L. Tisza. 'The theory of liquid Helium'. In: *Phys. Rev.* 72 (1947), p. 838.
[218] P. J. J. Tol et al. 'Large numbers of cold metastable helium atoms in a magneto-optical trap'. In: *Phys. Rev. A* 60 (1999), p. 761.
[219] PJJ Tol. 'Trapping and Evaporative Cooling of Metastable Helium'. PhD thesis. 2005, pp. 1–178.
[220] E Toth, Ana Maria Rey and P. Blair Blakie. 'Theory of correlations between ultracold bosons released from an optical lattice'. In: *Phys. Rev. A* 78.1 (2008), p. 013627.
[221] J. M. Tranquada et al. 'Evidence for stripe correlations of spins and holes in copper oxide superconductors'. In: *Nature* 375 (1995), pp. 561–563.
[222] S Trotzky et al. 'Suppression of the critical temperature for superfluidity near the Mott transition'. In: *Nat Phys* 6.12 (2010), pp. 998–1004.
[223] C. Valentin et al. 'One-dimension sub-Doppler molasses in the presence of static magnetic field'. In: *Europhys. Lett.* 17 (1992), p. 133.
[224] B. J. vanWees and et al. 'Quantized conductance of point contacts in a two-dimensional electron gas'. In: *Phys. Rev. Lett.* 60 (1988), pp. 848–850.

[225] Wim Vassen et al. 'Cold and trapped metastable noble gases'. In: *Rev. Mod. Phys.* 84.1 (2012), pp. 175–210.
[226] S Wessel et al. 'Quantum Monte Carlo simulations of confined bosonic atoms in optical lattices'. English. In: *Phys. Rev. A* 70.5 (2004), p. 053615.
[227] D. A. Wharam and et al. 'One-dimensional transport and the quantisation of the ballistic resistance'. In: *J. Phys. C* 21 (1988), p. L209.
[228] R. J. Wild et al. 'Measurements of Tan's Contact in an Atomic Bose-Einstein Condensate'. In: *Phys Rev Lett* 108 (2012), p. 145305.
[229] D. J. Wineland. 'Nobel Lecture: Superposition, entanglement, and raising Schrödinger's cat'. In: *Rev. Mod. Phys.* 85 (2013), p. 1103.
[230] J L Wiza. 'Microchannel plate detectors'. In: *Nuclear Instruments and Methods* 162 (1979), pp. 587–601.
[231] K Xu et al. 'Observation of Strong Quantum Depletion in a Gaseous Bose-Einstein Condensate'. In: *Phys. Rev. Lett.* 96.18 (2006), p. 180405.
[232] H. Yao et al. 'Tan's Contact for Trapped Lieb-Liniger Bosons at Finite Temperature'. In: *Phys Rev Lett* 121 (2018), p. 220402.
[233] Y. Yudkin and L. Khaykovich. 'Laser cooling at resonance'. In: *Phys. Rev. A* 97 (2018), p. 053403.
[234] Qi Zhou et al. 'Direct Mapping of the Finite Temperature Phase Diagram of Strongly Correlated Quantum Models'. In: *Phys. Rev. Lett.* 103.8 (2009), p. 085701.
[235] X. Zhu et al. 'Interaction of phonons and dirac fermions on the surface of Bi2Se3: A strong Kohn anomaly'. In: *Phys. Rev. Lett.* 107 (2011), p. 186102.
[236] P. Zin, J. Chwedenczuk and M. Trippenbach. 'Elastic scattering losses from colliding Bose-Einstein condensates'. In: *Phys Rev A* 73 (2006), p. 033602.
[237] P. Zin et al. 'Quantum Multimode Model of Elastic Scattering from Bose-Einstein Condensates'. In: *Phys Rev Lett* 94 (2005), p. 200401.
[238] P. Zupancic et al. 'Ultra-precise holographic beam shaping for microscopic quantum control'. In: *Optics Express* 24 (2016), pp. 13881–13893.
[239] M. W. Zwierlein et al. 'Condensation of pairs of fermionic atoms near a Feshbach resonance'. In: *Phys. Rev. Lett.* 92 (2004), p. 120403.